MECHANISMS THAT REGULATE BLOOD-BRAIN BARRIER DYSFUNCTION AND HYPERPERMEABILITY

A Dissertation

by

HIMAKARNIKA ALLURI

Submitted to the Office of Graduate and Professional Studies of
Texas A&M University
in partial fulfillment of the requirements for the degree of

DOCTOR OF PHILOSOPHY

Chair of Committee,	Binu Tharakan
Committee Members,	Cynthia J. Meininger
	Travis W. Hein
	Vincent J. VanBuren
Head of Department,	Paul E. Ogden

December 2015

Major Subject: Medical Sciences

ABSTRACT

Blood-brain barrier (BBB) disruption is the hallmark feature of the secondary injuries that occur following traumatic and ischemic brain injuries. Microvascular hyperpermeability that occurs consequently leads to vasogenic edema and elevated intracranial pressure. Structurally, the BBB is comprised of the brain endothelial cells and the tight junction between them formed by the tight junction proteins (TJPs). Zonula occludens-1 (ZO-1) is an important membrane-bound scaffolding TJP that links transmembrane TJPs to intracellular actin cytoskeletal assembly.

Studies indicate that adenosine triphosphate (ATP) that is released into the extracellular space following trauma binds to and activates the purinergic receptor (P2X7R), leading to the production of interleukin-1β (IL-1β); which in turn is shown to activate various downstream proteases. Matrix metalloproteinase-9 (MMP-9) and calpains are proteases known to induce BBB breakdown. However, the mechanisms by which ATP and IL-1β induce BBB dysfunction and hyperpermeability and the involvement of proteases in this process are vastly unknown. We hypothesize that ATP and IL-1β-induced BBB dysfunction and hyperpermeability occurs via P2X7R and /MMP-9/calpain-mediated pathways, respectively. And thus, P2X7R/MMP-9/calpain inhibitions play an important role in mediating BBB dysfunction and hyperpermeability following traumatic injuries in brain.

The results from these studies demonstrate that MMP-9/calpain inhibition attenuated IL-1β-induced monolayer hyperpermeability, *f*-actin stress fiber formation, and loss of ZO-1/TJ integrity and enhanced MMP-9/calpain activity in RBMECs. However, IL-1β treatment did not alter intracellular calcium levels, total number of viable cells, total ZO-1 protein, and mRNA expression. Purinergic receptor (P2X7R) inhibition attenuated Bz-ATP (potent agonist of

P2X7R)-induced endothelial cell hyperpermeability, loss of ZO-1/TJ integrity and *f*-actin stress fiber formation. Although Bz-ATP treatment reduced ZO-1 protein expression, it did not alter total number of viable cells or ZO-1 mRNA expression *in vitro*. Melatonin (a pineal hormone with MMP-9 inhibitory properties), calpain inhibitor III (calpain inhibitor), and KN-62 (PX7R inhibitor) pretreatment attenuated TBI-induced BBB hyperpermeability in C57BL/6 mice. P2X7R knockout mice demonstrated reduced TBI-induced BBB hyperpermeability compared to the wild-type animals.

In conclusion, ATP-sensitive P2X7R are involved in promoting BBB dysfunction and hyperpermeability via IL-1β-mediated activation of MMP-9/calpain pathways and subsequent disorganization of the TJs. Inhibition of this pathway can provide potential therapeutic targets against TBI-induced BBB hyperpermeability *in vivo*.

DEDICATION

I would like to dedicate my humble effort to my beloved parents. Their encouragement, support, patience, and kindness have been enormous in helping me reach such success and honor.

ACKNOWLEDGEMENTS

My education and development, both as a scientist and a person are due to more people than I will ever know. I owe my deepest gratitude to all the people who have helped me reach my potential in ways direct or indirect. I would like to kindly acknowledge all the people whose scientific contributions have led to this dissertation.

I would most whole-heartedly like to thank my mentor ***Dr. Binu Tharakan,*** Assistant Professor, Department of Surgery, Baylor Scott&White Health & Texas A&M University Health Science Center College of Medicine for providing me an opportunity to work in his laboratory. I am very grateful for his constant encouragement, valuable guidance, and support throughout my graduate work. His expertise on trauma and blood-brain barrier dysfunction helped me to improve my research skills and prepared me for future challenges. I really appreciate Dr. Tharakan for his kind, generous and friendly nature without his support this dissertation would not have been possible.

I would like to thank my committee members, ***Dr. Cynthia J. Meininger***, Professor, Department of Medical Physiology, Director of vascular biology division and graduate studies in Temple campus, Texas A&M University Health Science Center College of Medicine for her support and guidance throughout my graduate school education.

Dr. Travis W. Hein, Professor, Department of Surgery, Texas A&M University Health Science Center College of Medicine has been very helpful in my scientific

progress. His emphasis on in-depth knowledge and thorough understanding of basic concepts has been very helpful in my growth and advancement as a scientist.

I would like to thank ***Dr. Vincent J. VanBuren***, Assistant professor, Department of Medical Physiology, Director of Computational Biology and Bioinformatics Laboratory, Texas A&M University Health Science Center for kindly accepting to be part of my graduate committee, his suggestions and scientific input have been helpful during my study. He has been supportive while I was taking Biostatistics course under his guidance.

Dr. Ruth Murell-Lagnado, Department of Pharmacology, University of Cambridge has been very instrumental in developing conceptual ideas for the P2X7R project. Her scientific inputs in figuring out the ATP doses for our studies have been very useful.

Contribution of ***Dr. Shenyuan Zhang*** has been significant in performing calcium mobilization studies.

Collaboration with ***Dr. Xu Peng*** helped us tremendously in performing the RT-PCR experiments and western blots. His encouragement and guidance have been very valuable in seeking professional advice and help.

Dr. Yang Liu has been supportive and encouraging during my stay in Texas A&M University Health Science Center at Temple campus, both as research assistant and as a graduate student. She has been very helpful in holding scientific discussions and providing input. She has helped us with the RT-PCR studies presented in the dissertation.

Thanks goes to ***Dr. Carl Tong*** for helping me during the application process to graduate school at Texas A&M University Health Science Center.

Ms. Anna Webb, research technician at ***Texas A&M University Health Science Center College of Medicine Integrated Microscopy and Imaging Laboratory*** in Temple campus, helped us with various imaging techniques and obtaining good confocal images.

I would like to thank our past and present lab members:

Ms. Chinchusha Anasooya Shaji for her support and making sure that the research work in the laboratory runs smoothly. Contribution of Ms. Anasooya Shaji has been significant in completing the intravital microscopy imaging studies presented in this dissertation.

Dr. Katie C. Wiggins-Dohlvik, postdoctoral researcher in our lab was very helpful in completing the review, "Blood-brain barrier dysfunction following traumatic brain injury". Collaborating and assisting her in various projects has been very productive resulting in various research papers.

Ms. Mercene Grimsley, summer research student helped us in conducting experiments for calpain studies.

Ms. Rickesha L Wilson, medical student helped us with the interleukin-1 beta time and dose studies.

Tremendous thanks goes to ***Dr. Harry T. Papaconstantinou***, Chairman of Department of Surgery without his support this dissertation would not have been complete.

I would like to thank ***Baylor Scott and White Health Academic Operations*** and ***Texas A&M University Health Science Center*** for providing the infrastructure, core facilities and support which were very important for conducting good quality research.

I would like to thank '***Metabolic Brain Disease***' Journal and the publisher '***Springer***', for giving me the permission to use the review article, 'Blood-brain barrier dysfunction following traumatic brain injury' (PMID: 25624154), along with full-text and figures used this dissertation.

Thanks also go to my friends and colleagues and the department faculty and staff of both Department of Surgery and College of Medicine at Texas A&M University Health Science Center for their support and guidance for my excellent education.

Most importantly, I am very thankful to my husband ***Chander S. Peddaboina***, for his loving-kindness and support.

TABLE OF CONTENTS

Page

LIST OF FIGURES

FIGURE Page

CHAPTER I

INTRODUCTION TO ENDOTHELIAL HYPERPERMEABILITY AND TRAUMATIC BRAIN INJURY*

VASCULAR ENDOTHELIAL HYPERPERMEABILITY

Vascular endothelial hyperpermeability is a significant clinical problem in conditions associated with traumatic and ischemic injuries, sepsis, atherosclerosis, acquired respiratory distress syndrome, diabetic retinopathy, thrombosis, inflammatory bowel disease and cancer [1; 2; 3]. Of those conditions, traumatic injuries are a public health problem in the USA, that accounts for 2.3 million admissions, 41 million emergency department visits annually and are also considered as a leading cause of death among the age group of 1 to 44 (http://www.nationaltraumainstitute.org/). One of the most common traumatic injuries is the traumatic brain injury (TBI). Traumatic brain injury is defined as any damage to the brain due to external forces like rapid acceleration/deceleration, blast waves, crush, or penetration by a projectile [4; 5; 6]. Disruption of the blood-brain barrier (BBB; the protective vascular barrier of the brain)

---

*Parts of this chapter are reprinted with permission from "Blood-brain barrier dysfunction following traumatic brain injury" by Alluri H, Wiggins-Dohlvik K, Davis ML, Huang JH, Tharakan B, 2015. *Metab Brain Dis.*, 30(5):1093-104, Copyright 2015 by Springer.

is the chief secondary injury that occurs following TBI and is often associated with microvascular hyperpermeability. Microvascular hyperpermeability can be defined as the leakage of fluid and proteins from the intravascular space into the extravascular space leading to tissue edema and multiple organ dysfunction [7]. Currently, there is no treatment to retard or halt the progression of secondary injuries that occur following TBI [8].

BLOOD-BRAIN BARRIER

The brain is an extremely compact organ, tasked with performance and regulation of numerous activities, chief among these is maintenance of homeostasis in the body [9]. The delicate structure of the brain parenchyma renders it highly susceptible to injury, such as changes in forces and pressure [10] and consequently it is protected by a rigid skull. In addition to this macroscopic protection, the brain is also isolated from the blood or its fluid spaces on a microscopic level by three barrier layers: 1) BBB formed by cerebrovascular endothelial cells [11; 12], 2) the epithelium of the choroid plexus, and 3) the arachnoid epithelium [13; 14]. Of these, the BBB demonstrates the greatest influence over the microenvironment of the brain and plays the largest role in promoting optimal neuronal function [15; 16].

Paul Ehlrich first described the BBB in the 1880s [17; 18]. During his investigations, he injected water-soluble dyes into the systemic circulation and noted that they did not enter the central nervous system (CNS). Later Edwin E. Goldman injected the same dyes into the cerebrospinal fluid (CSF) and demonstrated that they did

not pass into the systemic circulation [19; 20]. These discoveries paved the way for our current understanding of the BBB. It is now known that the "barrier" identified by Ehlrich and Goldman is due to the complex interaction of the cerebral microvascular endothelial cells and the tight junctions between them [21]. The attachment of these endothelial cells forms a physical barrier. Additionally, the transport systems on the luminal and abluminal membranes regulate transcellular traffic and within the brain exhibit decreased endocytosis and transcytosis when compared to peripheral endothelium, thus forming a "transport barrier" [15]. Furthermore, the endothelial cells of the BBB are able to metabolize many toxic and neuroactive substances, functioning as a "metabolic barrier" [15]. Brain endothelial cells along with the other cells in the brain including astrocytes, pericytes, neurons and extracellular matrix (ECM) comprises the neurovascular unit (NVU) [22]. While the BBB is an essential and protective barrier of the brain its tightness is one of the limitations in transporting the therapeutic molecules across the BBB [23]. Efforts have been made to open the BBB transiently to permit the transit of various drug therapies following the breach in the BBB [23].

Brain endothelial cells

The vasculature of the brain is lined entirely with endothelial cells and these cells are normally the "front line defense" of the BBB. The integrity and permeability of the BBB is dictated mainly by tight junctions and adherens junctions between endothelial cells [22]. Tight junctions comprise integral transmembrane proteins

(claudins, occludin and junctional adhesion molecules) and accessory cytoplasmic membrane proteins (zonula occludens [ZO], cingulin and others) [24; 25] [28][29].

In addition to these junctional proteins, endothelial cells also possess several other unique characteristics. Brain endothelial cells completely lack fenestrations, have high reflective coefficients and high electrical resistance [21; 23; 26; 27]. Brain endothelial cells have abundant mitochondria. This supports their numerous transport systems and high number of ionic channels, which regulate the contraction of vessels and activate signaling pathways. They also lack MHC class II molecules. Together these mechanisms allow restriction of leukocyte transmigration and ionic movement from blood into tissue [15; 27; 28], which is paramount in maintaining homeostasis in the brain.

Tight junction proteins

Tight junction proteins make up the structural and functional units of the BBB. Tight junctions are expressed as early as embryonic day 12, reflecting their importance in growth and development [29], and are normally composed of a variety of proteins, including claudins, occludin, zonula occludens, and tricellulin. These proteins can be bicellular, like claudins or occludin, or they can be tricellular, as in tricellulin [30; 31]. Further, they encompass cytoplasmic proteins, like cingulin, afadin (AF6), 7H6, and zonula occludens (ZO)-1,-2, and -3 that bind the actin cytoskeleton within the cell [24; 32; 33].

Tight junctions regulate major functions of endothelial cells such as polarity, gene expression, signal transduction, differentiation, and undergo several post-translational modifications in order to regulate these processes [34; 35; 36]. Tight junction proteins, because of their importance in regulation of the BBB, are clearly deranged with the fluid extravasation and swelling as seen after TBI but have also been shown to be involved in many pathological states including inflammatory bowel disease (IBD), cancers, and tumor metastasis [18].

Zonula occludens

Zonula occludens (ZO) proteins belong to the membrane associated guanylate kinases (MAGUK) family and are expressed as one of three major forms (ZO-1, -2, or -3), all of which share sequence homology [37]. These proteins are multi-domain scaffolding cytoplasmic phosphoproteins, which link the transmembrane tight junction proteins like claudin to actin cytoskeleton via actin binding proteins cingulin and afadin. Domains at the C terminal are known to be, not only important for tight junction localization, but also in interaction with other tight junction proteins and immunoglobulins [33]. Zonula occludens proteins are important in regulating tight junction integrity, cell-cell interaction and adhesion, and signal transduction and, as such, are thought to possible play a large role in regulation of vascular permeability within the BBB, although this area is only beginning to be examined [18; 38]. Global gene knockout mouse model for ZO-1 have also been developed, however these animals exhibited lethal phenotype at embryonic day ten [39], further confirming its significance

in embryonic development. Unpublished data from our lab also demonstrate that ZO-1 siRNA transfected monolayers but not claudin-5 or occludin siRNA transfected monolayers showed significant hyperpermeability ($p<0.05$). These studies further support the role of ZO-1 in maintaining the BBB tight junction integrity and permeability.

TRAUMATIC BRAIN INJURY

Traumatic brain injury (TBI) could be simply defined as any injury to the brain resulting from an external force. Brain injuries are commonly sustained during motor vehicle accidents, sporting events, slips and falls, assaults, construction accidents, firearm mishaps and various military activities leading to a wide array of personality, cognitive, mental and emotional deficits [40]. Annually, it is estimated that around 10 million people are affected by TBI worldwide, and of these, 5.3 million people are from the United States (US) [41]. According to the Centers for Disease Control and Prevention in 2012, the lifetime (the direct and indirect) costs of medical care and lost wages/productivity for patients with TBI are estimated to be $76.5 billion [42]. Two issues complicate examination of these numbers. First, many patients who suffer TBI are predisposed to development of other neurological diseases like seizures, epilepsy, dementia and Alzheimer's disease [7; 43]. It is unknown how many people diagnosed with neurodegenerative disorders actually are suffering from the sequela of head injury. Secondly, 75% of all TBIs are mild injuries, commonly referred to as concussions. Many of these patients never seek medical attention, and consequently the injuries go

undiagnosed [4]. Therefore, the true cost and impact of TBI may be much higher than estimated. Even so, we speculate by the year 2020, TBI will be one of the leading causes of death and disability worldwide.

Traumatic brain injury and the blood-brain barrier

Both traumatic and non-traumatic brain injury can precipitate BBB breakdown [44; 45; 46]. Derangements in the BBB have been studied both clinically and in the laboratory. They have been implicated in numerous pathologic states including cerebral ischemia, subarachnoid hemorrhage, concussive brain injury, meningitis, vascular dementia, CNS vasculitis, ischemic-reperfusion injury, epilepsy, seizures, cerebral malaria, neurologic inflammation, auto immune diseases like Alzhemier's, Parkinson's, multiple sclerosis, various cancers, acquired immune deficiency syndrome (AIDS), insulin resistance, obesity, stroke, infarction, and TBI. Of these, TBI affects the most patients annually, and consequently warrants close and careful examination [23; 45; 46; 47; 48].

Traumatic brain injury has a very complex, dynamic and heterogeneous pathology, leading to a wide variety of injuries. Initially, direct tissue damage, known as the primary injury, occurs leading to immediate (usually in milliseconds to seconds), irreversible blood vessel and cellular damage. Such injuries set into motion a cascade of events that can precipitate secondary injuries, a term referring to the perpetuation of damage either through host cellular response or by ongoing physiologic insults. Secondary injuries are multifactorial, often ranging from few hours to days after the

initial insult and, with proper treatment; they can be avoided, or reversed. During the secondary phase, abnormalities in the BBB can be linked to several derangements that ultimately affect a patient's clinical course and, although BBB dysregulation is a highly transient and acute phenomenon, the secondary injuries that are triggered can be debilitating and can last a lifetime [49; 50]. The sequence of secondary events and clinical outcomes that occur following TBI are presented in Figure 1. Therefore, a better understanding of TBI, secondary injuries and the role of the BBB therein is paramount. Compromises in BBB permeability following brain injury may last from less than 4 hours to up to 4 days, based on the molecular weight of the compounds [51].

Several pathophysiologic stresses contribute to the breakdown of the BBB following TBI. Some of the significant secondary injury events in the brain include: 1) oxidative stress leading to free radical production and lipid peroxidation, 2) inflammation due to the release of various pro-inflammatory cytokines, nitric oxide and prostaglandins, 3) excitotoxicity occurring through NMDA receptor activation and calcium influx, 4) mitochondrial dysfunction occurring due to increase in Poly (ADP-Ribose) Polymerase 1 (PARP-1) and calpains activation and decrease in NAD+/ATP levels, 5) apoptotic and necrotic cell death mechanisms, and 6) BBB disruption leading to cerebral edema, hypoxia and ischemic events [52]. Proteases, reactive oxygen species (ROS), angiogenic factors, pro-inflammatory cytokines, autoantibodies, leukocytes adhesion and migration, infection and pathogens can all contribute to BBB dysfunction, which includes hyperpermeability, loss of tight junction integrity and transporters, inadequate clearance of cell debris, detachment from other brain cells like pericytes,

astrocytes and interrupted basement membrane and activation of brain immune cells i.e. glial cells [53]. Activation of caspases, translocases and phopholipases not only trigger changes in membranes and DNA, but also cause cleavage of tight junctions and their reorganization [54]. Some of the substances released from neurons, connective tissue and blood cells include substance P, serotonin, histamine, and ATP, which can affect the BBB both on the blood and the brain side [15].

Neuroinflammation following TBI plays an important role in determining its pathophysiology. A few inflammatory molecules that increase in production following TBI, including interleukin-1 beta (IL-1β) and tumor necrosis factor-alpha (TNF-α), further worsen the pathologic insult by activating various matrix metalloproteinases (MMPs) [55; 56]. BBB dysfunction, if not addressed in a timely manner, can lead to neuronal dysfunction, neuroinflammation and neurodegeneration [53].

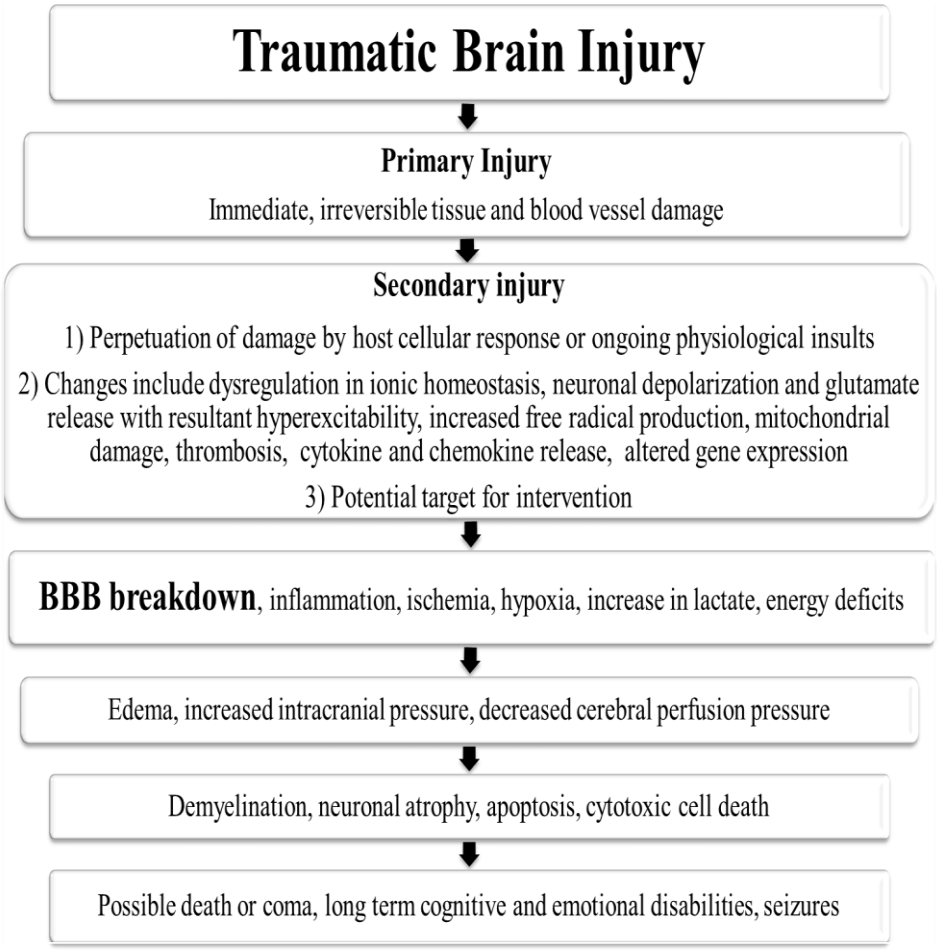

Figure 1: Schematic of various events and clinical outcomes that occur following TBI.

Models used in the study of TBI

Although impressive strides have been published since 1900s, the current understating in TBI and the role of the BBB therein is far from complete and warrants continued investigation. A variety of models have been developed and employed for this task. *In vitro* models examine the response of brain tissue to different components of mechanical stimuli in real-time, including hydrostatic pressure, shear stress, stretch and strain, and compression. Morrison and co-workers explain these studies in detail in their review Morrison et al, 2011 [57]. *In vitro* models provides advantages such as repeatability, the ability to control conditions, and the ability to isolate variables to better understand specific facets of TBI, including the mechanisms that affect the BBB and how it responds to certain conditions [57; 58; 59]. However, promising, *in vitro* models thus far lack validation with *in vivo* models; as they do not fully represent the multiple dimensions and complex pathophysiology seen in an intact organism after injury [60].

Various *in situ* and *in vivo* imaging techniques were utilized to study the BBB at the molecular level after TBI, including fluid extravasation and leukocyte diapedesis through the BBB. However, at this time these techniques are not cost-effective and present many logistic hurdles [4].

Several *in vivo* models have been developed to examine TBI. As with most scientific models, each exhibits strengths and weaknesses and in the study of TBI, these unfortunately are compounded by the heterogeneous nature of brain injuries. It is difficult to develop an *in vivo* model that mimics the diversity in patient age, gender,

baseline health, medication use, substance abuse, injury pattern and severity that are seen in actual TBIs [4; 32; 59; 61; 62]. With that said, invaluable insights into the pathophysiology of TBI have been gleaned utilizing animal models. The most commonly used models include: controlled cortical impact (CCI), fluid percussion injury (FPI), penetrating ballistic brain injury (PBBI) model, weight drop model, blast injury model, and acceleration head injury models [63]. Of them, CCI was the chosen model for this dissertation due to its various advantages as described in detail in the following section.

Controlled cortical impact (CCI)

This technique was developed first by Light Hall in 1988. It is widely used to study a range of neurological, cardiovascular, and histopathological variables. This is an invasive impact technique, widely used for studies in various animals. This technique uses a pneumatic or electromagnetic pump that drives the impactor onto the exposed dura. This technique is widely used to study cortical tissue loss, acute subdural hematoma, axonal injury, BBB dysfunction and coma [5]. This model is highly reproducible of many features of brain injuries like motor deficits, memory loss neuronal loss and also has the advantage of having lower mortality rate in animals [64; 65; 66; 67]. Its drawback is the need for a craniotomy, which blurs its direct translation to human injury [5; 68; 69]. Blood-brain barrier opening in CCI model of TBI is biphasic in nature and maxed for the first time 4-6 hours after TBI, and then 3 days after [49]. Controlled cortical impactor has been shown to increase BBB permeability after

injury and interestingly, quantitative T1 magnetic resonance imaging techniques have shown that BBB disruption exacerbates with age following CCI [70]. Pictorial representation of the CCI instrument used in this dissertation is presented in Figure 2.

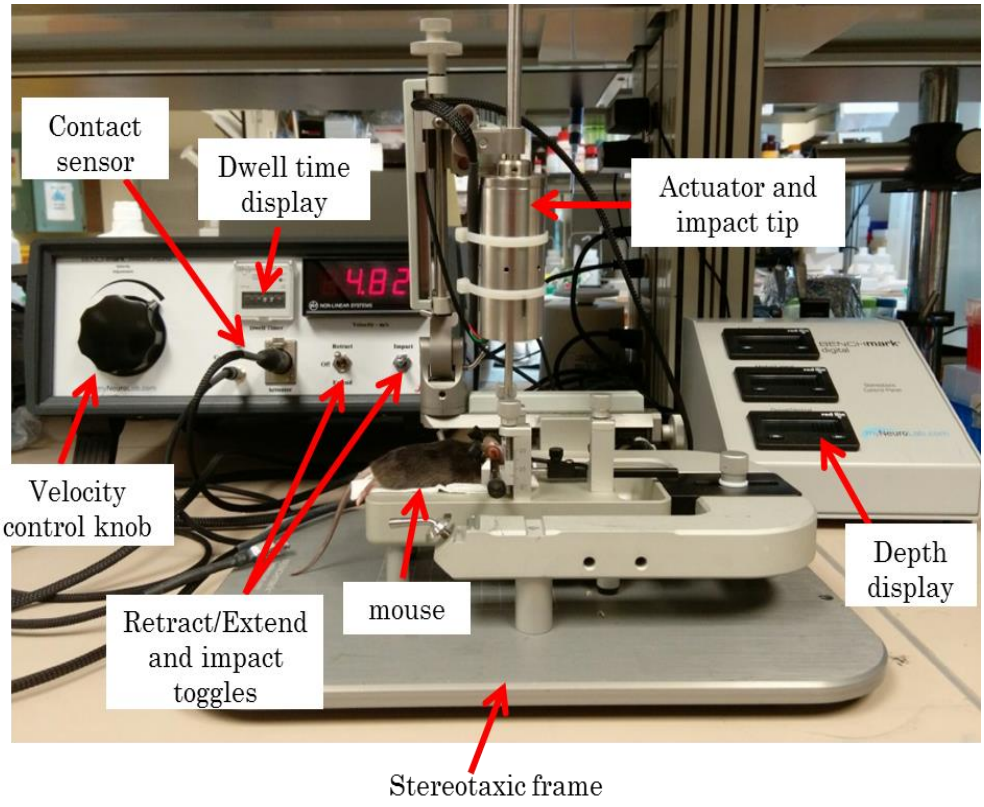

Figure 2: Pictorial representation of the controlled cortical impact model of TBI. Above is the picture of Leica Benchmark stereotaxic impactor. In this technique, following craniotomy surgery, head of the mouse is positioned under the probe of a controlled cortical impactor on the stereotaxic frame as shown in the picture. Settings for velocity and dwell time can be adjusted using the velocity control knob and dwell time display. Depth of the probe into the brain cortex can be adjusted using the digital manipulator on the right side with a depth display.

I*N VITRO* AND *IN VIVO* METHODS TO ASSESS PERMEABILITY

Permeability in the microvasculature works on the Starling principle, which illustrates the role of hydrostatic and oncotic pressures on the movement of fluid across capillary membranes. At the arteriolar end, hydrostatic pressure dominates the oncotic pressure, pushing the fluid into the extravascular space; while on the venular end, the oncotic pressure dominates the hydrostatic pressure, absorbing the proteins into the intravascular space. Thus, permeability is tightly regulated in the microvasculature. However, under pathological conditions, Lp, hydraulic conductivity which determines the permeability property of the capillary to water is increased leading to accumulation of large number of proteins into interstitial space producing an oncotic pressure that drives the flow into the extravascular space leading to edema. However, edema may also be affected by high capillary fluid pressure and increases in plasma proteins [71; 72]. Many methods exist to measure permeability of fluid/solutes. Most of them aim to determine one of the several different factors of the capillary wall that determine permeability like the filtration coefficient (K_f), hydraulic conductivity (L_p), solute permeability coefficient (P_s), or the osmotic reflection coefficient (σ).

Starling equation: $$J_v = K_f([P_c - P_i] - \sigma[\pi_c - \pi_i])$$

J_v is the net fluid movement between compartments and $[P_c - P_i] - \sigma [\pi_c - \pi_i]$ is the net driving force. P_c is the capillary hydrostatic pressure, P_i is the interstitial hydrostatic pressure, π_c is the capillary oncotic pressure, π_i is the interstitial oncotic pressure, K_f is the filtration coefficient (proportionality constant), and σ is the reflection coefficient. The most common *in vitro* technique used to study permeability is the membrane

permeability assay, while the most commonly studied *in vivo* method is Evans blue extravasation technique. Intravital microscopy (IVM) is an established technique that has gained a lot of popularity recently for measuring vascular permeability in animal models.

In vitro techniques

Quantitative measurements are more challenging to perform in the intact physiologically functional tissues. Hence, *in vitro* methods provide flexibility by employing cultured endothelial cell monolayers; enabling us to control various experimental conditions and allowing quantitative measurements. However, they also suffer from some limitations due to a chance for inadequate representations of real microvasculature.

The artificial membrane permeability assay has become a very popular, versatile and extremely useful technique as an *in vitro* tool for measuring permeability across the membranes. In this design there is a polycarbonate/polystyrene filter separating the donor and the acceptor compartment. After growing the endothelial cells on the membrane (step 1 in figure 3), the test drug is usually added to the donor compartment and is allowed to diffuse through the polycarbonate membrane (step 2 in figure 3) [71; 72]. At the end of the drug treatment study, fluorescent-tagged albumin or dextran of known molecular weight is added to the donor chamber and allow it to leak into acceptor chamber for 30 minutes (step 3 in figure 3). Fluorescence intensity is a

measure of FITC-dextran-10 kDa leakage into the lower chamber. Pictorial representation of an *in vitro* permeability assay is presented in Figure 3.

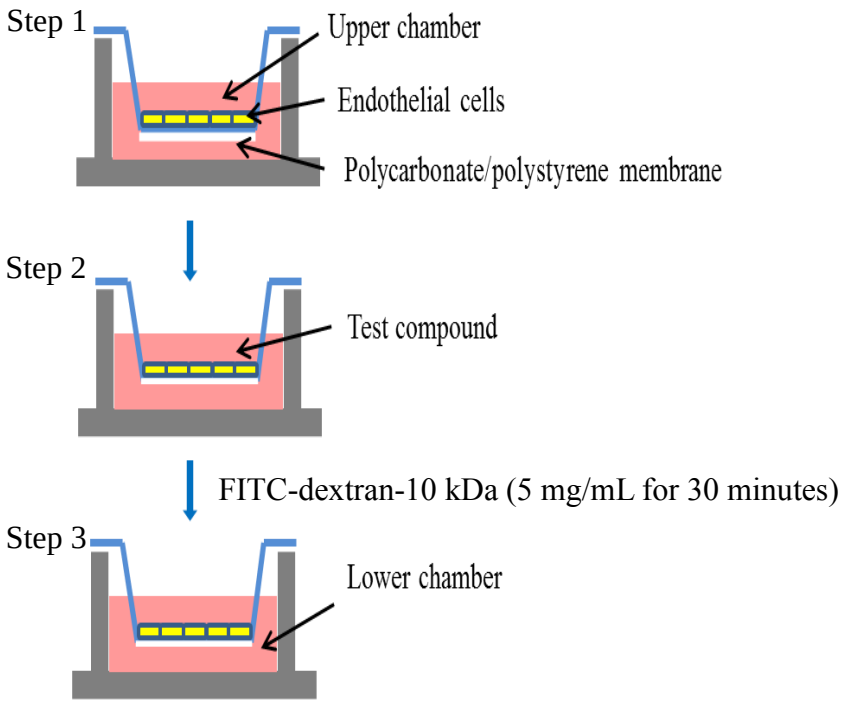

Figure 3: Pictorial representation of *in vitro* permeability assay. This assay employs Transwell inserts (shown in blue color). Transwell insert consists of polycarbonate or polystyrene membrane (white color) that separates the upper/donor chamber (luminal) from the lower/acceptor chamber (alumina chamber; shown in gray color). In this procedure, brain endothelial cells (shown in yellow color) are initially grown as monolayers on Transwell inserts and brain endothelial cell complete medium (shown in pink color) is added both to donor as well as acceptor chamber as depicted in step 1. A test compound is added to the donor and acceptor chamber and allowed to act on the endothelial cell monolayers (step 2). Finally, in step 3, FITC-dextran-10 kDa is applied to the donor chamber and allowed to diffuse into the lower chamber for 30 minutes. Later, a small sample is collected from the lower chamber and measured fluorometrically at 485/535 nm (Excitation/Emission).

In vivo techniques

Intravital microscopy (IVM) and Evans blue dye (EBD) extravasation techniques are commonly used *in vivo* techniques to study BBB endothelial hyperpermeability. These techniques employ either dyes (e.g., Evans Blue) or fluorescently tagged albumin or dextrans of known molecular weight as markers of permeability. *In vivo* techniques work on the principle that brain is impermeable to leakage of intravascular dyes (e.g. Evans blue dye that binds to the serum albumins) or fluorescent-tagged albumin or dextrans into the extravascular space; due to the high molecular weight of the dye-albumin complex or fluorescently tagged albumin or dextrans. However, when the BBB integrity is compromised, the dye-albumin complex or fluorescently tagged albumins/dextrans leak into the extravascular space of the brain and the extent of leakage into the extravascular space is a direct indication of vascular permeability as demonstrated in Figure 4.

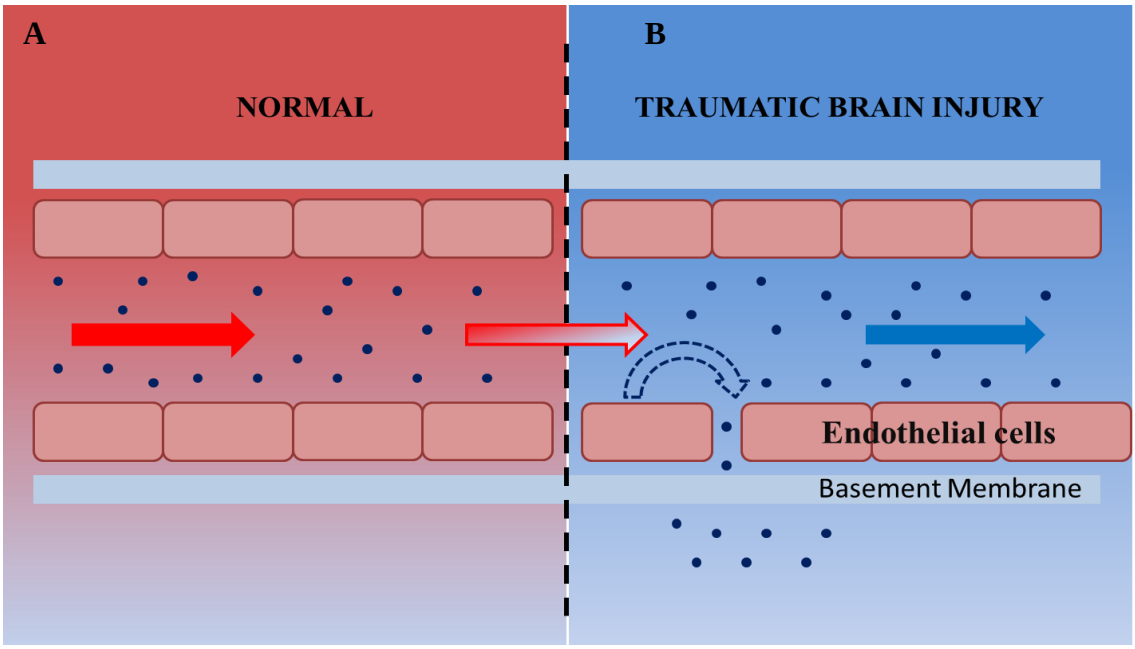

Figure 4: Principle of *in vivo* permeability studies. Under normal conditions, brain endothelial cell lining (pink color boxes) separates the blood from the extravascular space, preventing any leakage of dye/fluorescently tagged molecules from passing through the BBB (A); however, following brain trauma an increase in endothelial permeability results in leakage of plasma and proteins into the extravascular space of the brain (B). The extent of permeability can be determined as a ratio of extravascular to intravascular leakage or by comparing the total dye leakage into brain tissue compared to a control animal.

Intravital microscopy imaging

Wagner first described intravital microscopy (IVM) in the 19th century, which has evolved considerably by the advent of modern microscopy and imaging techniques. It is a powerful visualization technique used to study the vascular changes in live

animals. Pictorial representation of an intravital microscope is shown in the Figure 5. In this technique, fluorescein isothiocyanate (FITC) labeled dextran is injected intravenously into the animal and its leakage into the brain tissue over a period is monitored. In this procedure, mice are anesthetized with urethane, i.p. injection (2 mL/kg body weight) followed by FITC-dextran-10 kDa, i.v. injection (50 mg/mL; 100 μL) via the tail vein. FITC-dextran is injected into the animal five minutes prior to sham surgery (only craniotomy) or traumatic brain injury using a controlled cortical impactor. The craniotomy process involves making a circular window on the chosen (in this case, right hemisphere) hemisphere of the brain between bregma and lambda on the skull of the animal using a microdrill. The surgical site is cleaned and a cover glass is placed over the surgical site followed by sealing it with super glue. The animal is then placed under the microscope and the images were captured at 30, 50, and 70 minutes using Leica 40X N2 objective. Typically, vessels ranging from 20-40 μm were chosen for imaging pial microcirculation using FITC imaging cube with emission wavelength of 525 nm. Y-axis represents the ratio of FITC-fluorescence intensity values extravascular to intravascular space normalized to FITC-fluorescence intensity values obtained at 30 minutes baseline.

Pictorial and graphical representation of IVM images obtained from animals subjected to sham and mild TBI (2 millimeter depth; 0.5 meters/second velocity and 100 milliseconds contact time) injury over a period of 30, 50 and 70 minutes are presented in the figure 6A and B.

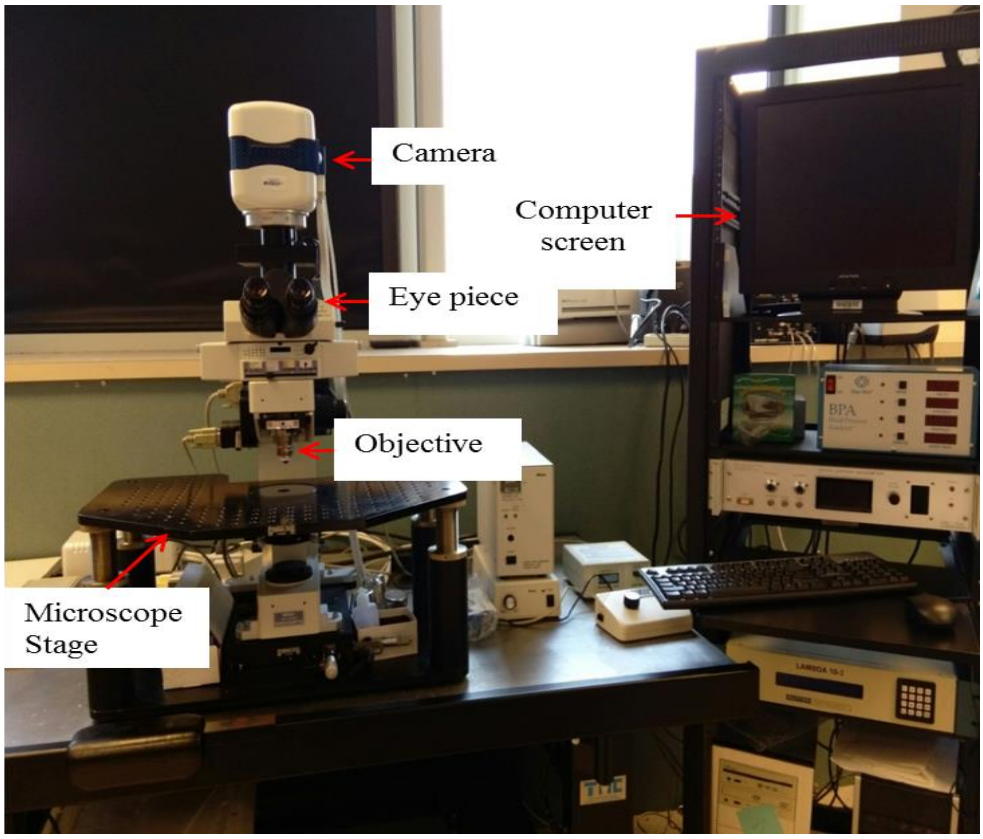

Figure 5: Pictorial representation of the intravital microscopy technique. This technique is employed to study the extent of vascular leakage of fluorescein isothiocyanate (FITC) dextran into the extravascular space. Animals will be placed on a warming pad on the microscope stage and imaged using a 40X water immersion objective over a period of time. Images will be collected using the computer and analyzed using NIS-Elements-Nikon imaging software.

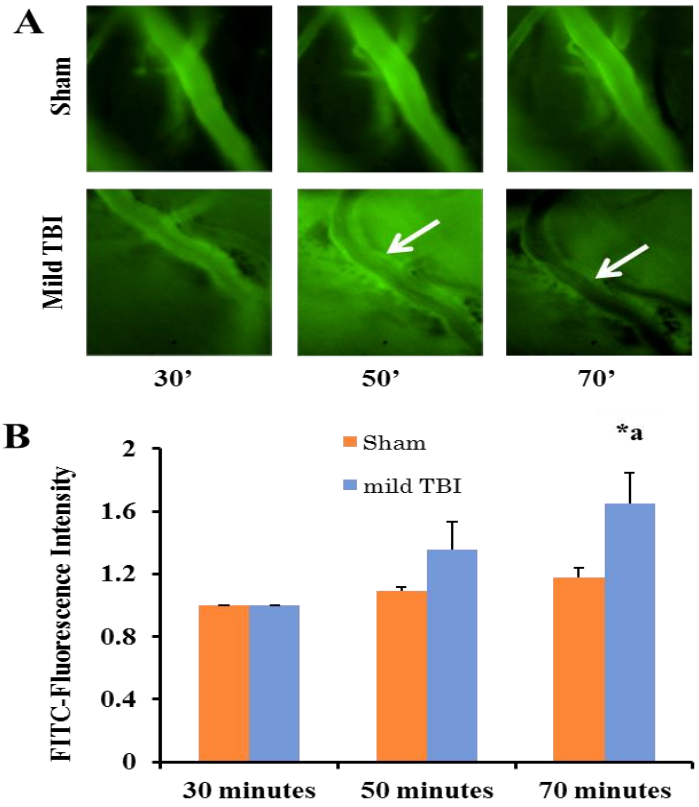

Figure 6: Effect of TBI on FITC-dextran leakage in mouse pial microvasculature. In this procedure, animals were subjected to sham injury (only craniotomy; n=5) or mild TBI injury (n=5). Pictorial representation of mice subjected to sham vs. mild TBI over a period of 30, 50, and 70 minutes (figure A).

Quantitative analysis further confirmed that animals subjected to TBI demonstrated more leakage of FITC-dextran-10 kDa into the extravascular space (figure B). Y-axis represents ratio of FITC-dextran fluorescence intensity outside of the vessel to inside (figure B). Data shown here are represented as mean ± SEM; $p \leq 0.05$. '*a' indicates significant increase compared to the sham group. Statistical significance was determined by two-way ANOVA followed by Tukey post-hoc test.

Evans blue extravasation study

Evans blue is an alkaline dye that binds to albumin in the blood. It is a popular dye used to study vascular permeability in various physiological disorders. In this procedure, the animals are anesthesized with urethane, i.p. injection (2 mL/kg body weight). Head is shaven and lubricating eye ointment is appplied to the eyes. Animals are then injected with Evans blue (2% wt/vol in saline, 4mL/Kg body weight) via the tail vein and allowed to circulate for 30 minutes, following which the animals were subjected to either sham (only craniotomy) or TBI (craniotomy followed by CCI-TBI injury). Settings for mild TBI injury included: 1 millimeter depth of injury, 5 meters/second velocity and 300 milliseconds contact time, while that for moderate TBI included: 2 millimeters depth of injury, 5 meters/second velocity and 300 milliseconds contact time. These settings were chosen for our preliminary studies in order to confirm that TBI induces BBB hyperpermeability *in vivo*. However, based on a thorough literature review, different settings were used for further chapters and the corresponding results are described in the various chapters. Drug treatments to be studied, can be administered along with Evans blue as pretreatment prior to sham or TBI. Pictorial representation of animals prior to and following Evans blue injection are shown in the Figure 7A and B. Figure 7C presents the pictures of Evans blue-injected mice following sham injury and TBI injury .

One hour post-TBI, mice were transcardially perfused with ice-cold saline for atleast 20 minutes and brains were extracted. Ipsilateral brain cortices were carefully isolated and homogenized in 1 mL of 50% (wt/vol) trichloroacetic acid (TCA) in saline.

The resulting samples were then centrifuged at 6000*g* for 20 minutes at 4 °C. Supernatants extracted were then diluted in 3 parts of 95% ethanol and measured fluorometrically at 620/680nm (Excitation/Emission). Evans blue concentrations in the samples were then evaluated using external standards of Evans blue ranging from 0-5000 ng/mL, prepared in the same solvent (1:3; TCA: 95% ethanol). Evans blue amount in the samples was expressed as ng/brain cortex ± SEM. Statistical differences among groups were determined by one-way analysis of variance (ANOVA) followed by Bonferroni post hoc test to determine significant differences between specific groups. A value of $p<0.05$ was considered statistically significant. Quantitative analysis of TBI-induced Evans blue leakage in mice is shown in Figure 8.

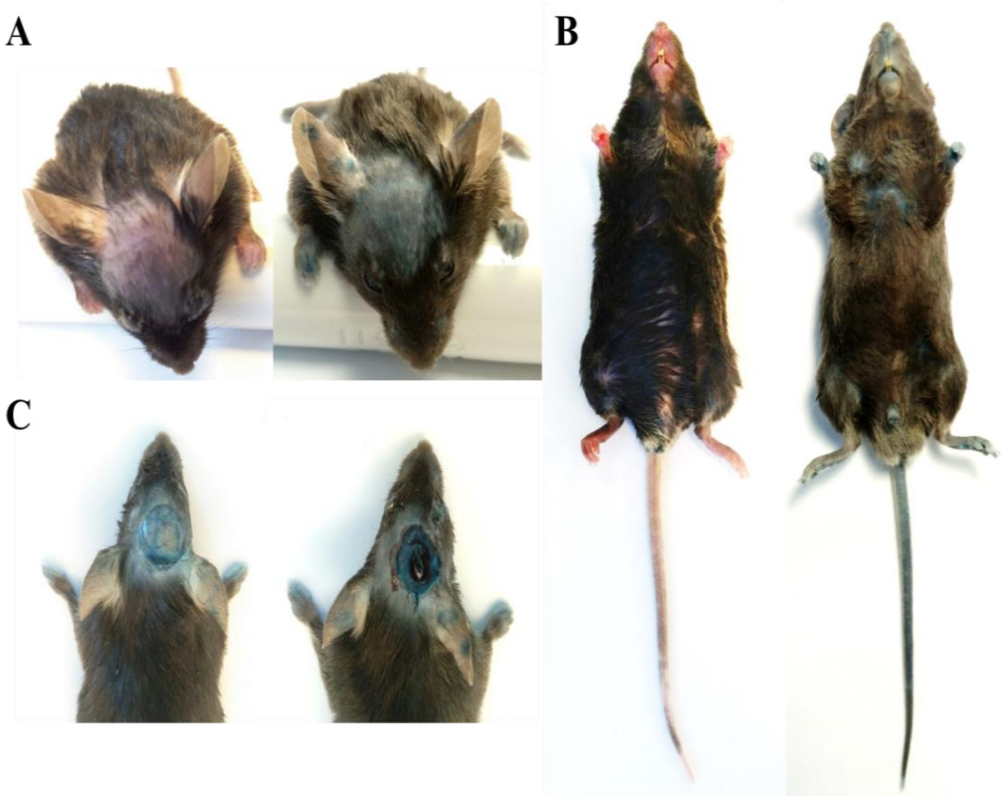

Figure 7: Pictorial representation of Evans blue-injected mice following sham injury and TBI. Figure A shows the dorsal side of the animal head prior to (left) and after Evans blue injection. Figure B shows the ventral side of the animal prior to (left) and after Evans blue injection (right). Evans blue binds to the albumin in the blood. Tail vain injection of Evans blue turns the blood blue by dyeing the entire systemic circulation. C shows animal with craniotomy surgery only i.e. sham (left) and after TBI (right).

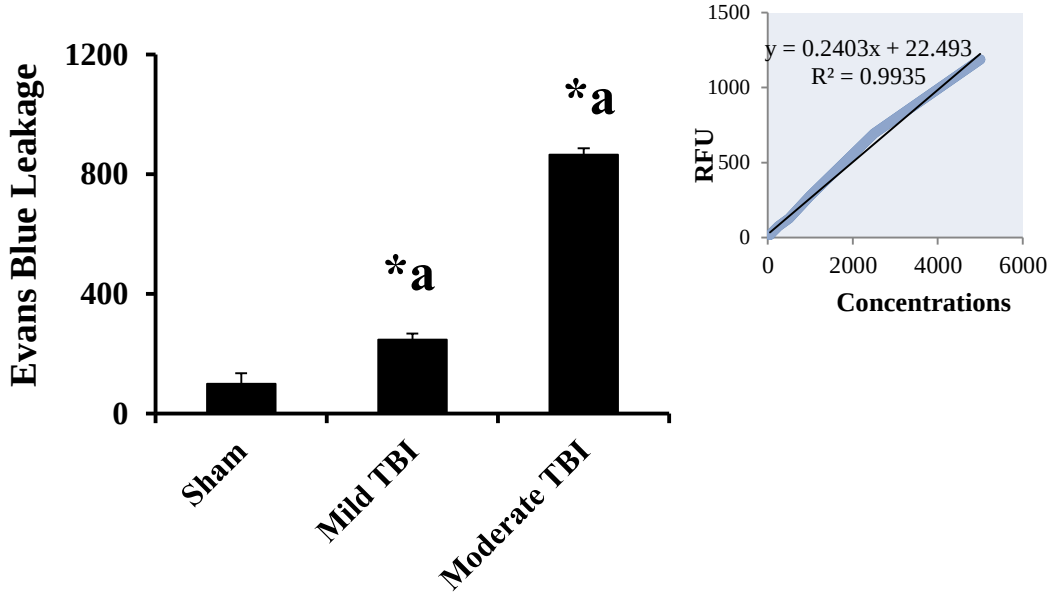

Figure 8: Effect of TBI on Evans blue leakage in mouse brain cortex. Animals were grouped into sham injury (n=4), mild TBI injury (n=5) and moderate TBI injury (n=5). Data are represented as ng/brain cortex ± SEM; $p \leq 0.05$. '*a' indicates significant increase compared to the sham group.

The graph on the right hand corner shows a standard curve for Evans blue concentrations ranging from 0 to 5000 ng/mL prepared in TCA: ethanol (1:3); plotted on X-axis. Y-axis represents relative fluorescence units (RFU), measured at 620/680 nm.

CONCLUSION

Blood-brain barrier (BBB) dysfunction and its contribution towards various diseases have been identified and explained in detail by Obermeier et al, 2013 [53]. Optimal functioning of BBB is essential for neuronal activity and normal brain functioning. A better understanding of the complex mechanisms involved in TBI-induced BBB dysfunction will lead to identification of potential drug targets. As tight junctions govern much of the function of the BBB and thus are paramount in mediating the vascular permeability changes in the BBB seen after TBI, focus on these proteins as therapeutic targets may be of benefit. Understanding the roles of tight junction proteins and the manner in which they are targeted by various proteases after TBI may assist in understanding BBB hyperpermeability, edema and the associated elevation of intracranial pressure (ICP) after TBI and may even provide therapeutic targets to combat this process. Knowledge of the interplay between the various components of the BBB and the molecular pathways that regulate them is critical and a more thorough understanding of the mechanisms that govern these interactions is important. Conditional knockouts of specific components of BBB or various molecular mediators can provide a deeper understanding of the functionality of the molecular players and our lab is currently moving towards that direction.

A multitude of medical and scientific advancements have been made in the field of trauma and brain research since the 1900s. Studies that focus on the basic mechanisms of brain injury and BBB dysfunction are beginning to emerge and may shed light on potential new therapeutic interventions. Although understanding the

pathophysiology of the BBB is intricate and extremely complex, the mechanisms involved in its breakdown in TBI require further study and hold great promise for treatment options for brain injury.

CHAPTER II

MATRIX METALLOPROTEINASE-9-MEDIATED MECHANISMS IN REGULATING BLOOD-BRAIN BARRIER DYSFUNCTION AND HYPERPERMEABILITY

SUMMARY

Microvascular hyperpermeability is the excessive leakage of fluid and proteins from the intravascular space into the interstitium. Hyperpermeability that occurs at the level of the blood-brain barrier (BBB) often leads to vasogenic brain edema following traumatic and ischemic brain injuries. At the cellular level, the tight junction proteins (TJPs) regulate the properties of the BBB. Zonula occludens-1 (ZO-1) is an important TJP that binds to the transmembrane TJPs and actin cytoskeleton intracellularly. The pro-inflammatory cytokine, interleukin-1 beta (IL-1β) activates downstream signaling pathways as well as various proteolytic enzymes. Matrix metalloproteinases (MMPs) play an important role in promoting secondary injuries following trauma/ischemia. Recent studies demonstrate melatonin, a pineal hormone, as a potential inhibitor of MMP-9. We hypothesized that melatonin pretreatment provides protection against IL-1β treatment-induced BBB dysfunction and hyperpermeability *in vitro* and following traumatic brain injury (TBI) *in vivo*.

Rat brain microvascular endothelial cells (RBMECs) were used for *in vitro* studies. RBMEC monolayers were grown on Transwell inserts and the cells were pretreated with GM6001 (broad-spectrum MMP inhibitor), MMP-9 inhibitor-1 (MMP-9

specific inhibitor), melatonin or transfected with MMP-9 siRNA followed by treatment with IL-1β. Tight junction integrity and cytoskeletal assembly were assessed by ZO-1 immunofluorescence and rhodamine phalloidin labeling for *f*-actin respectively. Protein and mRNA expression of ZO-1 was evaluated by Western blotting and RT-PCR techniques respectively. Cell viability and MMP-9 activity were assessed fluorometrically. Effect of melatonin pretreatment on TBI-induced BBB hyperpermeability in a mouse model was evaluated fluorometrically by Evans blue extravasation assay.

The results from our study demonstrate that acute IL-1β treatment-induced BBB hyperpermeability was significantly attenuated on pretreatment with GM6001, MMP-9 inhibitor-1, melatonin or MMP-9 siRNA transfection *in vitro*. Melatonin and MMP-9 inhibitor-1 pretreatment attenuated IL-1β-induced MMP-9 activity, loss of ZO-1 junctional integrity and *f*-actin stress fiber formation. IL-1β treatment affected neither ZO-1 protein or mRNA expression nor cell viability. Melatonin pretreatment attenuated TBI-induced BBB hyperpermeability *in vivo*.

These results demonstrate that MMP-9-mediated mechanisms play an important role in regulating IL-1β-induced BBB dysfunction and hyperpermeability. Melatonin treatment can be a potential strategy in attenuating TBI-induced BBB hyperpermeability in a mouse model of TBI.

INTRODUCTION

Microvascular hyperpermeability is the abnormal extravasation of plasma proteins and fluid into extravascular space leading to vasogenic edema. Hyperpermeability in the brain occurs at the level of blood-brain barrier (BBB). The BBB is a semipermeable membrane that separates the systemic circulation from the brain parenchyma. Optimal functioning of the BBB is crucial for maintaining the homeostasis of the brain. The key structural and functional elements in maintaining the integrity of the BBB are the tight junctions [63]. Tight junctions primarily include transmembrane (occludin, claudins, junctional adhesion molecules) and membrane bound tight junctions (zonula occludens [ZO]). Zonula occludens-1 (ZO-1) acts as a scaffolding molecule mediating the link between the transmembrane tight junctions and the actin cytoskeleton [63]. It plays an important role in maintaining the important properties of the BBB including resistance and permeability [63]. Alterations in BBB integrity leading to hyperpermeability and vasogenic edema often occur following inflammation [73; 74].

A variety of pro-inflammatory molecules are activated following various vascular disorders associated with traumatic brain injury (TBI), ischemia, cerebral infections, stroke, brain diseases, etc [75; 76]; leading to various ill-pathologies like microvascular leakage, brain edema leading to swelling, neuronal injury and death [74; 77]. Interleukin-1 beta (IL-1β) plays a central role in mediating the process of neuroinflammation [78]. It is a well-established pro-inflammatory cytokine known to induce BBB hyperpermeability in endothelial cell monolayers [74; 76; 79; 80]. It also

plays an important role in TBI pathophysiology [76]. Interleukin-1β levels and matrix metalloproteinase-9 (MMP-9) activity increase in brain following TBI; also, the role of MMP-9 in BBB tight junction disruption is also well studied [81; 82; 83]. Studies done by Wu et al, 2010 in intracerebral hemorrhagic (ICH) models suggest that IL-1β may be a key mediator molecule in MMP-9 activation and subsequent ZO-1 disruption [84]. So far, there are no evidences that confirm the direct contribution of MMP-9 in mediating IL-1β-induced BBB hyperpermeability, although other pro-inflammatory molecules like tumor necrosis factor-alpha (TNF-α) are shown to induce MMP-9 activity and endothelial hyperpermeability [85]. Hence, we hypothesized that IL-1β treatment-induced BBB hyperpermeability may occur via MMP-9-mediated mechanisms.

Our studies further explored the role of melatonin as a potential MMP-9 inhibitor apart from being a pineal hormone with anti-inflammatory and anti-oxidant properties. Recent studies by Rudra et al, 2013 indicate that melatonin inhibits MMP-9 by binding to its active catalytic site [86]. Anti-MMP-9 properties of melatonin following burn injury-induced endothelial hyperpermeability are also explored [87]. However, role of melatonin in attenuating IL-1β-induced BBB hyperpermeability is yet unknown. Furthermore, we employed melatonin to study its effect in mouse model of TBI. This study aims to address the following questions:

- What is the effect of acute IL-1β treatment on BBB endothelial cell permeability *in vitro*?

- What is the effect of melatonin and MMP-9 specific inhibitors on IL-1β treatment-induced BBB hyperpermeability, loss of tight junctional integrity, changes in actin cytoskeletal assembly and MMP-9 activity?
- What is the effect of IL-1β treatment on total number of viable cells and ZO-1 protein and mRNA expression *in vitro*?
- Can melatonin be used as a protective therapeutic agent against TBI-induced BBB hyperpermeability *in vivo*?

MATERIALS AND METHODS

Materials

Rat Brain Microvascular Endothelial Cells (RBMECs) and RBMEC Medium were obtained from Cell Applications Inc. (San Diego, CA). SensoLyte® 520 MMP-9 fluorometric Assay Kit was purchased from Anaspec Inc. (San Jose, CA). Transwell® 24-well plates were obtained from Corning Costar (New York, USA). Nunc Lab Tek II-CC, 8-well glass chamber slides, Interleukin-1β human, melatonin, fibronectin from bovine plasma, β-actin, albumin from bovine serum, Evans blue, trichloroacetic acid and fluorescein isothiocyanate-dextran-10 kDa were purchased from Sigma Aldrich (St. Louis, MO). Rabbit anti ZO-1 (Cat # 617300), mouse anti ZO-1 (Cat # 339100), 0.25% Trypsin (1X), Opti-MEM (1X)/reduced serum medium, Dulbecco's modified Eagle's medium (DMEM; with high glucose, HEPES, no phenol red (1X)), NuPAGE Novex® 10% Bis-Tris protein gels, NuPAGE® MOPS SDS Running Buffer, NuPAGE® Transfer Buffer, HyClone Dulbecco's phosphate buffered saline (PBS, without calcium,

magnesium, or phenol red), TRIzol® Reagent, SuperScript® IV First-Strand Synthesis System, Halt® Protease Inhibitor Cocktail (100X), Pierce™ ECL Western Blotting substrate and rhodamine phalloidin were purchased from Thermo Fisher Scientific (Carlsbad, CA). Goat anti-mouse IgG-HRP and donkey anti-rabbit IgG-FITC secondary antibodies were purchased from Santa Cruz Biotechnology, Inc. (Santa Cruz, CA). EZViable™ Calcein AM Cell Viability fluorometric assay kit was bought from Biovision (Milpitas, CA). We also purchased Vector VECTASHIELD® Mounting Media with DAPI from Vector Laboratories (Burlingame, CA). Pierce™ BCA Protein Assay Kit and RT² qPCR Primer Assay for Mouse GAPDH were purchased from Qiagen (Valencia, CA). GM6001 (also called as Ilomastat or Galardin) and MMP-9 inhibitor 1 were purchased from Calbiochem (Billerica, MA). Cell Lysis Buffer (10X) was bought from Cell Signaling Technology, Inc. (Danvers, MA). Primers were purchased from Thermo Fisher Scientific (Carlsbad, CA). MMP-9 siRNA and control siRNA (ON-TARGETplus siRNA) were purchased from Dharmacon, General Electric (Pittsburgh, PA).

In vitro BBB model

Primary cultures of RBMECs derived from the brain of adult Sprague Dawley rat were purchased from the Cell Applications Inc. (San Diego, CA). RBMECs were initially grown on 0.05% fibronectin-coated cell culture dishes, using the RBMEC medium in a cell culture incubator (95% O_2, 5% CO_2 at 37 °C). Endothelial cells were treated with 0.25% trypsin-EDTA for cell detachment. Detached cells were then grown

on fibronectin-coated Transwell® inserts, chamber slides or 100 mm dishes for experimental purposes. RBMEC passages 8-10 were chosen for all the experiments.

Animals and surgeries

C57BL/6 mice (25-30 g) were purchased from Charles River Laboratories (Wilmington, MA). Animals were maintained at the Texas A&M University Health Science Center College of Medicine and Baylor Scott and White Health animal facility on a 12:12 hour dark/light cycle, with free access to food and water. The room temperature was maintained at 25° ± 2 °C. Surgical and experimental procedures used in this study were conducted after approval by the Institutional Animal Care and Use Committee. The facility is approved by the Association for Assessment and Accreditation of Laboratory Animal Care International in accordance with the National Institutes of Health guidelines.

Craniotomy procedure

The head of the animal was shaven and the surgical site on the surface of the head was cleaned with an alcohol wipe. Lubricating ointment was applied to the eyes. Midline incision on the scalp helps to remove the skin from top of the skull exposing the sagittal suture, bregma and lambda. A circular craniotomy window, 3-4 mm in diameter was made on ipsilateral hemisphere, between lambda and bregma using a microdrill. The resulting bone flap was removed. Sham animals received only craniotomy surgery,

while TBI injury group receives brain injury via controlled cortical impactor following craniotomy procedure.

Controlled cortical impactor

These studies employ Benchmark™ Stereotaxic Impactor from Leica, for inflicting traumatic brain injury in mice. Following craniotomy procedure, the animals were mounted on the stereotaxic frame. An impactor probe of 3 mm diameter was used to impact the exposed part of the brain. The depth of the injury was used to determine the severity of the injury. Settings for mild TBI used in this study are: 2 millimeters depth, 0.5 meters/second velocity and 100 milliseconds contact time as described in Chen et al, 2014 [88].

Treatments

Melatonin at a dose of 10 mg/kg was used for the acute drug administration studies. This dose was chosen based on the studies done in mouse model of TBI [89]. Melatonin was administered via the tail vein along with Evans blue injection and allowed to circulate for 30 minutes prior to TBI.

Monolayer permeability assays

RBMECs were grown on fibronectin-coated Transwell® inserts as monolayers for 72-96 hours and regularly checked for confluency. Monolayers were initially exposed to phenol red free DMEM for 45 minutes to an hour. DMEM treated cells were

then treated with various concentrations of IL-1β (1-100 ng/mL) for 2 hours or IL-1β (10 ng/mL) treatment at various time points (1-4 hours). At the end of the treatment, FITC labeled dextran-10 kDa (5 mg/mL; 30 minutes) was applied to the luminal compartment. One hundred microliters of sample was collected from the abluminal compartment at the end of 30 minutes and measured fluorometrically at 485 nm/520 nm (Excitation/Emission) using Fluoroskan Ascent™ FL Microplate Fluorometer and Luminometer (Vantaa, Finland). These studies provided information on the minimal dose and time exposure of IL-1β to induce BBB endothelial cell hyperpermeability.

Using the above information, a separate set of experiments were conducted to study the effect of GM6001 (10 μM; 1 hour), MMP-9 inhibitor 1 (5 nM; 1 hour) and melatonin (10 μg/mL; 1 hour) pretreatment on IL-1β (10 ng/mL; 2 hours) treatment-induced monolayer hyperpermeability. At the end of the experiment, FITC-dextran-10 kDa was added to the donor chamber and fluorescence intensity measurements were performed as described above.

Melatonin dose and time exposure were chosen from the studies done in our lab in burn trauma models [87]. MMP-9 inhibitor 1 used in these studies is a cell-permeable, potent, selective and reversible MMP-9 inhibitor with IC_{50} at 5nM for MMP-9 inhibition. It inhibits other MMPs at concentrations higher or lower than 5nM, hence 5nM was specifically chosen for these studies. MMP-9 inhibitor 1 concentrations were chosen from the studies done in our lab to study the effect of TNF-α-induced BBB hyperpermeability [85]. The dose and exposure time for GM6001 were obtained from Simaro et al, 2012 [90].

Untreated cells served as control. Each experiment was repeated four times. Fluorescence intensity values were plotted on the Y-axis and represented as % control. Data were expressed as mean ± % SEM and statistical differences among groups were determined by one-way analysis of variance (ANOVA) followed by Bonferroni post hoc test to determine significant differences between specific groups. A value of $p<0.05$ was considered statistically significant.

MMP-9 knockdown studies

RBMECs were grown on fibronectin-coated Transwell® inserts for 24 hours and treated with control siRNA or MMP-9 siRNA at a concentration of 25 nM for 48 hours. Transfection was performed according to manufacturer's instructions. Transfected monolayers were then exposed to IL-1β (10 ng/mL; 2 hours) and permeability was determined based on the leakage of FITC-dextran-10 kDa (5 mg/mL; 30 minutes) leakage from the luminal to the abluminal chamber. One hundred microliters of the sample was obtained from the abluminal chamber and fluorescence intensity was measured at 485/520 nm (Excitation/Emission) using Fluoroskan Ascent™ FL Microplate Fluorometer and Luminometer.

Untreated cells were used as control. Each experiment was repeated four times. Fluorescence intensity was plotted on the Y-axis and represented as % control. Data were expressed as mean ± % SEM and statistical differences among groups were determined by one-way analysis of variance (ANOVA) followed by Bonferroni post hoc

test to determine significant differences between specific groups. A value of $p<0.05$ was considered statistically significant.

Measurement of MMP-9 activity

A SensoLyte® 520 MMP-9 fluorometric Assay Kit was employed to measure the MMP-9 activity in the cells. This kit detects the MMP-9 activity in samples by using a 5- carboxyfluorescein Ser - Leu - Gly - Arg - Lys - Ile - Gln - Ile - Gln - Lys(QXL®520) - NH_2 (5-FAM/QXL™ 520 fluorescence resonance energy transfer (FRET) peptide). In intact FRET peptide, the fluorescence of 5-FAM is quenched by the QXL™ 520. However, on cleavage of the peptide by MMP-9 fluorescence is recovered and measured at 490/520 nm (Excitation/Emission).

In this procedure, RBMECs were grown in petri dishes until confluency is achieved. Cells were then pretreated with MMP-9 inhibitor 1 (5 nM; 1 hour) or melatonin (10 μg/mL; 1 hour) followed by IL-1β (10 ng/mL; 2 hours). At the end of the experiment, cells were washed twice in PBS and exposed to the assay buffer provided in the kit. Cells were then scraped and the cell lysates were collected. Cell lysates were briefly sonicated and centrifuged in order to collect supernatants. Supernatants were used to measure the MMP-9 activity in the cells. Equal amounts of proteins were taken in each well and 4-aminophenylmercuric acetate (APMA) was added to samples and incubated for 2 hours in dark; in order to activate the pro-MMPs. To the activated samples, MMP-9 substrate, 5-FAM/QXL 520 FRET peptide was added and incubated

for another 30 minutes in dark and read fluorometrically at 490/520 nm (Excitation/Emission).

Untreated cells served as control. Each experiment was repeated four times. MMP-9 activity was expressed as relative fluorescence units (RFU) and plotted on the Y-axis. Data were expressed as mean ± SEM and statistical differences among groups were determined by one-way analysis of variance (ANOVA) followed by Bonferroni post hoc test to determine significant differences between specific groups. A value of $p<0.05$ was considered statistically significant.

ZO-1 immunofluorescence and rhodamine phalloidin labeling for *f*-actin

Zonula occludens-1 junctional localization and *f*-actin stress fibers were assessed. RBMECs were grown on chamber slides for overnight. Cells were initially exposed to Opti-MEM/reduced serum medium, followed by pretreatment with melatonin (10 μg/mL; 1 hour) and MMP-9 inhibitor 1 (5 nM; 1 hour) and subsequently IL-1β (10 ng/mL; 2 hours) treatment. Cells were then fixed in 4% paraformaldehyde in PBS for 10-15 minutes and permeabilized in 0.5% Triton-X 100 in PBS for another 10-15 minutes. Cells were blocked using 2% bovine serum albumin (BSA) in PBS for an hour at room temperature. Cells were then incubated overnight in anti-rabbit primary antibodies against ZO-1 (#617300; 1:150) in 2% BSA-PBS, followed by incubation with anti-rabbit IgG-FITC conjugated secondary antibody for an hour at room temperature. Cells were then washed and mounted using VECTASHEILD® Antifade Mounting Media with DAPI for nuclear staining.

Following treatment study, cells were fixed, permeabilized, and blocked in 2% BSA-PBS as described earlier. Cells were then labeled with rhodamine phalloidin (1:50) in 2% BSA-PBS for 20 minutes. Chamber slides were then washed and mounted using VECTASHIELD® Antifade Mounting Media with DAPI for nuclear staining.

Cells were visualized and scanned at a single optical plane with an Olympus Fluoview 300 Confocal Microscope (Center Valley, PA), with a PLA PO 60X water immersion objective. Untreated cells served as control. Each experiment was repeated four times.

Real time-PCR studies

RBMECs were grown on 100 mm cell culture dishes until 80-90% confluency was reached. Cells were then pretreated with melatonin (10 μg/mL; 1 hour) and MMP-9 inhibitor 1 (five nM; 1 hour) followed by IL-1β (10 ng/mL; 2 hours). Following treatments, cells were washed thrice in PBS and total RNA was then extracted using TRIzol® reagent according to the manufacturer's instructions. RNA concentration and quality were determined by employing the ratio of absorbance at 260/280 nm using Biotek Synergy Hybrid Spectrophotometer (Winooski, VT). Reverse transcription was performed using the SuperScript® IV First-Strand Synthesis System. Quantitative real time PCR was performed using the RT² SYBR Green Fluor qPCR Mastermix with the following primer pairs for ZO-1: Forward primer: 5′-CCTCTGATCATTCCACACAGTC-3′, Reverse primer: 5′-TAGACATGCGCTCTTCCTCTCT-3′, MMP-9: Forward primer: 5'-

GGCTAGGCTCAGAGGTAA-3', Reverse primer: 5'-GACGTTGTGTGAGTTCCAG-3' and GAPDH: Forward primer: 5′-AATGTATCCGTTGTGGATCT-3′, Reverse primer: 5′-CAAGAAGGTGGTGAAGCAGG-3′ were used. Real-time PCR detection was carried out using Stratagene Mx3000P qPCR System, Agilent Technologies (La Jolla, CA), using 1 μL of cDNA for 10 minutes at 95°C, followed by 40 cycles of 15 sec at 95°C for denaturation and 1 min at 60°C for annealing. Relative abundances of target genes were calculated by normalizing Ct values to endogenous control glyceraldehyde 3-phosphate dehydrogenase (GAPDH).

Cells were treated with IL-1β, while untreated cells served as control. Each experiment was repeated three times. Relative gene expression of ZO-1 was obtained by normalizing the C_t values to the endogenous control GAPDH for each repeat. Normalized C_t values were expressed as mean ± SEM. Statistical differences among groups were determined by one-way analysis of variance (ANOVA) followed by Bonferroni post hoc test to determine significant differences between specific groups. A value of $p<0.05$ was considered statistically significant.

Western blot analysis

Western blot analysis was performed to investigate the expression of ZO-1 protein in RBMECs. Cells were initially exposed to reduced serum medium followed by IL-1β (10 ng/mL; 2 hours) treatment. At the end of the study, cells were washed twice in ice-cold PBS and incubated in ice-cold cell lysis buffer (1X) along with protease inhibitor cocktail (1X) for 5 minutes in cell culture dishes. Cells were then scraped,

sonicated and centrifuged at 14,000*g* for 10 minutes at 4°C. Supernatant was collected from the extracts and protein concentration was determined using protein assay kit. Equal amounts of total protein (50 μg) were separated by sodium dodecyl sulphate-polyacrylamide gel electrophoresis (SDS-PAGE) on 10% Bis-Tris precast gels at constant voltage (145 V) for 180 minutes. Proteins were then transferred onto the nitrocellulose membrane at constant voltage (30 V) for overnight and the membranes were blocked using 5% nonfat dry milk in Tris-Buffered Saline (TBS) with 0.05% Tween-20 for 3 hours and subsequently incubated with primary mouse monoclonal anti ZO-1 antibody (1:250 dilution). Membranes were washed thrice in TBS-T and incubated with the goat anti-mouse IgG-HRP conjugated secondary antibody. After washing, the immunoblots were visualized by ECL Western Blotting Substrate. Untreated cells served as control. Equal amount of protein sample loading was verified by assessing β-actin protein expression. Each experiment was repeated four times.

Cell viability studies

An EZViable™ Calcein AM Cell Viability Assay Kit (Fluorometric) was used for quantify the number of viable cells. Calcein AM is a non-fluorescent, hydrophobic compound that easily penetrates intact and live cells. Hydrolysis of the calcein AM by intracellular esterase produces a hydrophilic, strongly fluorescent compound that is retained in the cell cytoplasm, which can be measured at 485/530 nm (Excitation/Emission).

Equal numbers of cells were grown on sterile black 96 well trays. On reaching confluency, growth media is discarded and cells were washed in PBS and pre-exposed to phenol red-free medium for 1 hour. Cells were divided into control (untreated) and IL-1β (10 ng/mL) treatment groups. Following treatments, cells were then exposed to calcein buffer solution (calcein AM: calcein dilution buffer in 1:500 dilution) and incubated at 37°C for 30 minutes and a fluorometric reading was obtained.

Fluorescence intensity was plotted on the Y-axis and represented as % control. Data were expressed as mean ± % SEM and statistical differences among groups were determined by one-way analysis of variance (ANOVA) followed by Bonferroni post hoc test to determine significant differences between specific groups. A value of $p<0.05$ was considered statistically significant.

Evans blue leakage studies

Evans blue dye binds to the albumin in the blood enabling us to detect the vascular leakage into the extravascular tissue following traumatic brain injury. C57BL/6 mice (25-30 g) were anesthetized with urethane, i.p. injection (2 mL/kg body weight) followed by Evans blue dye, i.v. injection (2% wt/vol in saline; 4 mL/kg body weight). Evans blue was allowed to circulate in the animal for 30 minutes prior to performing sham surgery (only craniotomy) or TBI using controlled cortical impactor. Drugs were given to the animal along with Evans blue injection and allowed to circulate for 30 minutes as well. 75% ethanol was used a vehicle control. Settings for mild TBI are described in the CCI procedure.

Animals were grouped into Sham (only craniotomy; n=6), Vehicle + Sham (75% ethanol injection followed by craniotomy; n=6), Vehicle + TBI group (75% ethanol followed by mild TBI; n=5), and melatonin +TBI group (melatonin [10 μg/gram body weight of the animal] injection followed by mild TBI; n=6).

One-hour post-TBI, animals were transcardially perfused with sterile saline containing heparin (1000 U/mL) for at least 20 minutes. Brains were extracted and brain cortex was carefully separated and weighed. Brain cortices were then homogenized in 1 mL of 50% (wt/vol) trichloroacetic acid (TCA) in saline. Homogenate was then centrifuged at 6,000*g* for 20 minutes at 4°C. Supernatants were extracted and further diluted in 3 parts of ethanol (1:3; 50% TCA: 95% ethanol). Samples were then quantitated fluorometrically at 620/ 680 nm (Excitation/Emission) using Biotek Synergy Hybrid H1 spectrophotometer (Winooski, VT). Evans blue concentration in the samples were evaluated using external standards for Evans blue ranging from 50-1000 ng/mL, prepared in same solvent (1:3; TCA: 95% ethanol). Evans blue amount in the samples was expressed as ng/brain cortex ± SEM. Statistical differences among groups were determined by one-way analysis of variance (ANOVA) followed by Bonferroni post hoc test to determine significant differences between specific groups. A value of $p<0.05$ was considered statistically significant.

RESULTS

IL-1β treatment induces BBB endothelial cell monolayer hyperpermeability

Endothelial cell monolayers were pretreated with various concentrations of IL-1β ranging from 1-100 ng/mL for a 2-hour period. Result from these data confirmed that IL-1β treatment at 10 ng/mL for 2 hours was found to be the minimal dose to induce monolayer hyperpermeability (Figure 9 A; $p < 0.05$). In a separate set of experiments, RBMECs were then treated with IL-1β at 10ng/mL for various time periods ranging from 1 to 4 hours. Result from this study further confirmed that IL-1β treatment (10 ng/mL; 2 hours) was the minimal dose to induce RBMEC monolayer hyperpermeability (Figure 9 B; $p < 0.05$). Hence, IL-1β treatment at 10 ng/mL dose for a 2-hour period was used to induce monolayer hyperpermeability in the following experiments.

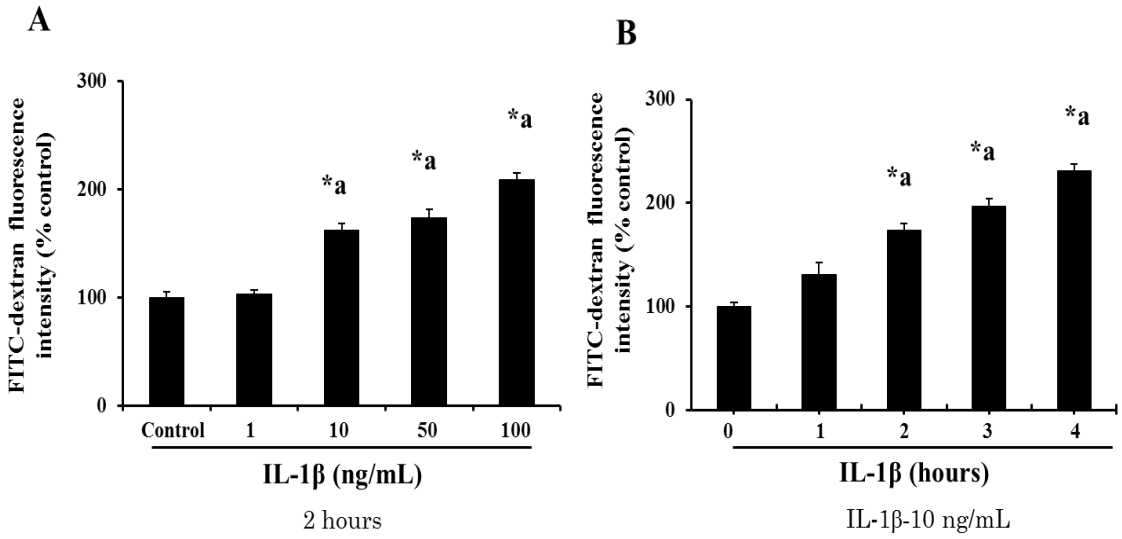

Figure 9: IL-1β treatment induces dose and time dependent increase in monolayer hyperpermeability. In figure A, IL-1β treatment at doses 10, 50 and 100 ng/mL for 2 hours are shown to significantly increase BBB permeability compared to the control group (n=4; $p<0.05$). Figure B indicates significant increase in IL-1β induced BBB permeability at 2, 3 and 4 hours compared to control (n=4; $p<0.05$). Monolayer permeability is expressed as a percentage control of FITC-dextran-10 kDa fluorescent intensity, plotted on the Y-axis. Data are expressed as mean ± % SEM. '*a' indicates significant increase compared to the control group.

MMP-9 specific inhibition attenuates IL-1β-induced BBB endothelial cell hyperpermeability

Initial preliminary studies to confirm the involvement of MMPs in mediating IL-1β-induced monolayer hyperpermeability; GM6001 (broad-spectrum MMP inhibitor) was used. Endothelial cell monolayers were pretreated with GM6001 (Figure 10 A; 10 μM; 1 hour) followed by IL-1β (10 ng /mL; 2 hours).

To study the effect of MMP-9 specific inhibition, MMP-9 inhibitor 1 and melatonin were employed. IL-1β (10 ng/mL; 2 hours) treatment-induced monolayer hyperpermeability was significantly attenuated on pretreatment with MMP-9 inhibitor 1 (Figure 10 B; 5 nM; 1 hour**)** or melatonin (Figure 10 C; 10 μg/mL; 1 hour). Permeability was assessed by monolayer permeability assays as described earlier.

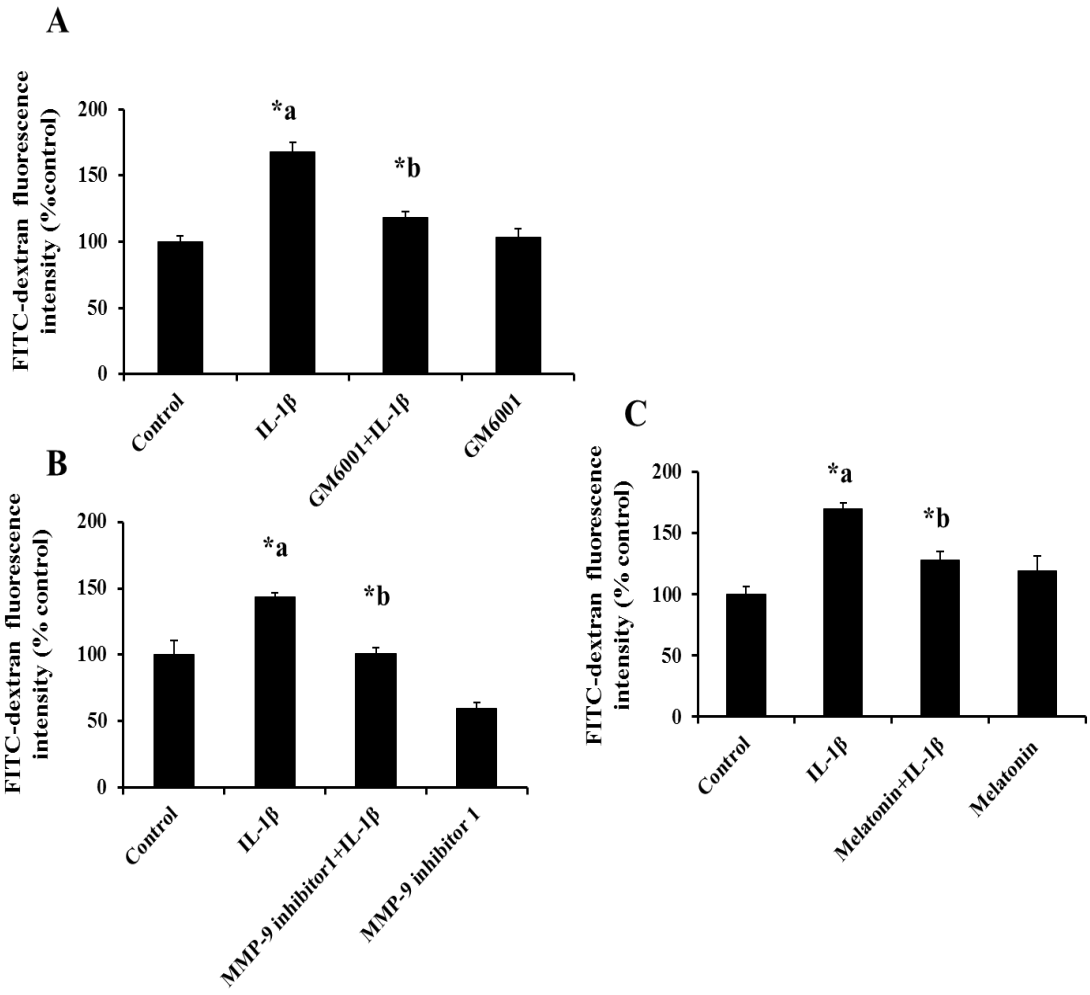

Figure 10: GM6001, MMP-9 inhibitor 1 and melatonin pretreatment attenuates IL-1β treatment-induced monolayer hyperpermeability. Figure A indicates the effect of GM6001 (broad-spectrum MMP inhibitor; n=4); while figure B and C employ MMP-9 specific inhibitors: MMP-9 inhibitor 1 (n=4) and melatonin (n=6) pretreatment on IL-1β-induced monolayer hyperpermeability. Monolayer permeability is expressed as a percentage control of FITC-dextran-10 kDa fluorescence intensity, plotted on Y-axis. Data are expressed as mean ± % SEM. '*a' indicates significant increase compared to control group; '*b' indicates significant decrease compared to the IL-1β treated group. $p<0.05$ was considered statistically significant.

MMP-9 knockdown attenuates IL-1β-induced endothelial cell hyperpermeability

Significant contribution of MMP-9 in attenuating IL-1β-induced endothelial cell hyperpermeability is further supported by siRNA transfection studies. IL-1β (10 ng/mL; 2 hours) treatment to MMP-9 knockdown (25 nM; 48 hours) cells significantly reduced IL-1β-induced monolayer hyperpermeability (Figure 11). siRNA treated groups were compared to the control siRNA group, while the IL-1β alone treated group was compared to the control group.

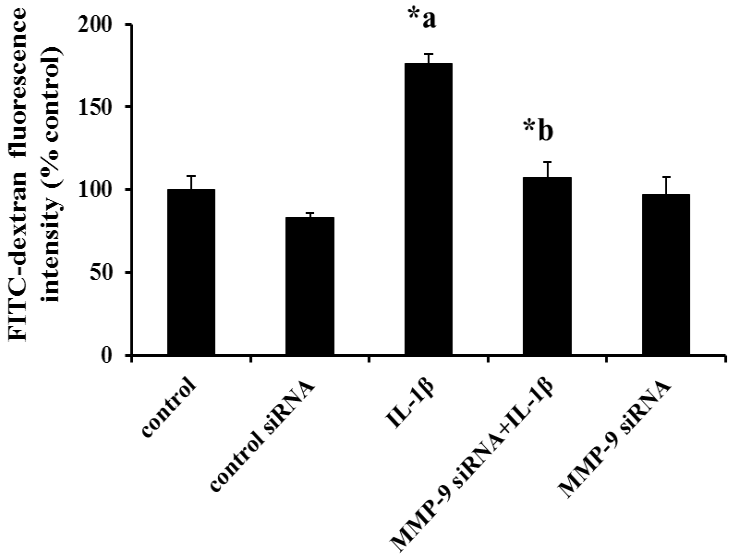

Figure 11: Knockdown of MMP-9 by siRNA attenuates IL-1β treatment-induced monolayer hyperpermeability. Monolayer permeability is expressed as percentage flux of FITC-dextran-10 kDa fluorescence intensity, plotted on Y-axis. Data are expressed as mean ± % SEM. '*a' indicates significant increase compared to the control group; '*b' indicates significant decrease compared to the IL-1β treatment group. siRNA transfected groups were compared to control siRNA transfected group (n=4; $p<0.05$).

IL-1β treatment-induces MMP-9 activity

IL-1β treatment significantly increased MMP-9 activity in RBMECs, while pretreatment with MMP-9 inhibitor 1 (5 nM; 1 hour) or melatonin (10 μg/mL; 1 hour) significantly attenuated IL-1β (10 ng/mL; 2 hours) treatment-induced MMP-9 activity (Figure 12 A and B). MMP-9 activity measurements were performed as described in the methods section. MMP-9 inhibitor 1 was used as a pharmacological inhibitor of MMP-9, however, anti-MMP-9 properties of melatonin are still not as well-established. Our studies support the role of melatonin as a potential MMP-9 inhibitor.

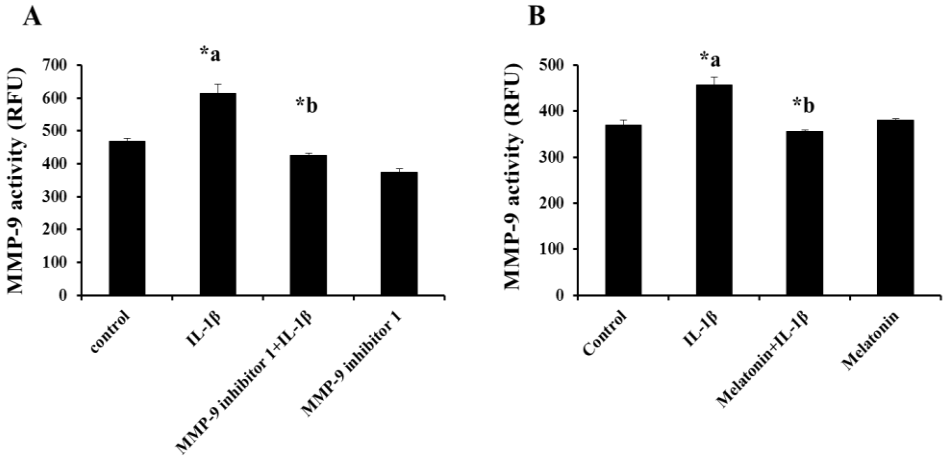

Figure 12: MMP-9 inhibitor 1 and melatonin pretreatment attenuates IL-1β treatment-induced MMP-9 activity. MMP-9 inhibitor 1 (n=4) and melatonin (n=5) pretreatment attenuated IL-1β-induced MMP-9 activity in rat brain endothelial cells. MMP-9 activity is expressed as relative fluorescence units (RFU), plotted on Y-axis. Data are expressed as mean ± SEM. '*a' indicates significant increase compared to the control group; '*b' indicates significant decrease compared to the IL-1β treatment group. $p<0.05$ was considered statistically significant.

MMP-9 inhibition provides protection against IL-1β treatment-induced loss of tight junction integrity and *f*-actin stress fiber formation

Cells were processed for immunofluorescence localization of tight junction protein, ZO-1. IL-1β (10 ng/mL; 2 hours) treatment-induced ZO-1 junctional discontinuity (white arrows; Panel 13 A and B) compared to the control cells. Pretreatment with MMP-9 inhibitor 1 (5 nM; 1 hour) and melatonin (10 μg/mL; 1 hour) decreased IL-1β treatment-induced ZO-1 junction integrity. Untreated cells served as control. These studies support that IL-1β treatment-induced monolayer hyperpermeability occurs via ZO-1 junctional disruption and possibly by ZO-1 redistribution.

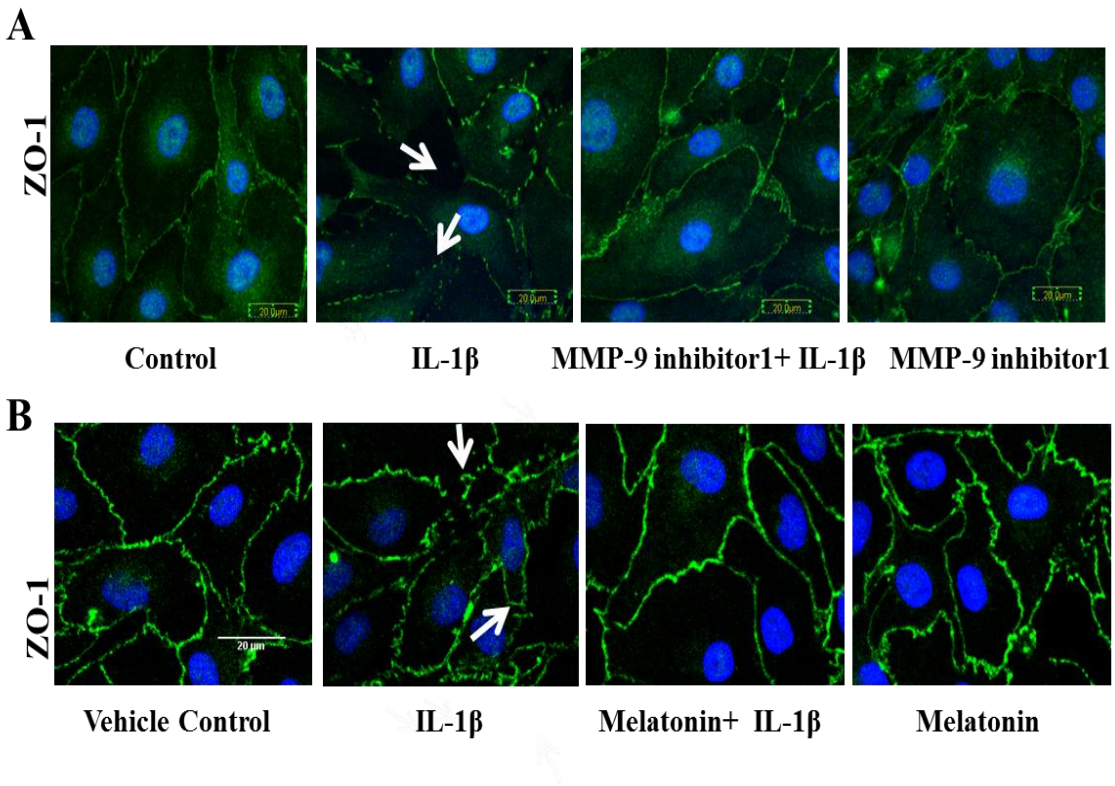

Figure 13: MMP-9 inhibitor 1 and melatonin pretreatment protects against IL-1β treatment-induced loss of ZO-1 junctional integrity. IL-1β treatment-induced ZO-1 junctional disruption (white arrows) was decreased on pretreatment with MMP-9 inhibitor 1 (n=4) and melatonin (n=4).

Melatonin and MMP-9 inhibitor provides protection against IL-1β induced *f*-actin stress fiber formation

For assessing the cytoskeletal assembly, rhodamine phalloidin labeling technique was performed. Untreated cells served as control. IL-1β treatment-induced *f*-actin stress fiber formation (white arrows; Figure 14 A and B) was reduced on pretreatment with MMP-9 inhibitor 1 and melatonin.

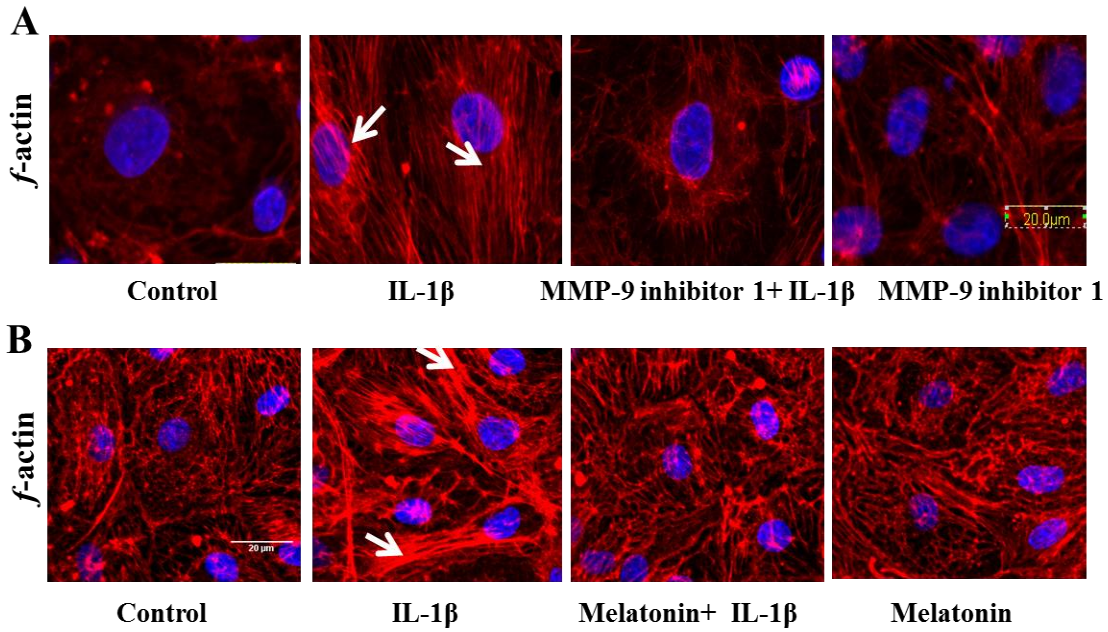

Figure 14: MMP-9 inhibitor 1 and melatonin pretreatment reduces IL-1β treatment-induced *f*-actin stress fiber formation. IL-1β treatment-induced *f*-actin stress fiber formation (white arrows) was decreased by pretreatment with MMP-9 inhibitor 1 (n=4) and melatonin (n=4).

IL-1β treatment neither induces ZO-1 mRNA expression nor alters ZO-1 protein expression

IL-1β treatment (10 ng/mL; 2 hours) did not alter ZO-1 or MMP-9 mRNA expression by RT-PCR studies (figure 15 A and B). IL-1β treatment (10 ng/mL; 2 hours) did not the alter ZO-1 protein expression (figure 15 C).

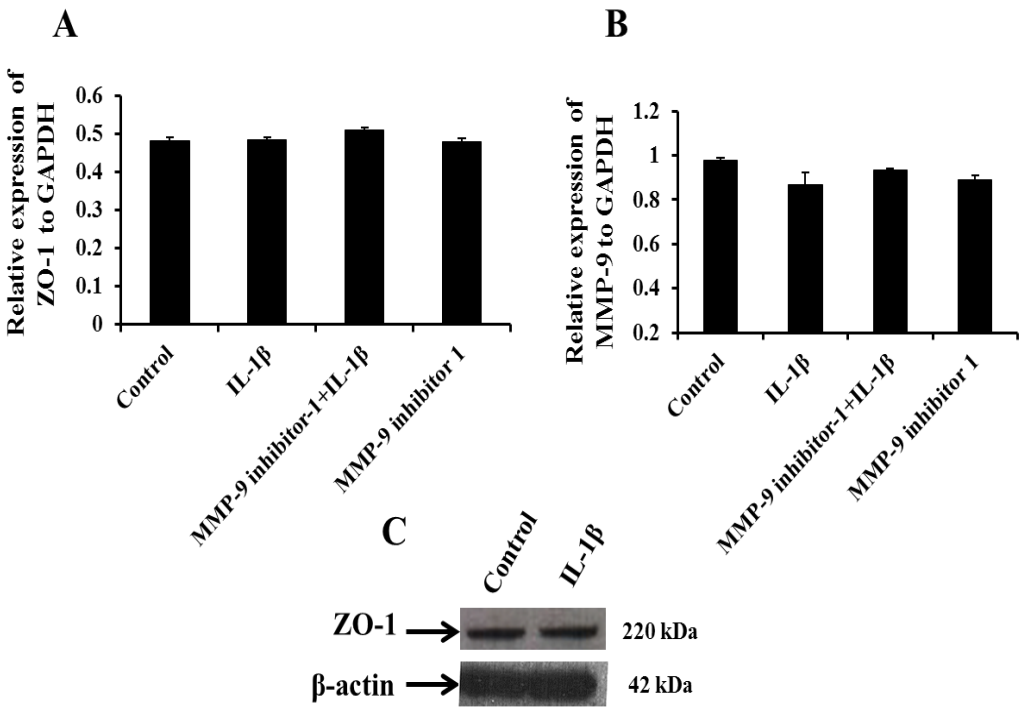

Figure 15: IL-1β treatment does not induce ZO-1 mRNA or protein expression. IL-1β treatment neither induces ZO-1/MMP-9 mRNA expression (n=3) nor alter ZO-1 protein expression (n=4). RT-PCR data plotted on the Y-axis are expressed as relative expression of ZO-1 normalized to GAPDH. Western blot studies had 4 replicates. Data are represented as mean ± SEM.

IL-1β treatment does not induce cell death in endothelial cells

IL-1β (10 ng/mL; 2 hours) treatment did not significantly decrease the number of viable cells compared to the control group (Figure 16). Hydrogen peroxide (100 mM; 2 hours) was used as a positive control.

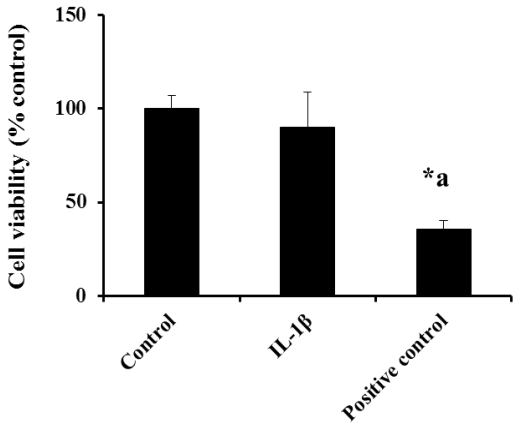

Figure 16: IL-1β treatment does not induce cell death. IL-1β treatment had no effect on cell viability (n=5). Hydrogen peroxide (used as a positive control) treatment decreases cell viability significantly ($p<0.05$). Data are expressed as mean ± % SEM. '*a' indicates significant decrease compared to the control group.

Melatonin pretreatment attenuates TBI-induced BBB hyperpermeability

Mice subjected to TBI demonstrated significant increase in Evans blue leakage compared to the sham animals. Evans blue extravasation was performed using ipsilateral brain cortices. Pretreatment with melatonin attenuated mild TBI-induced Evans blue leakage into the brain tissue (Figure 17 A & B). Evans blue leakage was assessed fluorometrically at 620/680 nm (Excitation/Emission). This study suggests that melatonin can be used as a potential therapeutic agent in attenuating BBB hyperpermeability that occurs following TBI.

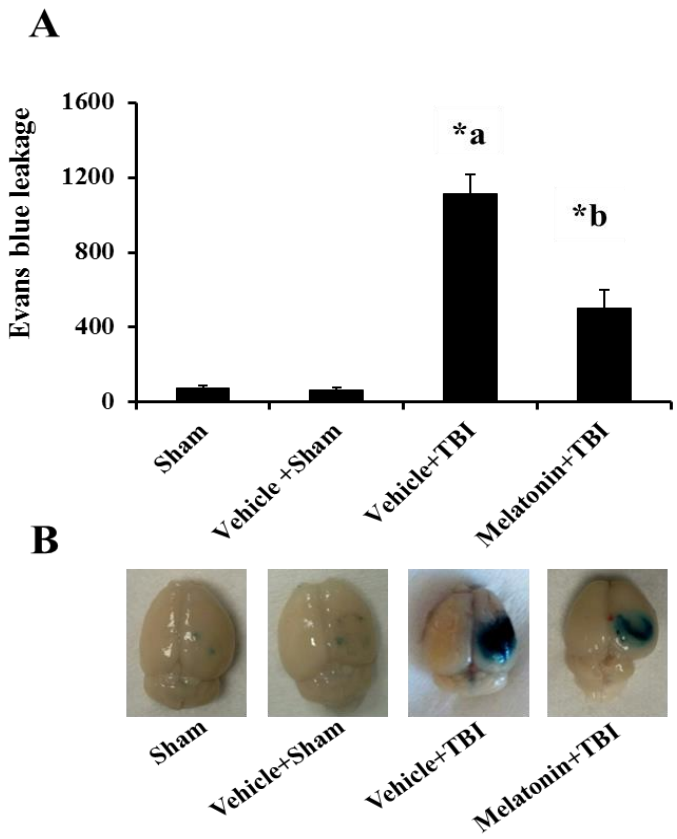

Figure 17: Melatonin pretreatment attenuates TBI-induced BBB hyperpermeability studied by Evans blue dye extravasation method. Pictorial representation of the brain tissue from various groups is shown in figure B. Sham injury group was used as the baseline for all comparisons. Melatonin (10 μg /gram body weight of the animal) pretreatment significantly attenuated TBI-induced Evans blue leakage into the extravascular tissue space ($p<0.05$). Animals were divided into sham (n=6), vehicle+sham (n=6), vehicle+TBI (n=5) and melatonin+TBI (n=6). Data are expressed as ng/brain cortex ± SEM. '*a' indicates significant increase compared to the sham injury/vehicle + sham injury group, '*b' indicates significant decrease compared to the vehicle + TBI group.

DISCUSSION

Matrix metalloproteinases (MMPs) are zinc and calcium proteases that play several roles in vascular physiology and pathophysiology [87; 91; 92]. Matrix metalloproteinase-9 levels are found to increase significantly in the cerebrospinal fluid (CSF) samples of the traumatic brain injury patients [82]. Identification of MMP-9 in the CSF may indicate their role in BBB disruption, which is supported by its ability to degrade various tight junction proteins such as claudin-5, occludin, and zonula occludens (ZO-1) in cultured brain endothelial cells [83]. Although studies done in intracerebral hemorrhagic (ICH) models suggest that IL-1β may induce MMP-9 activation and subsequent ZO-1 disruption [84], no elaborate studies have been done to imply its significance in regulating BBB dysfunction and hyperpermeability. Our studies further employ various MMP inhibitors like GM6001, MMP-9 inhibitor 1 and melatonin, in order to study the effect of MMP-9 inhibition on IL-1β-induced BBB dysfunction and hyperpermeability.

Interleukin-1β upregulation is also observed following experimental brain injuries [84; 93]. Our studies support the contribution of IL-1β in inducing BBB dysfunction and hyperpermeability as demonstrated in our permeability studies, ZO-1 junctional staining, and *f*-actin stress fiber formation. Although, IL-1β treatment at 10 ng/mL for 2 hours induced ZO-1 junctional disruption and BBB hyperpermeability we did not see changes in the total ZO-1 protein expression. These studies indicate a possibility that IL-1β treatment-induced alterations in the BBB may occur via intermediate signaling pathways that are activated by mitogen activated protein kinases

like c-Jun N-terminal kinases (JNK) and p38 [74; 94]. In addition, IL-1β treatment-induced loss of junctional integrity and *f*-actin stress fiber formation with no alterations in ZO-1 mRNA or protein expression indicate a possibility for ZO-1 protein relocalization.

IL-1β treatment induces MMP-9 activity in brain endothelial cells *in vitro* and one mechanism by which MMP-9 inhibitor 1 and melatonin pretreatment attenuates IL-1β-induced MMP-9 activity may occur by direct binding of MMP-9 inhibitor 1 and melatonin to MMP-9. However, these studies need to be explored further in order to understand how MMP-9 inhibitors inhibit IL-1β-induced BBB hyperpermeability. As MMP-9 is indicated to activate protein kinase C via extracellular signal-regulated kinases (ERK) in TBI [95], this can be a potential mechanism to explore further. Our studies employed pharmacological and endogenous MMP-9 inhibitors i.e. MMP-9 inhibitor 1 and melatonin in order to test their effect on IL-1β treatment-induced BBB dysfunction and hyperpermeability. Use of melatonin is advantageous for our studies as it can cross the BBB due to its lipophilic nature and can act as a neuroprotectant [96]; apart from the fact that it is an inexpensive drug that is available over-the-counter with no known adverse effects.

Although there is evidence that support the role of melatonin in attenuating TBI induced elevated ICP (1 hour post-TBI), BBB hyperpermeability and edema (72 hours post-TBI) [97]. Our studies further support and provide the mechanistic details for the observation that melatonin attenuates TBI-induced BBB hyperpermeability. Our studies emphasize on the significance of melatonin as a potential therapeutic agent for

attenuating TBI-induced BBB hyperpermeability, however, we do not believe its contribution is only owing to its MMP-9 inhibitory properties and these studies need further investigation. Future studies should aim to address the effect of melatonin on 1) tissue inhibitors of MMPs (TIMPs), 2) transcription factors responsible for MMP-9 expression such as nuclear factor kappa-light-chain-enhancer of activated B cells (NF-κB) and activator protein (AP-1), as suggested by Grossetete et al, 2009 [82], 3) on various ERK MAPK and 4) phosphorylation status of the tight junctions.

In conclusion, our studies indicate that melatonin has protective effects against IL-1β-induced BBB dysfunction and hyperpermeability via MMP-9 mediated mechanisms *in vitro*. IL-1β-induced acute barrier dysfunctions are not due to alterations in the endothelial cell viability or a decrease in the content or the expression of the key tight junction associated protein ZO-1. Protective effects of melatonin *in vitro,* parallels with its protective effects against TBI *in vivo*.

CHAPTER III

CALPAIN-MEDIATED MECHANISMS IN REGULATING BLOOD-BRAIN BARRIER DYSFUNCTION AND HYPERPERMEABILITY

SUMMARY

Microvascular hyperpermeability that occurs as a consequence of mechanical insult/pathological insult in brain leads to tissue vasogenic edema. At the cellular level, hyperpermeability is regulated by the tight junction proteins (TJPs); that comprise the blood-brain barrier (BBB). TJPs are intracellularly linked to the actin cytoskeleton via zonula occludens-1 (ZO-1). Calpains are shown to be involved in tight junction damage. However, their contribution in regulating BBB dysfunction and hyperpermeability following traumatic insults has not been explored. We hypothesize that calpain-mediated mechanisms play an important role in regulating IL-1β-induced BBB dysfunction and hyperpermeability.

Rat brain microvascular endothelial cell (RBMEC) monolayers were employed to study the effect of IL-1β treatment alone or following calpain inhibition via calpain inhibitor III, calpastatin, calpain-1 knockdown on monolayer hyperpermeability. Calpain activity following IL-1β treatment alone or following calpain inhibition by calpain inhibitor III was measured fluorometrically. Calcium mobilization and cell viability were measured following IL-1β exposure. Changes in cytoskeletal assembly and ZO-1 junctional integrity were assessed using immunofluorescence and rhodamine phalloidin labeling techniques respectively, following IL-1β treatment alone or

following calpain inhibitor III pretreatment. The effect of calpain inhibitor III pretreatment on Evans blue leakage following traumatic brain injury (TBI) was also assessed to study its potential effect in restoring BBB integrity.

IL-1β-induced monolayer hyperpermeability was significantly attenuated upon calpain inhibition by calpain inhibitor III, calpastatin and calpain-1 siRNA ($p<0.05$). IL-1β-induced calpain activity decreased significantly upon pretreatment with calpain inhibitor III and calpastatin ($p<0.05$). IL-1β treatment-induced TJ disruption and actin stress fiber formation were attenuated upon calpain inhibitor III pretreatment ($p<0.05$). Calpain inhibitor III pretreatment significantly attenuated TBI-induced Evans blue leakage in mice brain ($p<0.05$).

These findings suggest that calpain-mediated mechanisms play an important role in promoting IL-1β-induced BBB dysfunction and hyperpermeability and its inhibition provided protection via the preservation of TJ integrity. Calpain inhibition provides protection against TBI-induced BBB hyperpermeability in a mouse model of TBI. Calpain inhibitor III can be a potential therapeutic target in attenuating TBI-induced BBB hyperpermeability when established in humans.

INTRODUCTION

Secondary injuries that occur following traumatic brain injury (TBI) include blood-brain barrier (BBB) breakdown and hyperpermeability and often result in tissue vasogenic edema [98]. The BBB plays an important role in maintaining the homeostasis of the brain. The BBB is majorly composed of the cerebral endothelial cells and the

tight junctions between them. Tight junctions (TJs) between the endothelial cells include transmembrane TJs i.e., occludin, claudins and junctional adhesion molecules and membrane bound TJs i.e., zonula occludens [63]. Zonula occludens play an important role in regulating BBB permeability by binding to both transmembrane tight junctions as well as actin cytoskeleton intracellularly [17]. Various mediators of inflammation are shown to modulate BBB permeability as described in Abbott et al, 2000 [99].

Inflammation that occurs as a consequence of brain injuries is carried out by various pro-inflammatory cytokines [100]. IL-1β is the most implicated pro-inflammatory cytokine in various pathologies of the central nervous system including TBI [101; 102]. Blocking the interleukin-1 (IL-1) has beneficial effects as demonstrated in experimental models of brain damage [101]. IL-1β induces BBB breakdown in rat brain [102] and also increases human brain microvascular endothelial cell permeability [103]. However, IL-1β-induced mechanisms that lead to cellular dysfunction at the level of BBB are widely unknown.

We speculated the involvement of calpains in mediating BBB dysfunction and hyperpermeability, as they are involved in a wide array of neurological pathologies like trauma, ischemia-reperfusion injury, spinal cord injury and non-neurological pathologies [104; 105; 106; 107]. Intracellular calcium levels and the endogenous inhibitor of calpains namely calpastatin tightly regulate calpain levels endogenously [104; 108]. Calpains-1 and -2 are the predominant calpains in the central nervous systems [109; 110]. Calpain expression was found to increase in the endothelial cells of

the injured brain cortex following TBI in human patients compared to those who died from cardiac arrest [107]. Calpain-dependent cleavage of intracellular cytoplasmic protein zonula occludens-1 (ZO-1) has been studied in human lung endothelial cells [108]. However, their contribution in regulating BBB endothelial dysfunction and hyperpermeability is largely unknown.

We hypothesize that calpain-mediated mechanisms play an important role in promoting IL-1β-induced BBB dysfunction and hyperpermeability and that its inhibition will regulate this pathway. Furthermore, we studied the effect of calpain inhibition on TBI-induced BBB hyperpermeability in mouse model of TBI. We aim to address this hypothesis by answering the following questions:

- What is the effect of calpain inhibition on IL-1β-induced BBB endothelial hyperpermeability, tight junctional integrity, and actin stress fiber formation?
- Does IL-1β treatment induce calpain activity?
- Does IL-1β treatment induce intracellular calcium release?
- What is the effect of IL-1β treatment on total number of viable cells?
- Does IL-1β treatment induce ZO-1 mRNA or protein expression?
- What is the effect of calpain inhibition on TBI-induced BBB hyperpermeability in a mouse model of TBI?

MATERIALS AND METHODS

Materials

Rat brain microvascular endothelial cells (RBMECs) and RBMEC Medium were purchased from Cell Applications, Inc. (San Diego, CA). Transwell® 24-well plates were obtained from Corning Costar (New York, USA). Nunc Lab Tek II-CC, 8-well glass chamber slides, Interleukin-1β human, fibronectin from bovine plasma, β-actin, albumin from bovine serum, Evans blue, trichloroacetic acid and fluorescein isothiocyanate-dextran-10 kDa were purchased from Sigma Aldrich (St. Louis, MO). Rabbit anti ZO-1 (Cat#617300), mouse anti ZO-1 (Cat#339100), 0.25% Trypsin (1X), Opti-MEM (1X)/reduced serum medium, Dulbecco's modified Eagle's medium (DMEM; with high glucose, HEPES, no phenol red (1X)), NuPAGE Novex® 10% Bis-Tris protein gels, NuPAGE® MOPS SDS Running Buffer, NuPAGE® Transfer Buffer, HyClone Dulbecco's phosphate buffered saline (PBS, without calcium, magnesium, or phenol red), TRIzol® Reagent, SuperScript® IV First-Strand Synthesis System, Halt® Protease Inhibitor Cocktail (100X), Pierce™ ECL Western Blotting substrate and rhodamine phalloidin were purchased from Thermo Fisher Scientific (Carlsbad, CA). Goat anti-mouse IgG-HRP and donkey anti-rabbit IgG-FITC secondary antibodies were purchased from Santa Cruz Biotechnology, Inc. (Santa Cruz, CA). Calpain Activity Fluorometric Assay Kit (K240-100) and EZViable™ Calcein AM Cell Viability fluorometric assay kit were bought from Biovision (Milpitas, CA). We also purchased Vector VECTASHIELD® Mounting Media with DAPI from Vector Laboratories (Burlingame, CA). Pierce™ BCA Protein Assay Kit and RT² qPCR Primer Assay for

Mouse GAPDH were purchased from Qiagen (Valencia, CA). Carbobenzoxy-valinyl-phenylalaninal, also called as Calpain Inhibitor III or MDL 28170 was bought from Calbiochem (Billerica, MA). Cell Lysis Buffer (10X) was bought from Cell Signaling Technology, Inc. (Danvers, MA). Primers were purchased from Thermo Fisher Scientific (Carlsbad, CA). Calpain-1 siRNA and control siRNA (ON-TARGETplus siRNA) were purchased from Dharmacon, General Electric (Pittsburgh, PA).

In vitro BBB model

Primary cultures of RBMECs derived from the brain of adult Sprague Dawley rat were purchased from the Cell Applications Inc. (San Diego, CA). RBMECs were initially grown on 0.05% fibronectin-coated cell culture dishes, using the RBMEC medium in a cell culture incubator (95% O_2, 5% CO_2 at 37°C). RBMECs were treated with 0.25% trypsin-EDTA for cell detachment. Detached cells were then grown on fibronectin-coated Transwell® inserts, chamber slides or 100 mm dishes for experimental purposes. RBMEC passages 8-10 were chosen for all the experiments.

Animals and surgeries

C57BL/6 mice (25-30 g) were obtained from Charles River Laboratories (Wilmington, MA). Animals were maintained at the Texas A&M University Health Science Center College of Medicine and Baylor Scott and White Health animal facility on a 12:12 hour dark/light cycle, with free access to food and water. The room temperature was maintained at 25° ± 2 °C. Surgical and experimental procedures used

in this study were conducted after approval by the Institutional Animal Care and Use Committee. The facility is approved by the Association for Assessment and Accreditation of Laboratory Animal Care International in accordance with the National Institutes of Health guidelines.

Craniotomy procedure

The head of the animal was shaven and the surgical site on the surface of the head was cleaned with an alcohol wipe. Lubricating ointment was applied to the eyes. A midline incision was made to remove the skin from top of the skull exposing the sagittal suture, bregma and lambda. A circular craniotomy window, 3-4 mm in diameter was made on ipsilateral hemisphere, between lambda and bregma using a microdrill. The resulting bone flap was removed. Sham animals received only craniotomy surgery, while TBI injury group receives brain injury via controlled cortical impactor following craniotomy procedure.

Controlled cortical impact

Benchmark™ Stereotaxic Impactor from Leica was used for these studies. Following craniotomy procedure, the animal was mounted on the stereotaxic frame. An impactor probe of 3 mm diameter was used to impact the exposed part of the brain. The depth of the injury was used to determine the intensity of the injury. Settings for mild TBI used in this study are: 2 millimeters depth, 0.5 meters/second velocity and 100 milliseconds contact time as described in Chen et al, 2014 [88].

Monolayer permeability assays

RBMECs were grown on fibronectin-coated Transwell® inserts as monolayers for 72-96 hours and regularly checked for confluency. Monolayers were initially exposed to phenol red free DMEM for 45 minutes to an hour. DMEM treated cells were then pretreated with calpain inhibitors and subsequently with IL-1β (10 ng/mL; 2 hours). At the end of the treatments, FITC labeled dextran-10 kDa (5 mg/mL; 30 minutes) was applied to the luminal compartment. One hundred microliters of sample was collected from the abluminal compartment at the end of 30 minutes and measured fluorometrically at 485/520 nm (Excitation/Emission) using Fluoroskan Ascent™ FL Microplate Fluorometer and Luminometer (Vantaa, Finland).

Calpain inhibitor III (10 μM; 1 hour) was used for pharmacological inhibition of calpains, while calpastatin (10 μM; 1 hour), was used for endogenous inhibition of calpains. Calpain inhibitor III (MDL-28170; Carbobenzoxy-valinyl-phenylalaninal; Cbz-Val-Phe-H) is a potent, cell permeable inhibitor of both calpain-1 and -2 and calpastatin is a cell-permeable peptide (27 amino acids in length) that inhibits both calpains-1 and -2.

Untreated cells served as control. Each experiment was repeated four times. Fluorescence intensity was plotted on the Y-axis and represented as % control. Data were expressed as mean ± % SEM and statistical differences among groups were determined by one-way analysis of variance (ANOVA) followed by Bonferroni post hoc

test to determine significant differences between specific groups. A value of $p<0.05$ was considered statistically significant.

Calpain-1 knockdown studies

RBMECs were grown on fibronectin-coated Transwell® inserts as monolayers for 72-96 hours. Cells were transfected with control siRNA or calpain-1 siRNA on the following day or until they are about 50% confluent. RBMEC monolayers were transfected with calpain-1 and control siRNA at 25 nM concentration for 48 hours. Transfection was performed according to manufacturer's instructions. Transfected monolayers were then exposed to IL-1β and permeability was determined based on the leakage of FITC-dextran-10 kDa (5 mg/mL; 30 minutes) leakage from the luminal to the abluminal chamber. One hundred microliters of the sample was obtained from the abluminal chamber and measured fluorometrically at 485/520 nm (Excitation/Emission) using Fluoroskan Ascent™ FL Microplate Fluorometer and Luminometer. Untreated cells were used as control. Each experiment was repeated four times. Fluorescence intensity was plotted on the Y-axis and represented as % control. Data were expressed as mean ± % SEM and statistical differences among groups were determined by one-way analysis of variance (ANOVA) followed by Bonferroni post hoc test to determine significant differences between specific groups. A value of $p<0.05$ was considered statistically significant.

Calpain activity measurement

A Calpain Activity Fluorometric Assay Kit was used to measure the calpain activity in the cells. For this assay, RBMECs were grown in petri dishes until confluency is achieved. Cells were then trypsinized using lysis buffer, followed by resuspension in extraction buffer provided in the kit. The kit employs a synthetic calpain substrate, Ac-Leu-Leu-Tyr-7-Amino-4-trifluoromethylcoumarin (Ac-LLY-AFC) in order to detect the calpain activity. Equal amount of protein lysates were taken and subsequently exposed to the substrate Ac-LLY-AFC and incubated in the dark for an hour. Samples were then read using Fluoroskan Ascent™ FL microplate fluorometer and luminometer at 400/505 nm (Excitation/Emission).

Cells lysates were pretreated with calpain inhibitors (Calpain inhibitor III and calpastatin at 10 μM for 1 hour) and subsequently with IL-1β treatment. Untreated cells served as control. Each experiment was repeated five times. Calpain activity was expressed as relative fluorescence units (RFU) and plotted on the Y-axis. Data were expressed as mean ± SEM and statistical differences among groups were determined by one-way analysis of variance (ANOVA) followed by Bonferroni post hoc test to determine significant differences between specific groups. A value of $p<0.05$ was considered statistically significant.

Immunofluorescence localization and cytoskeletal assembly labeling

Zonula occludens (ZO-1) junctional localization and *f*-actin stress fiber formation were assessed. RBMECs were grown on chamber slides for overnight.

Pretreatment with calpain inhibitor III (10 μM; 1 hour) was followed by IL-1β treatment (10 ng/mL; 2 hours). Cells were then fixed in 4% paraformaldehyde in PBS for 10-15 minutes and permeabilized with 0.5% Triton-X 100 in PBS for another 10-15 minutes. Cells were blocked with 2% bovine serum albumin (BSA) in PBS for an hour at room temperature. Cells were then incubated overnight with anti-rabbit primary antibodies against ZO-1 (#617300) at 1:150 dilution, followed by incubation with anti-rabbit IgG-FITC conjugated secondary antibody for an hour at room temperature. Cells were then washed and mounted.

Following treatment study, cells were fixed, permeabilized and blocked in 2% BSA-PBS as described earlier. Cells were then labeled with rhodamine phalloidin at 1:50 dilution in 2% BSA-PBS for 20 minutes. Chamber slides were then washed and mounted using VECTASHIELDd® Antifade Mounting Media with DAPI for nuclear staining. Cells were visualized and scanned at a single optical plane with an Olympus Fluoview 300 Confocal Microscope (Center Valley, PA) with a PLA PO 60X water immersion objective. Untreated cells served as control. Each experiment was repeated four times.

Quantitative real time-PCR

RBMECs were grown on 100 mm cell culture dishes; total RNA was then extracted from the cells using TRIzol® reagent according to the manufacturer's instructions. RNA concentration and quality were determined by employing the ratio of absorbance at 260/280 nm using Biotek Synergy Hybrid Spectrophotometer (Winooski,

VT). Reverse transcription was performed using the SuperScript® IV First-Strand Synthesis System. Quantitative real time PCR was performed using the RT² SYBR Green Fluor qPCR Mastermix with the following primer pairs for ZO-1: Forward primer: 5′-CCTCTGATCATTCCACACAGTC-3′, Reverse primer: 5′-TAGACATGCGCTCTTCCTCTCT-3′, and GAPDH: Forward primer: 5′-AATGTATCCGTTGTGGATCT-3′, Reverse primer: 5′-CAAGAAGGTGGTGAAGCAGG-3′ were used. Real-time PCR detection was carried out using Stratagene Mx3000P qPCR System, Agilent Technologies (La Jolla, CA), using 1 μL of cDNA for 10 minutes at 95°C, followed by 40 cycles of 15 sec at 95°C for denaturation and 1 min at 60°C for annealing. Relative abundances of target genes were calculated by normalizing Ct values to endogenous control glyceraldehyde 3-phosphate dehydrogenase (GAPDH).

Cells were divided into 2 groups: control (untreated) and IL-1β (10 ng/mL; 2 hours) treatment groups. Each experiment was repeated three times. Relative mRNA expression of ZO-1 was obtained by normalizing the C_t values to the endogenous control GAPDH for each repeat. Normalized C_t values were expressed as mean ± SEM. Statistical differences among groups were determined by one-way analysis of variance (ANOVA) followed by Bonferroni post hoc test to determine significant differences between specific groups. A value of $p<0.05$ was considered statistically significant.

Western blot assays

Western blot analysis was performed to investigate the expression of ZO-1 protein in RBMECs. Following treatment studies, cells were washed twice in ice-cold PBS and incubated in ice-cold cell lysis buffer (1X) along with protease inhibitor cocktail (1X) for 5 minutes in cell culture dishes. Cells were then scraped, sonicated and centrifuged at 14,000*g* for 10 minutes at 4°C. Supernatant was collected from the extracts and protein concentration was determined using protein assay kit. Equal amounts of total protein (50 μg) were separated by sodium dodecyl sulphate-polyacrylamide gel electrophoresis (SDS-PAGE) on 10% Bis-Tris precast gels at constant voltage (145 V) for 180 minutes. Proteins were then transferred onto the nitrocellulose membrane at constant voltage (30 V) for overnight and the membranes were blocked using 5% nonfat dry milk in Tris-Buffered Saline (TBS) with 0.05% Tween-20 for 3 hours and subsequently incubated with primary mouse monoclonal anti ZO-1 antibody (1:250 dilution). Membranes were washed thrice in TBS-T and incubated with the goat anti-mouse IgG-HRP conjugated secondary antibody. After washing, the immunoblots were visualized by ECL Western Blotting Substrate. Cells were divided into untreated (control) and IL-1β (10 ng/mL; 2 hours) treatment groups. Each experiment was repeated four times. Equal amount of protein sample loading was verified by assessing β-actin protein expression. Each experiment was repeated four times.

Cell viability studies

An EZViable™ Calcein AM Cell Viability Assay Kit (Fluorometric) was used for quantify the number of viable cells. Calcein AM is a non-fluorescent, hydrophobic compound that easily penetrates intact and live cells. Hydrolysis of the calcein AM by intracellular esterase produces a hydrophilic, strongly fluorescent compound that is retained in the cell cytoplasm, which can be measured at 485/530 nm (Excitation/Emission).

Equal numbers of cells were grown on sterile black 96 well trays. On reaching confluency, growth media was discarded and cells were washed in PBS and pre-exposed to phenol red-free medium for an hour. Cells were divided into control (untreated) and IL-1β (10 ng/mL) treatment groups. Cells were treated with IL-1β for 2, 4 and 6 hours with hydrogen peroxide at 50, 25, 10 mM respectively, as a positive control. Following treatments, cells were then exposed to calcein buffer solution (calcein AM: calcein dilution buffer in 1:500 dilution) and incubated at 37°C for 30 minutes and a fluorometric reading was obtained.

Each experiment was repeated five times. Fluorescence intensity was plotted on the Y-axis and represented as % control. Data were expressed as mean ± % SEM and statistical differences among groups were determined by one-way analysis of variance (ANOVA) followed by Bonferroni post hoc test to determine significant differences between specific groups. A value of $p<0.05$ was considered statistically significant.

Fluo-4 based $[Ca^{2+}]_i$ measurements

For population measurements, RBMECs (monolayer) were incubated with 5 μM Fluo-4 AM (Thermo Fisher Scientific, Carlsbad, CA) at 37°C for 40 minutes and Fluo-4 fluorescence intensity was measured through a Biotek Synergy Hybrid Spectrophotometer (Winooski, VT). Ionomycin (Iono, 1 μM) and thapsigargin (TG, 2 μM) were used to increase $[Ca^{2+}]_i$ as positive controls. DMSO was used as a vehicle control. Each experiment was repeated four times. Data were presented as mean ± S.E.

Single-cell $[Ca^{2+}]_i$ imaging

RBMECs were grown on cover slips and incubated with 2 μM Fura-2 AM (ThermoFisher Scientific, Carlsbad, CA) in the culture medium at 37°C for 40 minutes. Ratiometric $[Ca^{2+}]_i$ imaging was performed on an IX-81 microscope (Olympus) based system as described previously from individual cells [111]. Data were analyzed using Metafluor software (Universal imaging) and OriginPro 8 software (Origin Lab) and expressed as mean ± S.E.

Evans blue leakage studies

Evans blue dye binds to albumin in the blood enabling us to study the vascular leakage into the extravascular tissue following TBI. For this study, C57BL/6 mice (25-30 g) were anesthetized with urethane, i.p. injection (2 mL/kg body weight) followed by Evans blue dye, i.v. injection (2% wt/vol in saline; 4 mL/kg body weight). Evans blue was allowed to circulate in the animal for 30 minutes prior to performing sham surgery

(only craniotomy) or TBI using controlled cortical impactor. Drugs were given to the animal along with Evans blue injection and allowed to circulate for 30 minutes as well. DMSO was used a vehicle control. Settings for mild TBI are described in the CCI procedure.

Animals were grouped into Sham (only craniotomy), Vehicle + Sham (DMSO injection followed by craniotomy), Vehicle + TBI group (DMSO followed by mild TBI), and Calpain inhibitor III+TBI group (calpain inhibitor III [10 μg/gram body weight of the animal] injection followed by mild TBI). Each group consisted of five animals.

One-hour post-TBI, animals were transcardially perfused with sterile saline containing heparin (1000 U/mL) for at least 20 minutes. Brains were extracted and brain cortex was carefully separated and weighed. Brain cortices were then homogenized in 1 mL of 50% (wt/vol) trichloroacetic acid (TCA) in saline. Homogenate was then centrifuged at 6,000*g* for 20 minutes at 4°C. Supernatants were extracted and diluted in 3 parts of ethanol (1:3; 50% TCA: 95% ethanol). Samples were then quantitated fluorometrically at 620/680 nm (Excitation/Emission) using Biotek Synergy Hybrid H1 spectrophotometer (Winooski, VT). Evans blue concentration in the samples were evaluated using external standards for Evans blue ranging from 50-1000 ng/mL, prepared in same solvent (1:3; TCA: 95% ethanol). Evans blue amount in the samples were expressed as ng/brain cortex ± SEM. Statistical differences among groups were determined by one-way analysis of variance (ANOVA) followed by Bonferroni post hoc

test to determine significant differences between specific groups. A value of $p<0.05$ was considered statistically significant.

RESULTS

Pharmacological or endogenous calpain inhibition attenuates IL-1β-induced endothelial cell hyperpermeability

RBMEC monolayers were pretreated with calpain inhibitor III or calpastatin to confirm the contribution of calpains in mediating IL-1β (10 ng /mL for 2 hours)-induced endothelial cell hyperpermeability. Figure 18 demonstrates that IL-1β treatment significantly increases endothelial cell hyperpermeability, while pretreatment with calpain inhibitor III (Figure 18 A, p <0.05) and calpastatin (Figure 18 B, p <0.05) significantly attenuates IL-1β-induced endothelial cell hyperpermeability.

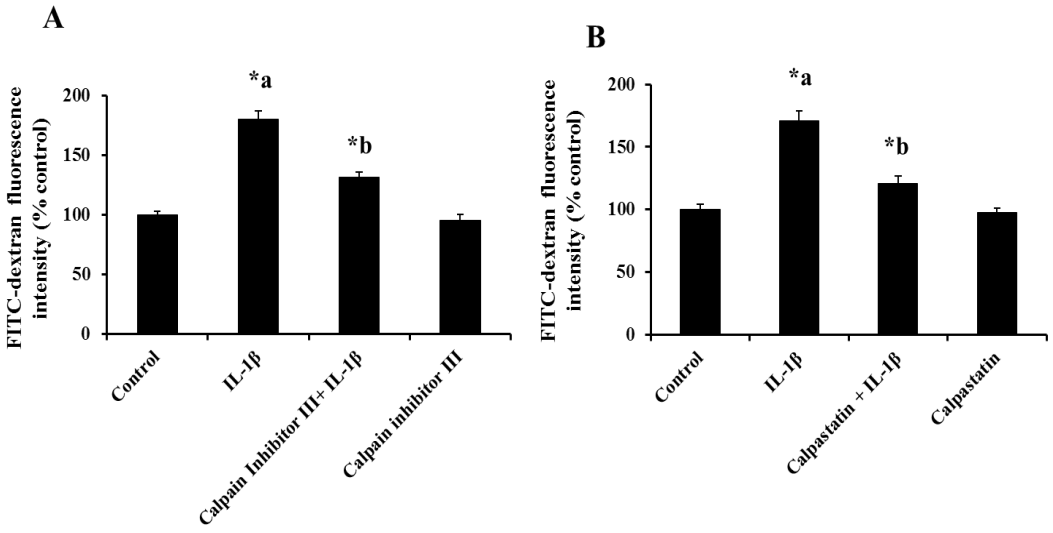

Figure 18: Calpain inhibitor III and calpastatin pretreatment attenuates IL-1β treatment-induced monolayer hyperpermeability. Calpain inhibitor III (figure A; n=4; $p<0.05$) and calpastatin (figure B; n=4; $p<0.05$) pretreatment attenuates IL-1β-induced monolayer hyperpermeability significantly. Monolayer permeability is expressed as a percentage control of FITC-dextran-10 kDa fluorescence intensity, plotted on Y-axis. Data are expressed as mean ± % SEM. '*a' indicates significant increase compared to the control group; '*b' indicates significant decrease compared to the IL-1β treatment group.

Calpain-1 knockdown attenuates IL-1β-induced endothelial cell hyperpermeability

Significant contribution of calpains-1 is further supported by calpain-1 siRNA transfection studies. Figure 19 demonstrates that IL-1β treatment-induced endothelial cell hyperpermeability was significantly reduced in calpain-1 knockdown cells compared to IL-1β treatment alone (p <0.05). Calpain-1 knockdown studies were performed using siRNA transfection technique as described earlier. siRNA treated groups were compared to the control siRNA group, while the IL-1β alone treated group was compared to the control group.

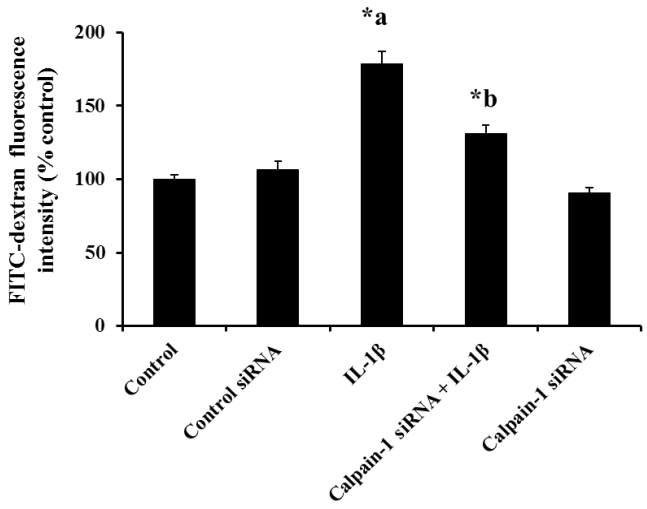

Figure 19: Knockdown of calpain-1 by siRNA attenuates IL-1β treatment-induced monolayer hyperpermeability. Monolayer permeability is expressed as percentage flux of FITC-dextran-10 kDa fluorescence intensity, plotted on Y-axis. Data are expressed as mean ± % SEM. '*a' indicates significant increase compared to the control group; '*b' indicates significant decrease compared to the IL-1β treatment group (n=4; $p<0.05$).

IL-1β treatment-induces calpain activity

IL-1β treatment significantly increased calpain activity in RBMECs, while pretreatment with calpain inhibitor III and calpastatin significantly attenuated IL-1β-induced calpain activity (Figure 20, p <0.05). Calpain activity measurements were performed as described in the methods section.

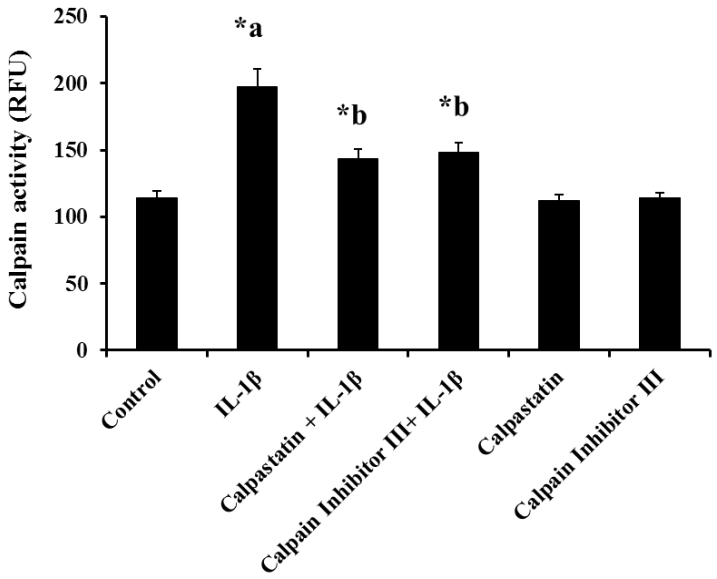

Figure 20: Calpastatin and calpain inhibitor III pretreatment attenuates IL-1β treatment-induced calpain activity. Calpain activity is expressed as relative fluorescence units (RFU), plotted on Y-axis. Data are expressed as mean ± SEM. '*a' indicates significant increase compared to the control group; '*b' indicates significant decrease compared to the IL-1β treatment group (n=4; $p<0.05$).

Calpain inhibition provides protection against IL-1β-induced loss of tight junction integrity and *f*-actin stress fiber formation.

Cells were processed for immunofluorescence localization of tight junction protein, ZO-1. IL-1β treatment-induced ZO-1 junctional discontinuity (white arrows; Panel 21 A) compared to the control cells. Pretreatment with calpain inhibitor III (10 μM; 1 hour) decreased IL-1β (10 ng/mL; 2 hours)-induced ZO-1 junction integrity.

For assessing the cytoskeletal assembly, rhodamine phalloidin labeling technique was performed. Untreated cells served as control. IL-1β (10 ng/mL; 2 hours)

treatment-induced *f*-actin stress fiber formation (white arrows; Figure 21 B) was reduced by pretreatment with calpain inhibitor III (10 μM; 1 hour).

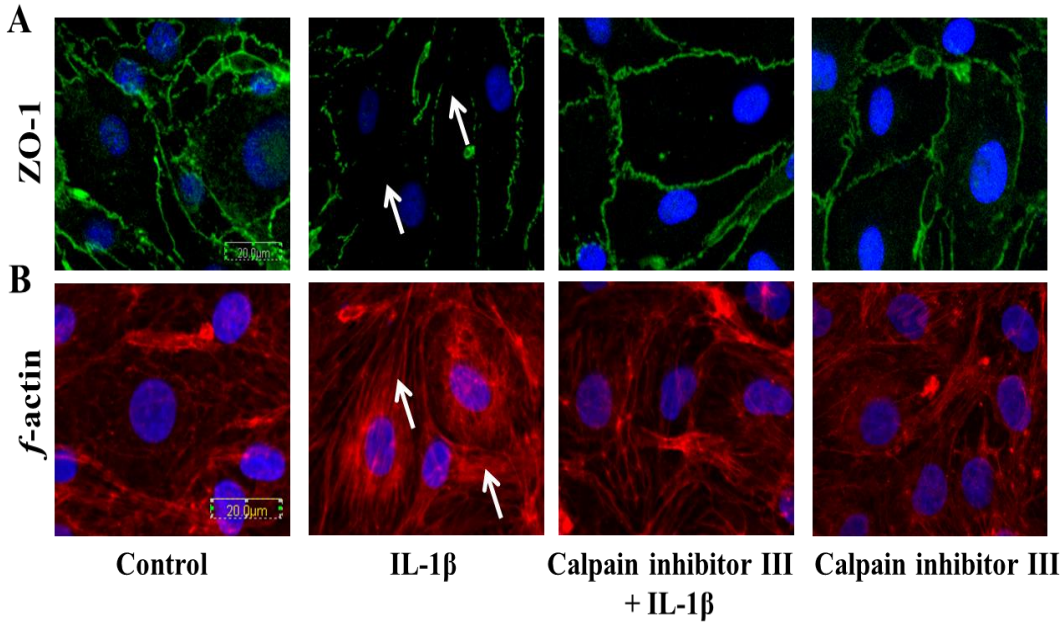

Figure 21: IL-1β treatment-induced ZO-1 junctional disruption and *f*-actin stress fiber formation is reduced by pretreatment with calpain inhibitor III. IL-1β treatment-induced ZO-1 junctional disruption and *f*-actin stress fiber formation are shown by white arrows in panel A and B respectively. ZO-1 junctional integrity and *f*-actin stress fiber formation were assessed using immunofluorescence localization and rhodamine phalloidin techniques respectively (n=4 for each study).

IL-1β treatment neither induces ZO-1 mRNA expression nor alters ZO-1 protein expression

IL-1β (10 ng/mL; 2 hours) treatment did not alter ZO-1 or MMP-9 mRNA expression by RT-PCR studies. IL-1β treatment did not alter ZO-1 protein expression.

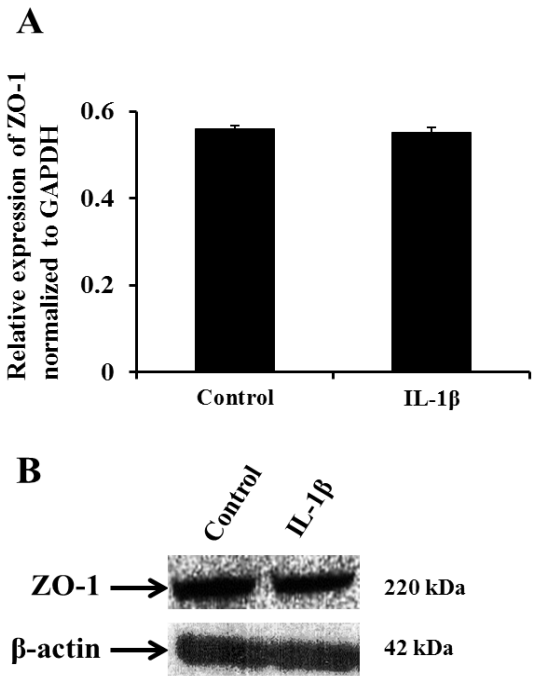

Figure 22: IL-1β treatment does not induce ZO-1 mRNA or protein expression. Fluorescence intensity from RT-PCR studies is expressed as relative expression of ZO-1 normalized to GAPDH and is plotted on Y-axis (n=3; figure A). Data are represented as mean ± SEM. ZO-1 protein expression did not change following IL-1β treatment (n=4; figure B).

IL-1β treatment does not induce cell death

IL-1β treatment did not significantly decrease the number of viable cells compared to the control group, as shown in Figure 23. Hydrogen peroxide (100 mM) was used as a positive control.

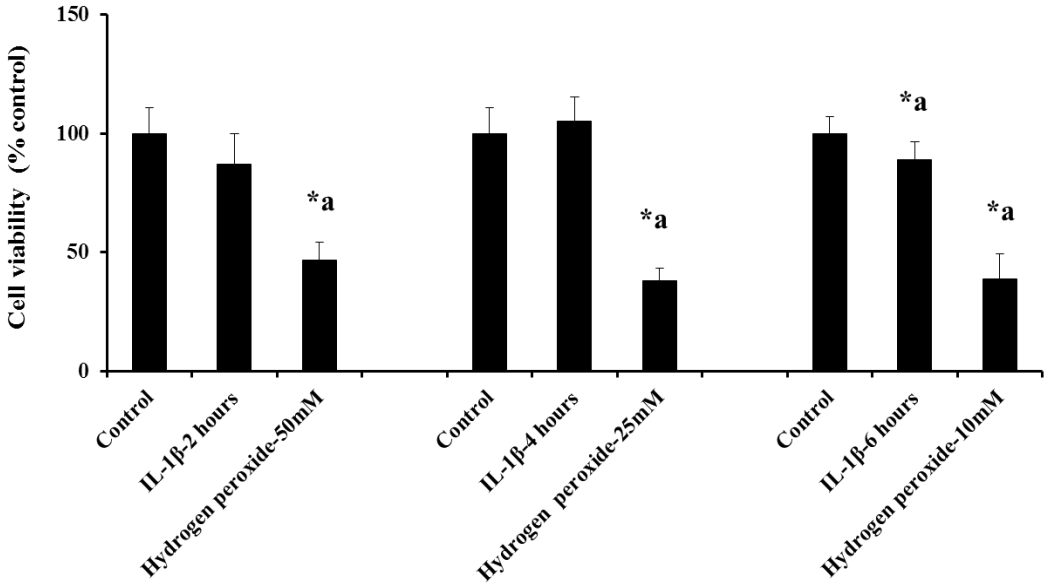

Figure 23: IL-1β treatment does not induce cell death. IL-1β treatment did not alter cell viability up to 4 hours. Treatment of hydrogen peroxide used as a positive control showed a significant decrease in cell viability compared to the untreated and IL-1β treatment groups (n=5; $p<0.05$). Data are expressed as mean ± % SEM. '*a' indicates significant decrease compared to the control group.

IL-1β treatment does not induce intracellular calcium mobilization

To test whether IL-1β upregulates the activity of calpains, a calcium-dependent cysteine protease, by increasing intracellular calcium concentration ($[Ca^{2+}]_i$), we directly measured $[Ca^{2+}]_i$ in RBMECs by two different approaches. Initially, RBMECs were grown as monolayers and loaded with Fluo-4 AM (a Ca^{2+} indicator). Fluo-4 signals were measured from cells before (F_0) and after (F) a 10-minute incubation of cells with IL-1β (10 ng/mL). In parallel, control cells were treated with thapsigargin (TG; 2 μM), ionomycin (Iono; 1 μM), or DMSO as the vehicle control for TG and Iono. TG is a sarco/endoplasmic reticulum Ca^{2+}-ATPase (SERCA) pump inhibitor, which passively depletes Ca^{2+} in the ER store in conjunction with triggering store-operated Ca^{2+} entry (SOCE). Ionomycin is an ionophore that increases membrane permeability to Ca^{2+}, therefore raising the intracellular level of Ca^{2+}. As expected, both stimulations by TG and ionomycin triggered a significant increase of $[Ca^{2+}]_i$ (Figure 24 A); however, there was only a negligible intracellular Ca^{2+} response to the IL-1β treatment (Figure 24 A).

It is possible that IL-1β triggers a relatively transient $[Ca^{2+}]_i$ response and/or a small population of cultured RBMECs has a dramatic $[Ca^{2+}]_i$ response to IL-1β, which could be masked during our Fluo-4 based $[Ca^{2+}]_i$ measurement. Accordingly, RBMECs were then loaded with Fura-2 AM, a ratiometric Ca^{2+} indicator, and $[Ca^{2+}]_i$ was continuously monitored at the single-cell level (15 seconds/frame). In the control experiments, TG could evoke a typical SOCE in RBMECs (Figure 24 B) that elevates $[Ca^{2+}]_i$ from 65 ± 6 nM up to 281 ± 22 nM (Figure 24 D). However, when RBMECs were incubated with 10 ng/mL IL-1β for 20 minutes, there were no cells showing

significantly increased $[Ca^{2+}]_i$ (data not shown). We then treated cells with a higher dose (100ng/mL) of IL-1β for 2 hours, which still did not significantly promote intracellular calcium levels in any cells (Figure 24 C and 24 D). As a conclusion, our results indicate that IL-1β treatment does not induce a dramatic $[Ca^{2+}]_i$ mobilization in RBMECs.

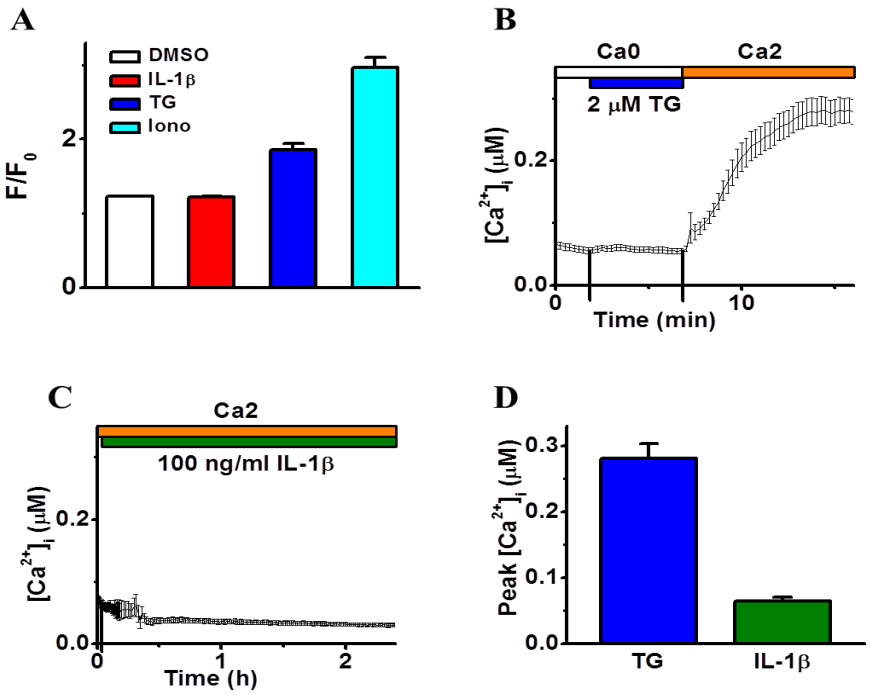

Figure 24: IL-1β treatment does not induce intracellular calcium mobilization. Figure A demonstrates the effect of IL-1β treatment on intracellular calcium mobilization (F) relative to basal Ca^{2+} (F_0) when measured 10 minutes after the application of DMSO (vehicle control), IL-1β (10 ng/mL), TG (2 μM), and Iono (1 μM), and displayed as mean ± SE (n = 4). Figure B and C are the representative intracellular free calcium recordings ($[Ca^{2+}]_i$, mean ± SE) showing cytosolic Ca^{2+} levels coupled to TG (2 μM, figure B) or IL-1β (100 ng/mL, C) stimulation. The top bars indicate the type of extracellular solutions applied to the RBMECs, and the vertical lines on the X-axis indicate the time of solution change. Figure D displays averaged peak value of $[Ca^{2+}]_i$ in response to TG (n = 40 cells) and IL-1β (n = 30 cells), respectively, are summarized.

Calpain inhibitor III pretreatment attenuates TBI-induced BBB hyperpermeability

Mice subjected to TBI demonstrated significant increase in Evans blue leakage compared to the sham animals. Pretreatment with calpain inhibitor III attenuated mild TBI-induced Evans blue leakage into the brain tissue (Figure 25 A & B; $p < 0.05$). Evans blue leakage was assessed fluorometrically at 620/680 nm (Excitation/Emission). This study suggests that calpains are a potential therapeutic target to attenuate BBB hyperpermeability that occurs following TBI.

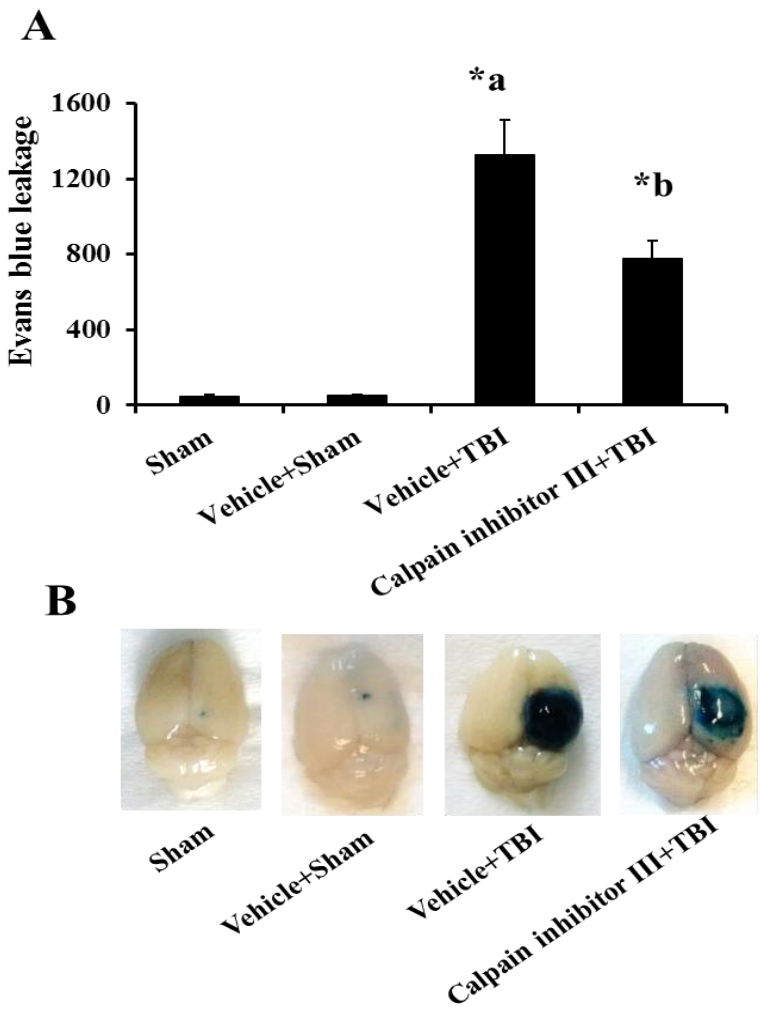

Figure 25: Calpain inhibitor III pretreatment attenuates TBI-induced BBB hyperpermeability studied by Evans blue dye extravasation method. Vehicle control group subjected to TBI demonstrated significant increase in Evans blue leakage compared to the sham injury group (figure A; $p<0.05$). Calpain inhibitor III (10 µg /gram body weight of the animal) pretreatment significantly attenuated TBI-induced Evans blue leakage into the extravascular tissue space (figure A; $p<0.05$). Pictorial representation of the brain tissue from various groups is shown in figure B. Each group consisted of five animals. Sham injury group is used as the baseline for all comparisons. Data are expressed as ng/brain cortex ± SEM. '*a' indicates significant increase compared to the sham injury group; '*b' indicates significant decrease compared to the vehicle + TBI group.

DISCUSSION

The major findings of this study are: 1) calpain(s) promote BBB dysfunction and hyperpermeability via disruption of the TJs *in vitro,* 2) IL-1β is an inducer of calpain-mediated BBB dysfunction and hyperpermeability *in vitro,* 3) inhibition of calpain activation provides protection against BBB hyperpermeability via preservation of TJ integrity *in vitro,* 4) calpain mediated loss of barrier functions are independent of Ca^{2+} mobilization or loss of cell viability, and 5) pharmacological inhibition of calpains provide protection against BBB hyperpermeability in a mouse model of TBI.

Calpains are thiol or cysteine proteases that are present in most of the mammalian cells. Under physiological conditions, calpains possess low activity and play an important role in regulating the kinases, transcription factors, and receptors apart from aiding in the cytoskeletal turnover [112]. Calpain deficiencies as well as its over activation are linked to a variety of diseases and pathological consequences described in Kampfl et al, 1997 [113]. Due to their multifaceted nature, they control various irreversible signaling events and other biological functions in the cell like endothelial cell adhesion, differentiation, migration, proliferation, cell cycle control, cytoskeletal remodeling, embryonic development, vesicular trafficking [107; 108; 109; 114; 115; 116]. Calpain-1 (also known as tau-calpain) and calpain-2 (also known as m-calpain) are predominantly expressed in the central and peripheral nervous systems [109; 110]. Calpain-1 is activated under low calcium concentrations (3-50 μM), while calpain-2 is activated only under high concentrations (400-800 μM) of calcium in the cell [115; 116]. Calpain knockdown data from our studies demonstrates the contribution

of calpain-1 but we do not disregard the contribution of calpain-2 in mediating BBB dysfunction and hyperpermeability and is an area open for further investigation.

Calpastatin and intracellular Ca^{2+} levels tightly regulate the calpain levels endogenously [107; 113]. This information was used to study the contribution of calcium and calpastatin in regulating IL-1β-induced endothelial hyperpermeability. To study the effect of IL-1β treatment on intracellular calcium, we performed calcium mobilization studies, which demonstrated that IL-1β treatment (10 ng/mL; 2 hours) does not induce significant intracellular mobilization of calcium in RBMECs. However, we do not rule out the possible involvement of calcium in inducing calpains as established in several other conditions. We speculate that IL-1β-induced calpain activation may occur due to changes in localized calcium, which can be studied by calcium sparks [117]. Calpastatin is an endogenous inhibitor of calpains; it regulates the activity of calpains by binding to the active site cleft of both calpains-1 and -2. Our results support the significance of calpain-calpastatin interactions in regulating BBB functions. Although, our studies demonstrate the ability of calpastatin in attenuating IL-1β-induced endothelial hyperpermeability, we have not further explored these studies *in vivo*. Understanding calpastatin-mediated regulation of BBB hyperpermeability can open new avenues for finding therapeutic agents that can alter the secondary injuries that occur following brain injury.

We have shown that pharmacological inhibition of calpains is effective in preserving barrier functions *in vitro* and *in vivo*. Calpain inhibitor III, is a well-studied cell permeable pharmacological inhibitor of calpains [107], was chosen for our *in vitro*

and *in vivo* studies. Calpain inhibitor III crosses the BBB efficiently and binds specifically to calpains -1 and -2, unlike other inhibitors of calpains like trypsin, plasmin, caspase-1, and cathepsin D [116]. Cytoskeletal and neuroprotective properties of calpain inhibitor III were examined using the controlled cortical impact (CCI) model of TBI in male CF-1 mice, 24 h post-TBI [118]. However, these studies do not aim to understand the effect of calpain inhibitor III on TBI-induced BBB hyperpermeability. Our study addresses this important question. While our *in vitro* studies support that calpain inhibition protected the BBB by preserving the TJ integrity and cytoskeletal organization this has not been confirmed in our *in vivo* studies.

Studies by Tsubokawa et al., 2006 indicate a link between calpain, cathepsin B, and matrix metalloproteinase-9 (MMP-9) upregulation [119]. MMP-2 and calpains have some common cleavage targets like sarcomeric proteins troponin I, myosin light chain-1 and titin in heart cells [120]. These studies support the possibility that calpain-induced BBB endothelial cell hyperpermeability may occur via MMP activation or vice-versa. Understanding this relationship is important to selectively target the appropriate pathways for therapeutic purposes. Our results demonstrate changes in cytoskeletal assembly evidenced by increased *f*-actin stress fiber formation following IL-1β treatment-induced calpain activation and BBB hyperpermeability. The stress fiber formation that occurs following IL-1β treatment may also involve tight junction cleavage via Ras homolog gene family, member A (RhoA)-dependent mechanisms leading to BBB permeability. RhoA-mediated mechanisms also activate cell division

control protein (cdc42) activation, which play an important role in maintaining the tight junction integrity and actin cytoskeletal assembly [121].

Our studies on understanding the role of calpains were focused more on the tight junction protein, ZO-1 and the actin cytoskeleton. However, understanding the contribution of calpains in mediating BBB hyperpermeability is extremely complicated as they target a wide range of proteins, which include: cytoskeletal proteins (α-spectrin, talin, filamin, paxillin, vinculin, ezrin, microtubule-associated proteins 2, myristoylated alanine-rich C-kinase substrate and neurofilament proteins), kinases (PP60 and proto-oncogene tyrosine-protein kinase src), phosphatases (protein tyrosine phosphatase 1B, focal adhesion kinase, talin, paxillin, protein tyrosine phosphatase), membrane–associated proteins, junctional proteins (β-catenin, E-cadherin, β-spectrin), and transcription factors such as c-fos, c-jun and p53 [108; 113; 114; 122; 123; 124; 125]. Although these molecules may not be expressed in the BBB, it is important to know how calpains interact with them and how these molecules contribute to BBB dysfunction or trauma-induced brain damage directly or indirectly.

In conclusion, our studies demonstrate the novel role of calpains in promoting IL-1β-induced BBB dysfunction and hyperpermeability and how calpain inhibition regulates this pathway. Our results further demonstrate that calpain inhibition has the potential to develop as a therapeutic target in controlling TBI-induced BBB hyperpermeability and edema when established in human patients.

CHAPTER IV

P2X7R-MEDIATED MECHANISMS IN REGULATING BLOOD-BRAIN BARRIER DYSFUNCTION AND HYPERPERMEABILITY

SUMMARY

Traumatic brain injury (TBI) is a serious cause of morbidity and mortality worldwide. Pathological consequences that occur following TBI include blood-brain barrier (BBB) dysfunction and hyperpermeability leading to vasogenic edema. Structurally, the BBB is comprised of brain endothelial cells and the tight junctions (TJ) between them, consisting of tight junction proteins (TJPs). Of these proteins, zonula occludens-1 (ZO-1) is an important scaffolding linker molecule that binds the transmembrane tight junctions to the actin cytoskeletal assembly of the cell. It plays an important role in regulating BBB hyperpermeability. Extracellular or intracellular factors that alter TJ integrity will promote BBB hyperpermeability. Traditionally, adenosine triphosphate (ATP) is known as a major source of energy in cell; however, ATP when released into extracellular space due to trauma or other reasons acts as a danger signal by acting via purinergic receptor (P2X7R). The objective of this study was to understand the role of P2X7R-mediated mechanisms in regulating BBB dysfunction and hyperpermeability using *in vitro* and *in vivo* approaches.

Rat brain endothelial cells (RBMEC) were used for the *in vitro* studies. Monolayer permeability assays using Transwell inserts were employed to determine the minimal concentration of Bz-ATP (potent agonist of P2X7R) to induce

hyperpermeability. Effect of Bz-ATP treatment alone or following P2X7R inhibition via A740003 or P2X7R siRNA on monolayer hyperpermeability was assessed. Changes in ZO-1 tight junctional localization and *f*-actin stress fiber formation following Bz-ATP treatment alone and following A740003 pretreatment were assessed via immunofluorescence and rhodamine phalloidin labeling respectively. Effect of Bz-ATP treatment on cell viability, ZO-1 mRNA, and protein expression were assessed by fluorescence assays, RT-PCR and western blot respectively. Evans blue extravasation assays and Intravital microscopy imaging techniques were employed to study the effect of TBI-induced BBB dysfunction in P2X7R knock out and wild type mice. Also, the effect of KN-62 (non-competitive P2X7R antagonist) pretreatment on TBI-induced BBB hyperpermeability was determined by Evans blue extravasation assays. Bz-ATP-induced monolayer hyperpermeability was attenuated by pretreatment with P2X7R inhibitors or transfection with P2X7R siRNA. Bz-ATP-induced disruption of tight junction integrity and *f*-actin stress fiber formation was attenuated by pretreatment with A740003. P2X7R knockout mice demonstrated less leakage of Evans blue and FITC-dextran into extravascular space compared to the wild type mice subjected to TBI. KN-62 pretreatment attenuated TBI-induced Evans blue leakage in mice.

Together, these findings implicate that ATP-sensitive P2X7R facilitates BBB hyperpermeability via alterations in TJ integrity and ZO-1 protein levels. P2X7R may be further studied as a novel therapeutic target to control TBI-induced BBB hyperpermeability and brain edema.

INTRODUCTION

Brain endothelial hyperpermeability that occurs at the level of the blood-brain barrier (BBB) is a common secondary injury that occurs as a consequence of various traumatic injuries to the brain, including traumatic brain injury (TBI). Hyperpermeability can be defined as the leakage of fluid and proteins into the extravascular space leading to vasogenic edema [126] with several adverse clinical consequences leading to patient death. Thus, understanding the mechanisms that are involved in the loss of BBB integrity leading to hyperpermeability is critical for therapeutic drug development against TBI. The integrity and permeability of the BBB is dictated mainly by the tight junctions (TJ) between the inter-endothelial cells [63] as they make up the structural and functional units of the BBB. Tight junctions proteins can be transmembrane in nature like occludin, claudins, junctional adhesion molecules or membrane bound, as in the case of zonula occludens proteins (ZOs) [63]. Among the ZOs, Zonula occludens-1 is an important scaffolding linker molecule in the BBB that binds to both transmembrane TJPs and actin cytoskeletal assembly intracellularly. BBB breakdown is a hallmark feature of the secondary injuries that occur following TBI.

Traumatic brain injury is the leading cause of mortality and morbidity worldwide. Annual incidence of TBI is accounted to be around 10 million people worldwide, with 5.3 million people from US alone, based on 2010 CDC statistics [63]. Accumulation of ATP metabolites in the cerebrospinal fluid correlates with edema formation and elevated intracranial pressure (ICP) as observed in a neurotrauma patient [127]. TBI is followed by depletion in cellular ATP [128]. Several evidences also

support the release of ATP from injured cells following trauma and TBI [129; 130; 131; 132].

ATP is essential for all living cells as a source of energy but when released extracellularly it acts in autocrine and paracrine fashion via purinergic receptors (P1 and P2) [9; 133; 134; 135]. Adenosine molecules activate P1 receptors, while ADP/ATP activates P2 receptors [136]. Purinergic receptors can be of two types: P2X (ligand-gated ion channels) and P2Y (G-protein coupled receptors) [133; 137; 138]. Studies by Gorodeski et al, 1997 demonstrate the role of extracellular ATP in regulating permeability in human cervical epithelial cells [139]. However, no information is currently available on the study of the role of ATP in the context of BBB dysfunction and hyperpermeability.

Extracellular ATP acts via purinergic receptor, P2X7 receptors (P2X7R) and are activated by high concentrations of ATP, usually >100 μM [140]. P2X7Rs exhibit low sensitivity to ATP and bind preferentially to Bz-ATP (2'(3')-*O*-(4-Benzoylbenzoyl) adenosine-5'-triphosphate tri (triethylammonium) salt) [134; 136]. Beneficial effects of P2X7R inhibition following neurotrauma are also studied [130; 141]. However, these studies do not aim to study the effect of P2X7R inhibition on TBI-induced BBB dysfunction and hyperpermeability. We hypothesize that P2X7R-mediated mechanisms play an important role in regulating ATP-induced BBB dysfunction and hyperpermeability. We investigated this hypothesis, by addressing the following questions:

- What is the effect of Bz-ATP treatment on BBB endothelial hyperpermeability?

- What is the effect of P2X7R inhibition on Bz-ATP-induced endothelial hyperpermeability, tight junction integrity and actin stress fiber formation.
- Does Bz-ATP treatment alter cell viability or alter ZO-1 mRNA or protein expression?
- What is the effect of TBI on BBB integrity in P2X7R global knockout mice?
- Can a pharmacological inhibitor of P2X7R such as KN-62 decrease TBI-induced BBB hyperpermeability?

MATERIALS AND METHODS

Materials

Rat brain microvascular endothelial cells (RBMECs) and Rat Brain Endothelial Cell Growth Medium were purchased from Cell applications, Inc. (San Diego, CA). Human brain microvascular endothelial cells (HBMECs) and CSC Complete Medium (containing CultureBoost-R and Bac-Off®), Attachment Factor were purchased from Cell systems (Kirkland, WA). Transwell® 24-well plates were obtained from Corning Costar (New York, USA). Nunc Lab Tek II-CC, 8-well glass chamber slides, 2′ (3′)-O-(4-Benzoylbenzoyl)adenosine 5′-triphosphate triethylammonium salt (Bz-ATP), fibronectin from bovine plasma, β-actin, albumin from bovine serum, Evans blue, trichloroacetic acid, fluorescein isothiocyanate-dextran-10 kDa were purchased from Sigma Aldrich (St. Louis, MO). Rabbit anti ZO-1 (Cat # 617300), mouse anti ZO-1 (Cat # 339100), 0.25% Trypsin (1X), Opti-MEM (1X)/reduced serum medium, Dulbecco's modified Eagle’s medium (DMEM; with high glucose, HEPES, no phenol red (1X)),

NuPAGE Novex® 10% Bis-Tris protein gels, NuPAGE® MOPS SDS Running Buffer, NuPAGE® Transfer Buffer, HyClone Dulbecco's phosphate buffered saline (PBS, without calcium, magnesium, or phenol red), TRIzol® Reagent, SuperScript® IV First-Strand Synthesis System, Halt® Protease Inhibitor Cocktail (100X), Pierce™ ECL Western Blotting substrate and rhodamine phalloidin were purchased from Thermo Fisher Scientific (Carlsbad, CA). Goat anti-mouse IgG-HRP and donkey anti-rabbit IgG-FITC secondary antibodies were purchased from Santa Cruz Biotechnology, Inc. (Santa Cruz, CA). EZViable™ Calcein AM Cell Viability fluorometric assay kit was bought from Biovision (Milpitas, CA). We also purchased Vector VECTASHIELD® Mounting Media with DAPI from Vector Laboratories (Burlingame, CA). Pierce™ BCA Protein Assay Kit and RT² qPCR Primer Assay for Mouse GAPDH were purchased from Qiagen (Valencia, CA). Cell Lysis Buffer (10X) was bought from Cell Signaling Technology, Inc. (Danvers, MA). Primers were purchased from Thermo Fisher Scientific (Carlsbad, CA). P2X7R siRNA and control siRNA (ON-TARGETplus siRNA) were purchased from Dharmacon, General Electric (Pittsburgh, PA). A740003 and KN-62 was purchased from Tocris Biosciences (Minneapolis, MA).

In vitro BBB model

Primary cultures of RBMECs derived from the brain of adult Sprague Dawley rat were purchased from the Cell Applications Inc. (San Diego, CA). RBMECs were initially grown on 0.05% fibronectin-coated cell culture dishes, using the RBMEC medium in a cell culture incubator (95% O_2, 5% CO_2 at 37°C). Primary cultures of

HBMECs derived from the normal human brain cortex were purchased from the Cell systems (Kirkland, WA). HBMECs were initially grown on attachment factor-coated cell culture dishes using CSC complete medium in a cell culture incubator (95% O_2, 5% CO_2 at 37°C). RBMECs and HBMECs were treated with 0.25% trypsin-EDTA for cell detachment. Detached cells were then grown on fibronectin/attachment factor-coated Transwell® inserts, chamber slides or 100 mm dishes for experimental purposes. RBMEC/HMBEC passages 5-10 were chosen for all the experiments.

Animals and surgeries

C57BL/6 mice (25-30 g) were purchased from Charles River Laboratories (Wilmington, MA). P2X7R knockout animals (male and female) were bought from Jackson Laboratories (Boston, MA) and bred at Texas A&M Institute for Genomic Medicine facility. C57BL/6 animals were maintained at the Texas A&M University Health Science Center College of Medicine and Baylor Scott and White Health animal facility on a 12:12 hour dark/light cycle, with free access to food and water. The room temperature was maintained at 25° ± 2°C. Surgical and experimental procedures used in this study were conducted after approval by the Institutional Animal Care and Use Committee. The facility is approved by the Association for Assessment and Accreditation of Laboratory Animal Care International in accordance with the National Institutes of Health guidelines.

Craniotomy procedure

The head of the animal was shaven and the surgical site on the surface of the head was cleaned with an alcohol wipe. Lubricating ointment was applied to the eyes. Midline incision on the scalp helps to remove the skin from top of the skull exposing the sagittal suture, bregma and lambda. A circular craniotomy window, 3-4 mm in diameter was made on ipsilateral hemisphere, between lambda and bregma using a microdrill. The resulting bone flap was removed. Sham animals received only craniotomy surgery, while TBI injury group receives brain injury via controlled cortical impactor following craniotomy procedure.

Controlled cortical impactor

These studies employ Benchmark™ Stereotaxic Impactor from Leica, for inflicting the TBI in mice. Following craniotomy procedure as described above, the animal was then mounted on the stereotaxic frame. An impactor probe of 3 mm diameter was used to impact the exposed part of the brain. The depth of the injury was used to determine the intensity of the injury. Settings for mild TBI used in this study are: 2 millimeters depth, 0.5 meters/second velocity and 100 milliseconds contact time as described in Chen et al, 2014 [88].

Treatments

KN-62 at a dose of 10 mg/kg was used for acute drug administration studies. This dose was chosen based on the studies done in rats, which demonstrated that

intravenous injection of KN-62 at 10 mg/kg, did not alter systemic arterial pressure of heart rate [142] and hence was a reasonable choice for our mice studies *in vivo*. KN-62 is a non-competitive antagonist of the P2X7R receptor, which also binds directly to the calmodulin binding site of the CaMKII (calcium-calmodulin-dependent protein kinase type II). KN-62 was administered via the tail vein along with Evans blue injection and allowed to circulate for 30 minutes prior to TBI.

Monolayer permeability assays

HBMECs or RBMECs were grown on fibronectin-coated Transwell® inserts as monolayers for 72-96 hours and regularly checked for confluency. Monolayers were initially exposed to phenol red free DMEM for 45 minutes to an hour. DMEM treated cells were then pretreated with P2X7R inhibitor, A740003 (100 μM; 30 minutes) and subsequently with Bz-ATP. At the end of the study, FITC labeled dextran-10 kDa (5 mg/mL; 30 minutes) was applied to the luminal compartment. One hundred microliters of sample was collected from the abluminal compartment at the end of 30 minutes and measured fluorometrically at 485 nm/520 nm (Excitation/Emission) using Fluoroskan Ascent™ FL Microplate Fluorometer and Luminometer (Vantaa, Finland).

Preliminary studies in HBMECs employed Bz-ATP treatment at a concentration of 5 mM for an hour. This experiment was repeated six times. In a separate set of experiments, minimal dose of Bz-ATP treatment to induce RBMEC monolayer hyperpermeability was determined. In this procedure, RBMECs were exposed to phenol red free DMEM for 45 minutes to an hour following which they were treated with

different concentrations of Bz-ATP ranging from 10 to 250 μM for 4 hours. Minimal dose of Bz-ATP treatment to induce RBMEC monolayer hyperpermeability was obtained. This information was then used to test the effect of P2X7R antagonist, A740003 (100 μM; 30 minutes) on Bz-ATP treatment-induced RBMEC monolayer hyperpermeability. These experiments were repeated four times.

Untreated cells served as a control group. Fluorescence intensity was plotted on the Y-axis and represented as % control. Data were expressed as mean ± % SEM and statistical differences among groups were determined by one-way analysis of variance (ANOVA) followed by Bonferroni post hoc test to determine significant differences between specific groups. A value of $p<0.05$ was considered statistically significant.

P2X7R knockdown studies

RBMECs were grown on fibronectin-coated Transwell® inserts for 24 hours and transfected with P2X7R and control siRNA at 25 nM concentration for 72 hours. Transfection was performed according to manufacturer's instructions. Transfected monolayers were then exposed to Bz-ATP (10 μM; 4 hours) and permeability was determined based on the leakage of FITC-dextran-10 kDa (5 mg/mL; 30 minutes) leakage from the luminal to the abluminal chamber. One hundred microliters of the sample was obtained from the abluminal chamber and measured fluorometrically at 485/520 nm (Excitation/Emission) using Fluoroskan Ascent™ FL Microplate Fluorometer and Luminometer.

Untreated cells were maintained as a control group. Each experiment was repeated five times. Fluorescence intensity was plotted on the Y-axis and represented as % control. Data were expressed as mean ± % SEM and statistical differences among groups were determined by one-way analysis of variance (ANOVA) followed by Bonferroni post hoc test to determine significant differences between specific groups. A value of $p<0.05$ was considered statistically significant.

Immunofluorescence localization and cytoskeletal labeling

In order to study tight junction integrity, ZO-1 junctional localization and formation of *f*-actin stress fibers were assessed. RBMECs were grown on chamber slides for overnight. The cells were pretreated with A740003 (100 μM; 30 minutes) followed by Bz-ATP (10 μM; 4 hours) treatment. The cells were then fixed in 4% paraformaldehyde in PBS for 10-15 minutes and permeabilized with 0.5% Triton-X 100 in PBS for another 10-15 minutes. Following this, the cells were blocked with 2% bovine serum albumin (BSA) in PBS for an hour at room temperature. The cells were then incubated overnight in an anti-rabbit primary antibody against ZO-1 (#617300; 1:150) in 2% BSA-PBS, followed by incubation with anti-rabbit IgG-FITC conjugated secondary antibody for an hour at room temperature. The cells were then washed and mounted using VECTASHIELD® Antifade Mounting Media with DAPI for nuclear staining.

Following this, the cells were fixed, permeabilized and blocked in 2% BSA-PBS as described earlier. The cells were then labeled with rhodamine phalloidin (1:50) in 2%

BSA-PBS for 20 minutes, washed and mounted using VECTASHIELD® Antifade Mounting Media containing DAPI for nuclear staining.

RBMECs were visualized and scanned at a single optical plane with an Olympus Fluoview 300 Confocal Microscope (Center Valley, PA) with a PLA PO 60X water immersion objective. Untreated cells served as control. Each experiment was repeated four times.

Quantitative real time-PCR

RBMECs were grown on 100 mm cell culture dishes. The total RNA was then extracted using TRIzol® reagent according to the manufacturer's instructions. RNA concentration and quality were determined by employing the ratio of absorbance at 260/280 nm using Biotek Synergy Hybrid Spectrophotometer (Winooski, VT). Reverse transcription was performed using the SuperScript® IV First-Strand Synthesis System. Quantitative real time PCR was performed using the RT² SYBR Green Fluor qPCR Mastermix with the following primer pairs for ZO-1: Forward primer: 5′-CCTCTGATCATTCCACACAGTC-3′, Reverse primer: 5′-TAGACATGCGCTCTTCCTCTCT-3′, MMP-9: Forward primer: 5'-GGCTAGGCTCAGAGGTAA-3', Reverse primer: 5'-GACGTTGTGTGAGTTCCAG-3' and GAPDH: Forward primer: 5′-AATGTATCCGTTGTGGATCT-3′, Reverse primer: 5′-CAAGAAGGTGGTGAAGCAGG-3′ were used. Real-time PCR detection was carried out using Stratagene Mx3000P qPCR System, Agilent Technologies (La Jolla, CA), using 1 μL of cDNA for 10 minutes at 95°C, followed by 40 cycles of 15 sec

at 95°C for denaturation and 1 min at 60°C for annealing. Relative abundances of target genes were calculated by normalizing Ct values to endogenous control glyceraldehyde 3-phosphate dehydrogenase (GAPDH).

Cells were divided into control (untreated), B-ATP (10 μM; 4 hours) treatment alone, pretreatment with A740003 (100 μM; 30 minutes) followed by Bz-ATP (10 μM; 4 hours) and A740003 (100 μM; 30 minutes) alone. Each experiment was repeated three times. Relative mRNA expression of ZO-1 was obtained by normalizing the C_t values to the endogenous control GAPDH for each repeat. Normalized C_t values were expressed as mean ± SEM. Statistical differences among groups were determined by one-way analysis of variance (ANOVA) followed by Bonferroni post hoc test to determine significant differences between specific groups. A value of $p<0.05$ was considered statistically significant.

Western blot assays

Western blot analysis was performed to investigate expression of ZO-1 in RBMECs. Cells were divided into control (untreated) and Bz-ATP (10 μM; 4 hours) treatment groups. Following treatments, the cells were washed twice in ice-cold PBS and incubated in ice-cold cell lysis buffer (1X) along with protease inhibitor cocktail (1X) for 5 minutes in cell culture dishes. The cells were then scraped, sonicated and centrifuged at 14,000*g* for 10 minutes at 4°C. Supernatant was collected from the extracts and protein concentration was determined using a protein assay kit. Equal amounts of total protein (50 μg) were separated by sodium dodecyl sulphate-

polyacrylamide gel electrophoresis (SDS-PAGE) on 10% Bis-Tris precast gels at constant voltage (145 V) for 180 minutes. Proteins were then transferred onto the nitrocellulose membrane at constant voltage (30 V) for overnight and the membranes were blocked using 5% nonfat dry milk in Tris-Buffered Saline (TBS) with 0.05% Tween-20 for 3 hours and subsequently incubated with primary mouse monoclonal anti ZO-1 antibody (1:250 dilution). Membranes were washed thrice in TBS-T and incubated with a goat anti-mouse IgG-HRP conjugated secondary antibody for an hour. After washing, the immunoblots were visualized by ECL Western Blotting Substrate. Untreated cells served as control. The loading of equal amount of protein sample was verified by assessing β-actin protein expression used as an internal control. Each experiment was repeated four times.

Cell viability studies

An EZViable™ Calcein AM Cell Viability Assay Kit (Fluorometric) was used to quantify the number of viable cells. Calcein AM is a non-fluorescent, hydrophobic compound that easily penetrates intact and live cells. Hydrolysis of the calcein AM by intracellular esterase produces a hydrophilic, strongly fluorescent compound that is retained in the cell cytoplasm, which can be measured at 485/530 nm (Excitation/Emission).

For this study, equal numbers of RBMECs were grown on a sterile black 96 well trays. When the cells reached confluency, growth media was discarded and the cells were washed in PBS and pre-exposed to phenol red-free medium for 1 hour. Cells were

divided into control (untreated), Bz-ATP treatment at 10 and 50 μM for 4 hours. Hydrogen peroxide (100 μM; 4 hours) was used as a positive control. Following treatments, the cells were then exposed to calcein buffer solution (calcein AM: calcein dilution buffer in 1:500 dilution) and incubated at 37°C for 30 minutes and a fluorometric reading was obtained.

Each experiment was repeated five times. Fluorescence intensity was plotted on the Y-axis and represented as % control. Data were expressed as mean ± % SEM and statistical differences among groups were determined by one-way analysis of variance (ANOVA) followed by Bonferroni post hoc test to determine significant differences between specific groups. A value of $p<0.05$ was considered statistically significant.

Intravital microscopy imaging

C57BL/6 mice (25-30 g) were anesthetized with urethane, i.p. injection (2 mL/kg body weight) followed by FITC-dextran-10 kDa, i.v. injection (50 mg/mL; 100 μL). FITC-dextran was allowed to circulate in the animal for 5 minutes prior to performing sham surgery (only craniotomy) or TBI using a controlled cortical impactor. Surgical site was then cleaned and a cover glass was placed on the surgical site with the help of super glue. The animal was then placed under a Nikon intravital microscope and the images were captured at 30, 50, and 70 minutes using a 40X objective. Vessels ranging from 20-40 μm were only chosen for imaging pial microcirculation using FITC imaging cube with emission wavelength of 525 nm.

FITC-fluorescence intensity values were obtained by choosing a small region in the intravascular (Ii) and extravascular space (Io) and dividing it by the area. The ratio of average extravascular to intravascular FITC-intensity values were obtained and normalized to the baseline ratio obtained at 30 minutes and plotted on the Y-axes. Mean ± SEM at different time points 30, 50 and 70 minutes were plotted on the X-axis. Each group consisted of five animals. Statistical differences among groups were determined by two-way analysis of variance (ANOVA) followed by Bonferroni post hoc test to determine significant differences between specific groups. Significant differences between the specific groups were further confirmed by repeated measures ANOVA for 95% confidence interval followed by Tukey post hoc test. If the 95% confidence interval does not overlap with 0, then the difference between group means is significant as seen for the comparisons between WT-sham and WT-TBI animals or WT-TBI and KO-TBI animals. A value of $p<0.05$ was considered statistically significant.

Evans blue extravasation assays

Evans blue dye binds to the albumin in the blood enabling us to study vascular leakage into the extravascular tissue following TBI when the dye is extracted and measured fluorometrically. C57BL/6 mice (25-30 g) were anesthetized with urethane, i.p. injection (2 mL/kg body weight) followed by Evans blue dye, i.v. injection (2% wt/vol in saline; 4 mL/kg body weight). Evans blue was allowed to circulate in the animal for 30 minutes prior to performing sham surgery (only craniotomy) or TBI using controlled cortical impactor. Drug was given to the animal along with Evans blue

injection and allowed to circulate for 30 minutes as well. DMSO was used a vehicle control. Settings for mild TBI are given in the CCI procedure described above.

One-hour post-TBI, animals were transcardially perfused with sterile saline containing heparin (1000 U/mL) for at least 20 minutes. Brains were extracted and brain cortex was carefully separated and weighed. Brain cortices were then homogenized in 1 mL of 50% (wt/vol) trichloroacetic acid (TCA) in saline. Homogenate was then centrifuged at 6,000*g* for 20 minutes at 4°C. Supernatants were extracted and further diluted in 3 parts of ethanol (1:3; 50% TCA: 95% ethanol). Samples were then quantitated fluorometrically at 620/680 nm (Excitation/Emission) or colorimetrically at 610 nm using Biotek Synergy Hybrid H1 spectrophotometer (Winooski, VT). Evans blue amount in the samples was evaluated using external standards for Evans blue ranging from 50-1000 ng/mL, prepared in same solvent (1:3; TCA: 95% ethanol).

To study the effect of P2X7R gene deletion on TBI-induced BBB hyperpermeability, in the initial studies, P2X7R-/- and wild type animals were subjected to TBI as described above. Each group consisted of four animals. Statistical differences among the groups were determined by student's *t*-test. Later studies employed P2X7R-/- and wild type animals, which were then divided into sham (only craniotomy) and mild TBI injury groups. In this study each group consisted of nine animals. Statistical differences among groups were determined by one-way analysis of variance (ANOVA) followed by Bonferroni post hoc test to determine significant differences between specific groups. A value of $p<0.05$ was considered statistically significant.

In order to study, the effect of a pharmacological inhibitor of P2X7R on TBI-induced BBB hyperpermeability, the drug KN-62 was used. For these studies, animals were grouped into a sham (only craniotomy), a Vehicle + Sham group (DMSO vehicle injection followed by craniotomy), a Vehicle + TBI group (DMSO vehicle injection followed by mild TBI), and a KN-62 + TBI group (KN-62 [10 μg/gram body weight] followed by mild TBI). Each group consisted of five animals. Brain tissue was collected, extracted and the amount of Evans blue dye was measured as described above. Evans blue amount in the samples were expressed as ng/per brain cortex ± SEM. Statistical differences among groups were determined by one-way analysis of variance (ANOVA) followed by Bonferroni post hoc test to determine significant differences between specific groups. A value of $p<0.05$ was considered statistically significant.

RESULTS

P2X7R inhibition attenuates Bz-ATP-induced endothelial cell hyperpermeability

RBMEC monolayers were pretreated with P2X7R inhibitor, A740003 (100 μM; 30 minutes) to confirm the contribution of P2X7R in mediating Bz-ATP (5 mM; 1 hour)-induced endothelial cell hyperpermeability. Bz-ATP treatment increased monolayer hyperpermeability significantly, while pretreatment with A740003 significantly attenuated Bz-ATP-induced hyperpermeability (p <0.05; Figure 26). Permeability was assessed by monolayer permeability assays as described earlier. This experiment was performed in HBMECs as preliminary studies to confirm the hypothesis. Each experiment was repeated six times.

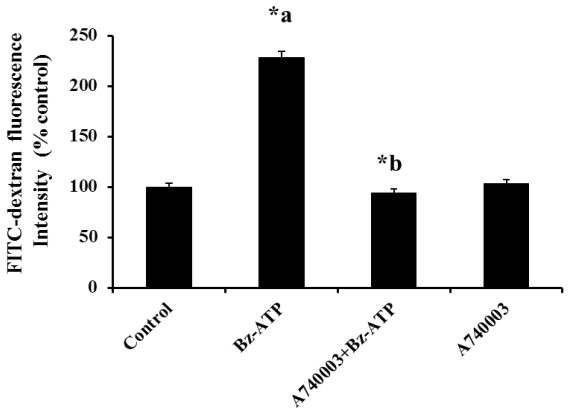

Figure 26: A740003 pretreatment attenuates Bz-ATP treatment-induced monolayer hyperpermeability in HBMECs (n=6; $p<0.05$). Monolayer permeability is expressed as a percentage control of FITC-dextran-10 kDa fluorescence intensity, plotted on the Y-axis. Data are expressed as mean ± % SEM. '*a' indicates significant increase compared to the control; '*b' indicates significant decrease compared to the Bz-ATP treatment group.

Bz-ATP treatment induces endothelial cell monolayer hyperpermeability, alters ZO-1 junctional localization, and decreases ZO-1 protein expression

Rat brain endothelial cell monolayers were treated with Bz-ATP at different concentrations varying from 10 μM to 250 μM for 4 hours. Bz-ATP treatment significantly increased endothelial cell hyperpermeability from 10 μM up to 250 μM (p <0.05; Figure 27 A). Hyperpermeability was evidenced by the increase in the FITC-dextran-10 kDa leakage to the lower chamber of the Transwell® insert. Four hours of Bz-ATP treatment was chosen as the earlier time point to induce monolayer hyperpermeability (2-3 hours did not show any significant increase in permeability from

our preliminary studies). Based on this information, we employed Bz-ATP treatment at 10 μM concentration for 4 hours in RBMECs.

In order to study the changes in integrity of BBB tight junctions, immunofluorescence of tight junction protein, ZO-1 was performed following Bz-ATP treatment. Bz-ATP (10 μM; 4 hours) treatment induced ZO-1 junctional discontinuity (white arrows; Panel 27 B) and decreased ZO-1 protein expression (Panel 27 C) compared to the untreated control cells.

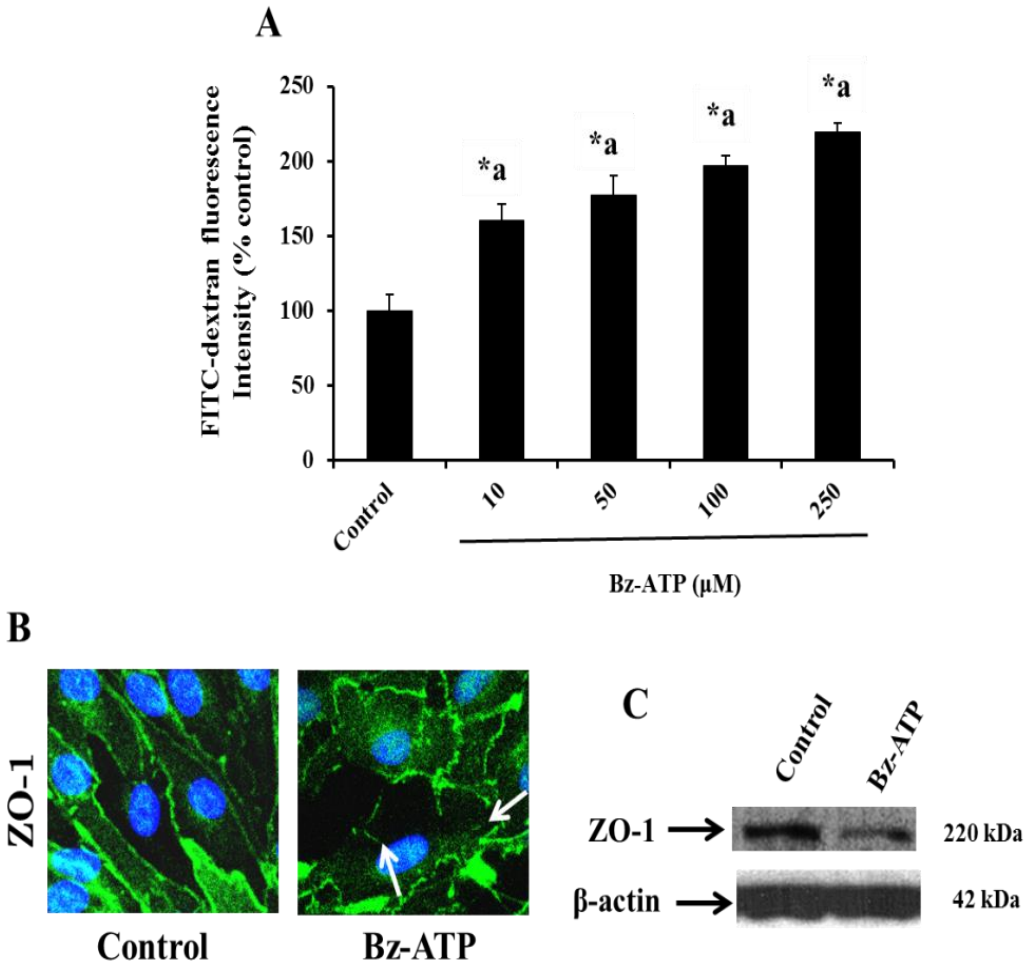

Figure 27: Bz-ATP treatment induces monolayer hyperpermeability, ZO-1 junctional disruption and decreases ZO-1 protein expression. Monolayer permeability was expressed as a percentage control of FITC-dextran-10 kDa fluorescence intensity, plotted on the Y-axis (figure A; n=4). Data are expressed as mean ± % SEM. '*a' indicates significant increase compared to the control group. $p<0.05$ is considered as statistically significant.

Bz-ATP treatment-induced ZO-1 junctional disruption is demonstrated by immunofluorescence localization of ZO-1 (figure B; n=4). Bz-ATP treatment reduces total ZO-1 protein expression as shown by western blot studies in rat brain endothelial cells (figure C; n=4).

P2X7R inhibition attenuates Bz-ATP-induced endothelial cell hyperpermeability

Bz-ATP (10 μM; 4 hours) treatment-induced endothelial cell monolayer hyperpermeability significantly, while pretreatment with A740003 (100 μM; 30 minutes) attenuated Bz-ATP-induced hyperpermeability significantly (p <0.05; Figure 28).

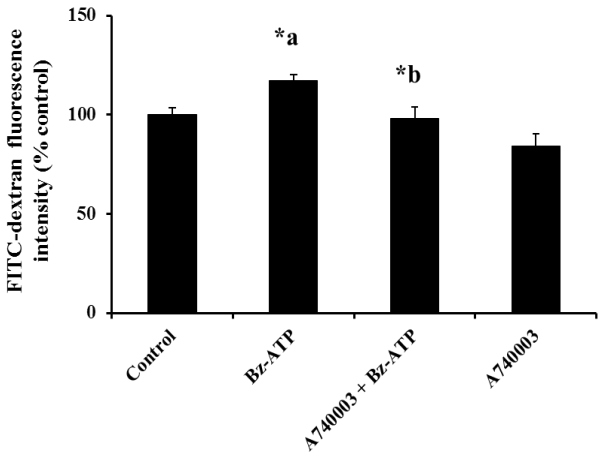

Figure 28: A740003 pretreatment attenuates Bz-ATP treatment-induced monolayer hyperpermeability in RBMECs (n=4; p<0.05). Monolayer permeability is expressed as a percentage control of FITC-dextran-10 kDa fluorescence intensity, plotted on the Y-axis. Data are expressed as mean ± % SEM. '*a' indicates significant increase compared to the control group; '*b' indicates significant decrease compared to the Bz-ATP treatment group.

P2X7R knockdown attenuates Bz-ATP-induced endothelial cell hyperpermeability

Bz-ATP (10 μM; 4 hours) treatment-induced monolayer hyperpermeability was blocked in P2X7R transfected (25 nM; 72 hours) monolayers (Figure 29, p <0.05).

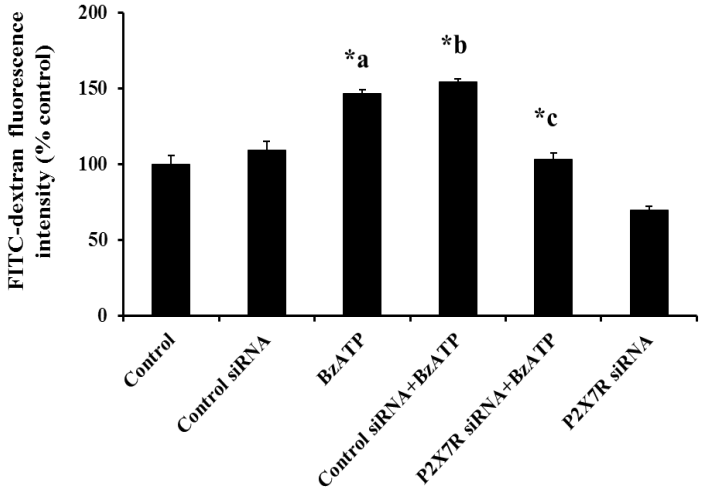

Figure 29: Knockdown of P2X7R by siRNA attenuates Bz-ATP treatment-induced monolayer hyperpermeability (n=5; p<0.05). Monolayer permeability is expressed as a percentage control of FITC-dextran-10 kDa fluorescence intensity, plotted on the Y-axis. Data are expressed as mean ± % SEM. '*a' indicates significant increase compared to the control group; '*b' indicates significant increase compared to the control siRNA treatment group and '*c' indicates significant decrease compared to the control siRNA+ Bz-ATP treatment group.

P2X7R inhibition protects against Bz-ATP-induced loss of tight junction integrity and *f*-actin stress fiber formation

RBMECs were processed for immunofluorescence localization of tight junction protein, ZO-1. Bz-ATP treatment (10 μM for 4 hours and 5 mM for 1 hour)-induced ZO-1 junctional discontinuity (white arrows; Panel 30 A and B) compared to the control cells. Pretreatment with A740003 (100 μM; 30 minutes) decreased Bz-ATP-induced loss of ZO-1 at the tight junctions. Panel A represents the data from higher concentration of Bz-ATP and panel B represents the data from lower concentration of Bz-ATP

For studying the changes in actin cytoskeletal assembly, rhodamine phalloidin labeling technique was performed. Bz-ATP (10 μM for 4 hours and 5 mM for 1 hour) treatment-induced *f*-actin stress fiber formation (white arrows; Figure 30 C and D) was reduced following pretreatment with A740003 (100 μM; 30 minutes). The data from the high concentration of Bz-ATP treatment (5 mM; 1 hour) is shown in the Figure 30, panel C, while panel D shows data from the study where Bz-ATP treatment at 10 μM was done for 4 hours.

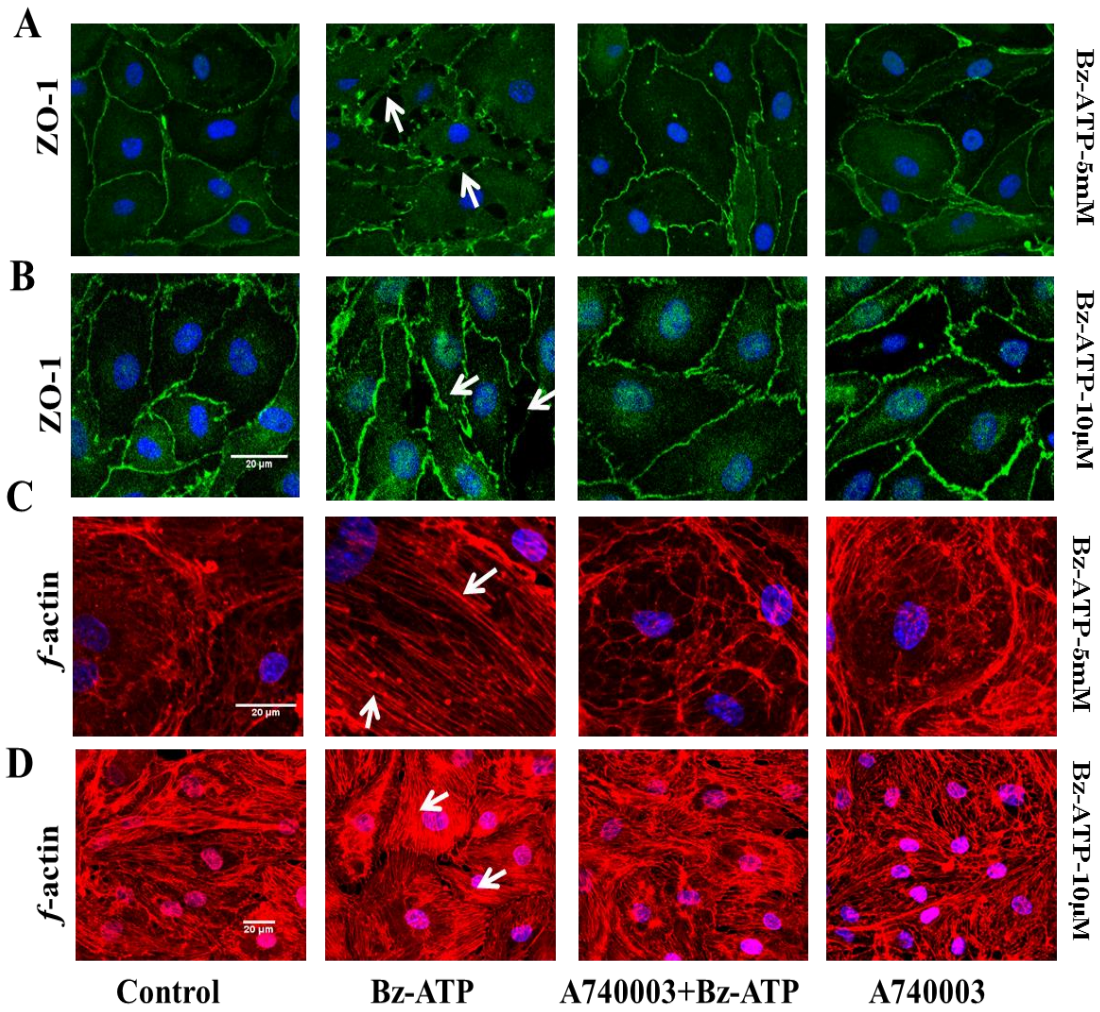

Figure 30: Bz-ATP treatment-induced ZO-1 junctional disruption and *f*-actin stress fiber formation is reduced by pretreatment with A740003. Immunofluorescence localization of ZO-1 (panel A and B) and rhodamine phalloidin labeling of actin cytoskeleton (panel C and D) are shown in the figure. Bz-ATP treatment-induced ZO-1 junctional disruption (white arrows; panel A and B; n=4) and *f*-actin stress fiber formation (white arrows; panel C and D; n=4) were preserved on pretreatment with A740003. Five millimolar of Bz-ATP treatment for an hour is shown in panel A and C; 10 μM Bz-ATP treatments for 4 hours are shown in panel C and D.

Bz-ATP treatment does not induce ZO-1 mRNA expression

RT-PCR study showed that Bz-ATP treatment at 10 μM for 4 hours did not alter ZO-1 or MMP-9 mRNA expression (Figure 31).

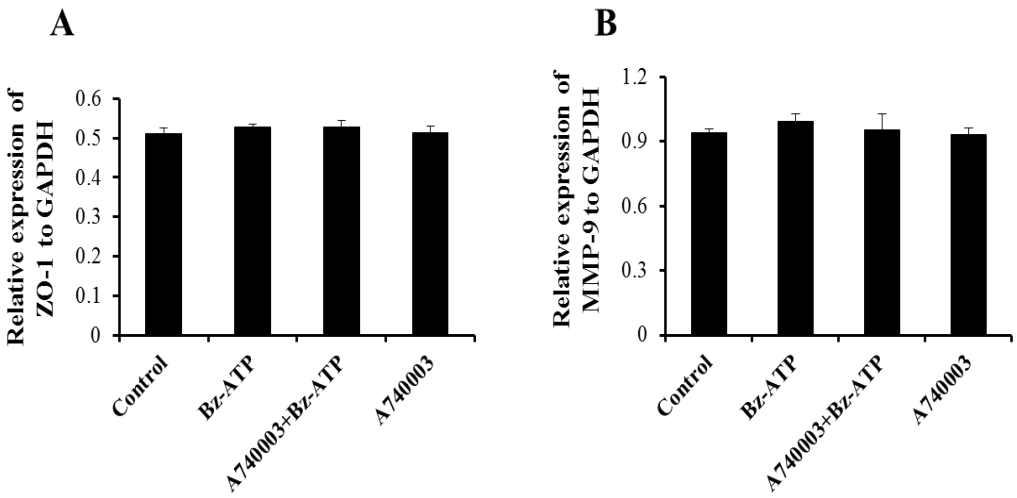

Figure 31: Bz-ATP treatment does not induce ZO-1 mRNA expression. RT-PCR data are expressed as relative expression of ZO-1 normalized to GAPDH is plotted on Y-axis. Data are represented as mean ± SEM (n=3).

Bz-ATP treatment does not induce cell death in endothelial cells

Bz-ATP treatment at 10 μM for 4 hours did not cause any significant change in the number of viable cells as shown in Figure 32. Hydrogen peroxide (100 μM; 4 hours) used as a positive control decreased cell viability significantly.

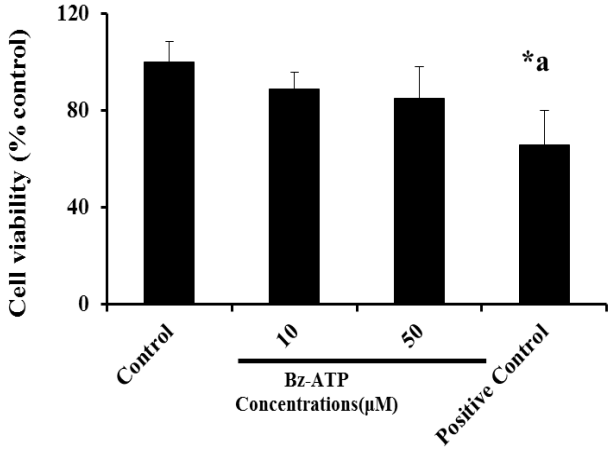

Figure 32: Bz-ATP treatment does not affect cell viability. Hydrogen peroxide was used as a positive control (n=5; $p<0.05$). Cell viability is expressed as a percentage control of fluorescence intensity, plotted on the Y-axis. Data are expressed as mean ± % SEM. '*a' indicates significant decrease compared to the control group.

Genetic ablation of P2X7R provides protection against TBI-induced FITC-dextran leakage

The effect of TBI-induced FITC-dextran-10 kDa (50 mg/mL) leakage in pial microvasculature of P2X7R -/- and wild type animals was assessed using intravital microscopy imaging as described above. Mice were studied at various time points (30, 50, and 70 minutes as shown in Figure 34) following TBI/sham injury. The wildtype mice subjected to TBI showed a significant increase in FITC-dextran extravasation compared to P2X7R -/- mice. $p<0.05$, n=5, Figure 34).

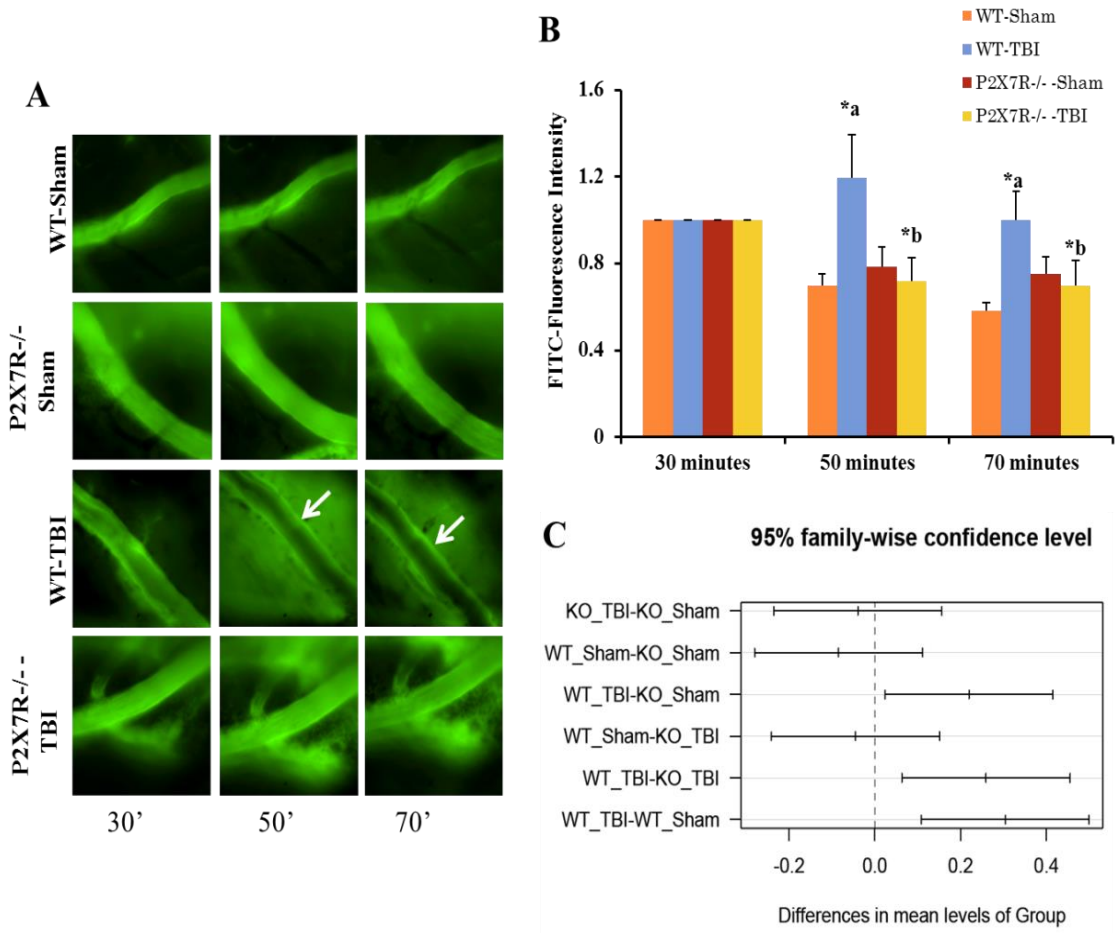

Figure 33: Effect of TBI on BBB permeability (studied by FITC-dextran leakage) in P2X7R knockout mice. Figure A demonstrates that P2X7R knockout animals subjected to TBI show a decrease in FITC-dextran-10 kDa leakage into the extravascular space of the pial vessel compared to the wild-type animals (shown by white arrows) subjected to TBI. Quantitative representation of FITC-fluorescence intensity values are shown in Figure B. Figure C represents the statistical analysis by repeated measures ANOVA using 95% confidence intervals, followed by Tukey HSD post hoc test for the FITC-fluorescence intensity values. Images using intravital microscopy were taken at 30, 50, and 70 minutes after inducing TBI. Each group had five animals. Ratio of FITC-dextran-10 kDa in the extravascular space to intravascular space relative to 30 minutes baseline is plotted on Y-axis. Data are expressed as mean FITC-fluorescence intensity ± SEM. '*a' indicates significant increase compared to the WT-sham injury group within the time point, '*b' indicates significant decrease compared to the WT-TBI group within the time point.

Genetic ablation of P2X7R provides protection against TBI-induced Evans blue leakage

Effect of TBI-induced Evans blue leakage was studied in P2X7R -/- knockout and wild type mice using the Evans blue extravasation assays as described earlier. Evans blue leakage was assessed colorimetrically at 610 nm. TBI-induced BBB hyperpermeability was significantly attenuated in P2X7R -/- mice compared to wild type mice (Figure 33 A & B, $p<0.05$).

Preliminary studies were performed using only four animals as shown in figure 33 A. A thorough study using all groups with nine animals per group is shown in figure 33 B.

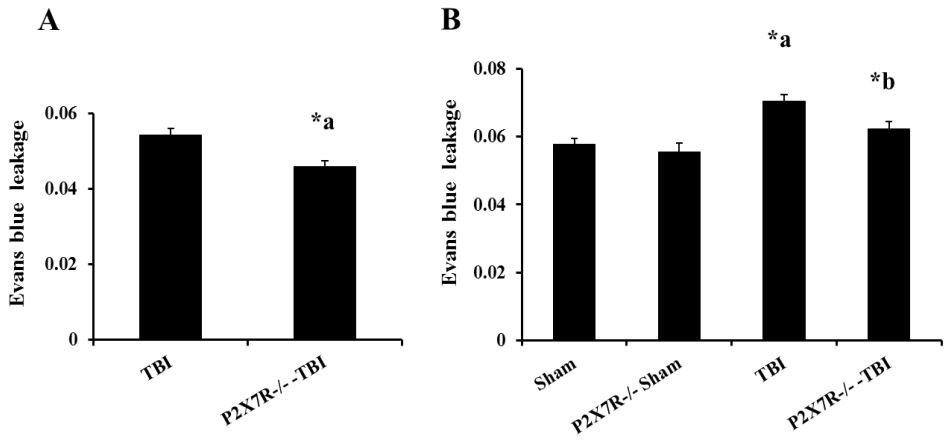

Figure 34: Effect of TBI on BBB permeability (studied by Evans blue leakage) in P2X7R knockout mice. P2X7R knockout mice demonstrated significantly reduced Evans blue leakage compared to the wild-type animals subjected to the TBI (figure A; n=4; p <0.05). Figure B shows the results of a separate study that further confirms the results in Figure A (n=9; p <0.05). Data are expressed as absorbance ± SEM. '*a' in figure A represents significant decrease compared to the wild type animals subjected to TBI. '*a' in figure B indicates significant increase compared to the wild-type sham animals; '*b' indicates significant decrease compared to wild-type animals subjected to TBI.

KN-62 pretreatment attenuates TBI-induced BBB hyperpermeability

Mice subjected to TBI demonstrated significant increase in Evans blue leakage compared to the sham animals. Pretreatment with KN-62 attenuated mild TBI-induced Evans blue leakage into the brain tissue (Figure 35 A & B; p <0.05). Evans blue leakage was assessed fluorometrically at 620/680 nm (Excitation/Emission). This study suggests that P2X7R inhibition as a potential drug target against BBB hyperpermeability that occurs following TBI.

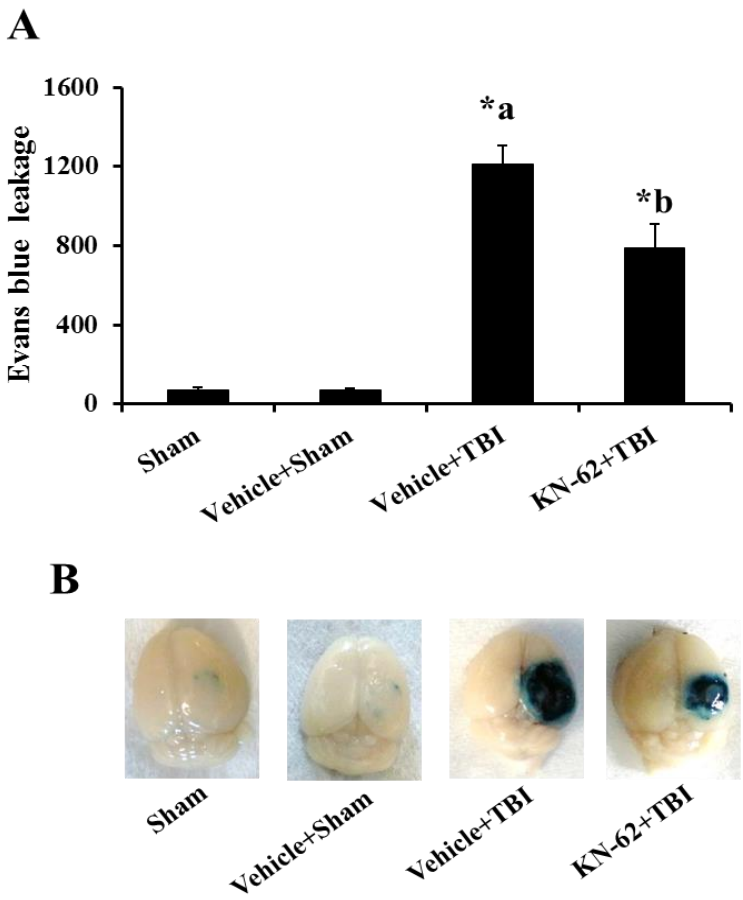

Figure 35: KN-62 pretreatment attenuates TBI-induced BBB hyperpermeability studied by Evans blue dye extravasation method. Vehicle control group subjected to TBI demonstrated significant increase in Evans blue leakage compared to the sham injury group (figure A; $p<0.05$). KN-62 (10 μg /gram body weight of the animal) pretreatment significantly attenuated TBI-induced Evans blue leakage into the extravascular tissue space (figure A; $p<0.05$). Pictorial representation of the brain tissue from various groups is shown in figure B. Each group consisted of five animals. Sham injury group is used as the baseline for all comparisons. Data are expressed as ng/brain cortex ± SEM. '*a' indicates significant increase compared to the sham injury group, '*b' indicates significant decrease compared to the vehicle + TBI group.

DISCUSSION

The major findings of this study are: 1) extracellular ATP induces the loss of tight junctional integrity, enhances *f*-actin stress fiber formation and BBB hyperpermeability via P2X7R receptors *in vitro*, 2) ATP/P2X7R-mediated loss of barrier function involves a decrease in ZO-1 protein expression but not mRNA expression and is independent of endothelial cell death, and 3) genetic and pharmacological inhibition of P2X7R provides protection against TBI-induced BBB hyperpermeability in a mouse model of TBI.

ATP is traditionally known as the energy source of the cell that drives all the cellular functions. Various pathological conditions like inflammation, ischemia and trauma lead to an increase in extracellular ATP [132]. ATP plays an important role in inflammation by aiding in the processing and release of pro-inflammatory cytokines like IL-1β and IL-6 [133]. However, the effect of ATP on IL-1β and IL-6 expression in brain endothelial cells are not clearly known and remains to be explored. ATP in extracellular space plays an important role in neurotransmission and inflammatory processes [133]. Millimolar concentrations of extracellular ATP are generated following local trauma leading to temporary increase in local nucleotide concentrations to >100 μM [143]. ATP is rapidly degraded in the extracellular environment by various cellular enzymes such as ecto-nucleotidases, ecto-nucleotide pyrophosphate, nucleotidase, phosphatases, and transphosphorylating enzymes like nucleoside diphosphokinase and adenylyl kinase, which breakdown ATP to ADP, AMP and adenosine [133; 144; 145]. Half-life of ATP is only a few seconds once it is released into the extracellular space, which makes its

detection further difficult [146]. For these reasons we employed Bz-ATP a potent and stable analogue of ATP in our *in vitro* studies.

ATP release that occurs following mechanical and biochemical stimulation regulates various cellular functions via purinergic receptors [147; 148]. P2X7R are involved in various cellular mechanisms like membrane permeabilization, caspase activation, cytokines release, cell proliferation and apoptosis [149]. The contribution of ATP-induced P2X7R is well studied in astrocytes, glial cells, and other immune cells of the brain; however, very little is known about its contribution in the brain endothelial cells [150]. Our results demonstrate that Bz-ATP promotes BBB hyperpermeability *in vitro* and ATP-induced hyperpermeability can be attenuated by pharmacological inhibition of P2X7R or by P2X7R mRNA silencing. Thus, our studies provide novel insight into the mechanisms by which ATP-sensitive P2X7R promote brain endothelial barrier dysfunction.

Pharmacologically, P2X7Rs are activated by high concentrations of ATP (>100 μM) and Bz-ATP has 30 times greater potency compared to ATP. EC_{50} of Bz-ATP is ~20 μM [150]. Hence, the lowest dose of Bz-ATP at a concentration of 10 μM was chosen in our *in vitro* studies. In our preliminary studies, exposure of Bz-ATP to endothelial monolayers for 2-3 hours did not significantly induce monolayer hyperpermeability. So, we chose a higher time period for Bz-ATP exposure at 4 hours. An interesting feature of P2X7R is its differential sensitivity across the species. For example, rat P2X7R are 10 fold more sensitive to Bz-ATP and ATP compared to mouse P2X7R [144]. Similarly, high concentrations of extracellular ATP induces cell death

[151]. Hence, the ATP concentration used in a particular study should be based on the specific features of that study and also the source of cell types used in the study. In our *in vitro* studies we employed A740003 a potent and highly competitive antagonist of P2X7R that effectively blocks both human and rat P2X7 receptors [152].

In our *in vivo* studies we have used KN-62, a well-studied pharmacological inhibitor of P2X7R which also acts as an inhibitor of the calcium dependent enzyme CaMKII. Stretch-induced TBI injury in mouse brain endothelial cells demonstrated elevated levels of intracellular calcium levels *in vitro* [153]. Inhibition of intracellular calcium by CaMKII strongly suppresses endothelial permeability in immortalized rat brain endothelial cells [154]. This information was critical in our studies to determine the effect of KN-62 (piperazine-derived antagonist that blocks CaMKII) on TBI-induced BBB hyperpermeability in mice. Our studies thus indicate that KN-62 pretreatment attenuates TBI-induced BBB hyperpermeability by P2X7R and the role of CaMKII cannot be ruled out. The relationship between P2X7R and CaMKII pathways in mediating BBB dysfunction and hyperpermeability was not studied here and needs further investigation.

At a cellular level, the cytoskeleton is critical to the cellular structure and also regulates various signal transduction processes in endothelial cells. In previous studies, Bz-ATP treatment is shown to alter *f*-actin cytoskeletal assembly and activate various cellular functions like exocytosis and cell migration [155]. Our studies also demonstrated an increase in *f*-actin stress fiber formation; however, the significance of this increase and how it regulates various cellular functions including barrier

functions/permeability remains to be explored in the context of ATP-P2X7R interactions. Studies conducted in rat parotid acinar cells reveal that extracellular ATP increases the activity and phosphorylation of protein kinase D (PKD) by acting via P2X7R. ATP and Bz-ATP treatment (P2X7R agonist) also increases tyrosine phosphorylation of protein kinase-Cδ (PKCδ) and extracellular signal-regulated protein kinase (ERK) activity in a PKC dependent manner [156]. In addition, PKC-mediated alterations in ZO-1 are known.

While our studies described in the previous chapters suggest that proteolytic enzymes such as MMP-9 and calpains are important in regulating barrier dysfunction, future studies should aim to understand the mechanisms by which ATP induces BBB dysfunction and hyperpermeability with a focus on specific protein kinase (C, D, etc.) or ERK and their relationship to P2X7R. In addition to the possibility of MMP-9 and calpain involvement, understanding how ATP treatment alters the phosphorylation status of the tight junctions may provide a rationale for the ZO-1 decrease observed in the present studies.

In conclusion, our results from *in vitro* and *in vivo* studies clearly demonstrate a key role for P2X7R in mediating BBB hyperpermeability. Targeting the P2X7R could provide a novel and promising approach for the regulation of BBB hyperpermeability and brain edema that occurs following TBI when established in human patients.

CHAPTER V

SUMMARY AND CONCLUSIONS

Microvascular endothelial hyperpermeability, the excessive leakage of fluid and proteins that takes place at the level of the blood-brain barrier (BBB) is a significant problem associated with various vascular conditions including traumatic, hemorrhagic and ischemic injuries that occur in the brain. One of the devastating injuries that occur in the brain is traumatic brain injury (TBI). Traumatic brain injury is the leading cause of death and disability worldwide in the younger population. Annual incidence of TBI is accounted to be around 10 million people worldwide, with 5.3 million people from US alone, based on 2010 CDC statistics. Thus, the basic, translational and clinical research that leads to deeper understanding of TBI and its pathophysiology is very critical. As one of the major clinical concerns in TBI is the inability to manage the TBI-associated brain edema and elevated intracranial pressure, focus must be given to understand the mechanisms that lead to brain edema formation and identification of potential therapeutic targets.

Disruption of the BBB is the hallmark feature of the secondary injuries that occur following TBI. BBB dysfunction and the associated hyperpermeability leads to tissue vasogenic edema, elevated intracranial pressure, decreased tissue perfusion pressure, multiple organ failure, and death. Currently, there are no medications that could enhance BBB integrity and thereby retard the progression of secondary injuries following TBI. An intact BBB and optimal functioning of the BBB is critical for normal

brain functioning and brain homeostasis. At the cellular level, microvascular dysfunction of the BBB is dictated by changes in endothelial cell-cell junctions, linker molecules, and actin cytoskeleton. Hence, studying and understanding the contribution of cell adhesion molecules in BBB would provide more insight into the significance of altered BBB structure and functions. Our studies were focused on understanding the contribution of the major BBB tight junction protein, zonula occludens-1 in regulating BBB hyperpermeability by employing rat brain microvascular endothelial cells and TBI as *in vitro* and *in vivo* study models respectively.

The two main goals of this dissertation are: 1) to understand the various cellular mechanisms that lead to the loss of BBB tight junction integrity leading to hyperpermeability and 2) to identify potential therapeutic targets against TBI-induced BBB dysfunction/hyperpermeability and cerebral edema. We addressed these goals by investigating the contribution of the proteolytic enzymes that are known to increase following TBI and also target TJ proteins, such as matrix metalloproteinase-9 (MMP-9) and calpains. Furthermore, we have investigated the role of ATP-sensitive P2X7R as an upstream enhancer of these pathways. Adenosine triphosphate (ATP) that is released into the extracellular space following trauma binds and activates P2X7R. P2X7R activation is further shown to activate downstream pathways that stimulate the release of pro-inflammatory cytokines like interleukin-1 β (IL-1β). IL-1β induces adverse changes in the BBB but the cellular mechanisms are not well understood. The proteolytic enzymes MMP-9 and calpains are also shown alter the BBB in various

conditions. This information served as the basis for our hypothesis, which we tested using various *in vitro* and *in vivo* approaches and models.

The first mechanism presented in this dissertation (CHAPTER-II) emphasizes the significance of MMP-9 inhibition in regulating IL-1β treatment-induced BBB dysfunction and hyperpermeability. Contribution of MMP-9 was confirmed both by employing pharmacological MMP-9 specific inhibitors (MMP-9 inhibitor 1) and endogenous MMP-9 inhibitor (melatonin). Melatonin is recently explored as a potential MMP-9 inhibitor. Melatonin was henceforth employed to study its effect on IL-1β-induced BBB dysfunction and hyperpermeability *in vitro*. Furthermore, we have also employed melatonin as a potential agent to attenuate TBI-induced BBB hyperpermeability *in vivo* in a mouse model of TBI. Although, our studies demonstrate the significance of MMP-9-mediated mechanisms in regulating BBB dysfunction and hyperpermeability, several questions remain unanswered. Future studies should focus on understanding: 1) how MMP-9 inhibition attenuates IL-1β treatment-induced hyperpermeability; is the via tissue inhibitors of metalloproteinases (TIMPs) or is it by altering the phosphorylation status of the tight junctions via various mitogen-activated protein kinases? 2) What is the cellular mechanism by which melatonin inhibits TBI-induced BBB hyperpermeability other than via MMP-9 inhibition; are various MAPK pathways involved, and/or is the status of tight junctions altered, including ZO-1 relocalization as found in our *in vitro* studies? What is the effect of melatonin on the well-known transcription factors of MMP-9: nuclear factor kappa-light-chain-enhancer of activated B cells and activator protein-1?. Although our results support melatonin-

MMP-9 interaction as a mechanism that leads to the protection of the BBB, the multiple other roles of melatonin (anti-inflammatory, antioxidant, etc.) still remains to be studied in more detail.

The second mechanism presented in this dissertation (CHAPTER-III) emphasizes the significance of calpain inhibition in regulating IL-1β treatment-induced BBB dysfunction and hyperpermeability. Contribution of calpains in mediating BBB dysfunction and hyperpermeability were studied both by employing a pharmacological calpain inhibitor (calpain inhibitor III) and by an endogenous calpain inhibitor (calpastatin). Furthermore, we have also employed calpain inhibitor III as a potential drug to attenuate TBI-induced BBB hyperpermeability *in vivo*. These studies demonstrate the significance of calpain-mediated mechanisms in regulating BBB dysfunction and hyperpermeability; several questions remain unanswered. Future studies should aim to address: 1) the mechanisms apart from calcium and calpastatin in mediating IL-1β-induced BBB hyperpermeability, 2) the main substrates for calpains in mediating IL-1β-induced BBB hyperpermeability, 3) whether changes in actin cytoskeletal assembly as observed following IL-1β treatment involve Ras homolog gene family, member A (RhoA), Ras-related C3 botulinum toxin substrate 1 (Rac1) and cell division control protein 42 homolog (cdc42), which in turn regulate tight junction integrity, and 4) whether there is an inter-relationship between calpains and MMP-9 upregulation.

The third mechanism presented in this dissertation (CHAPTER-IV) emphasizes the significance of P2X7R in regulating ATP-induced BBB dysfunction and

hyperpermeability. Contribution of P2X7R was confirmed by employing pharmacological inhibitors for P2X7R (A740003, KN-62). We further tested the importance of P2X7R by employing global knockout mice of P2X7R to study the effect of TBI. As hypothesized, P2X7R knockout animals demonstrated attenuated TBI-induced BBB hyperpermeability compared to the wild-type animals. Furthermore, we also employed KN-62 as a potential agent to attenuate TBI-induced BBB hyperpermeability *in vivo*. These studies demonstrate the significance of P2X7R-mediated mechanisms in regulating BBB dysfunction and hyperpermeability; several questions remain unanswered. Future studies should aim to address: 1) how P2X7R-mediated mechanisms induce the release of IL-1β in BBB; is it via inflammasome or caspase-1-mediated pathways? 2) How ATP binding to P2X7R affects MMP-9 or calpain activity in the endothelial cells as well as in *in vivo* models? 3) What is the effect of KN-62 (a P2X7R inhibitor; as well as CaMKII inhibitor) on MMP-9 and calpain levels in brain endothelial cells and following TBI. Pictorial representations of the various mechanisms and their interrelationship in regulating BBB hyperpermeability following brain trauma based on our studies are shown in Figure 36.

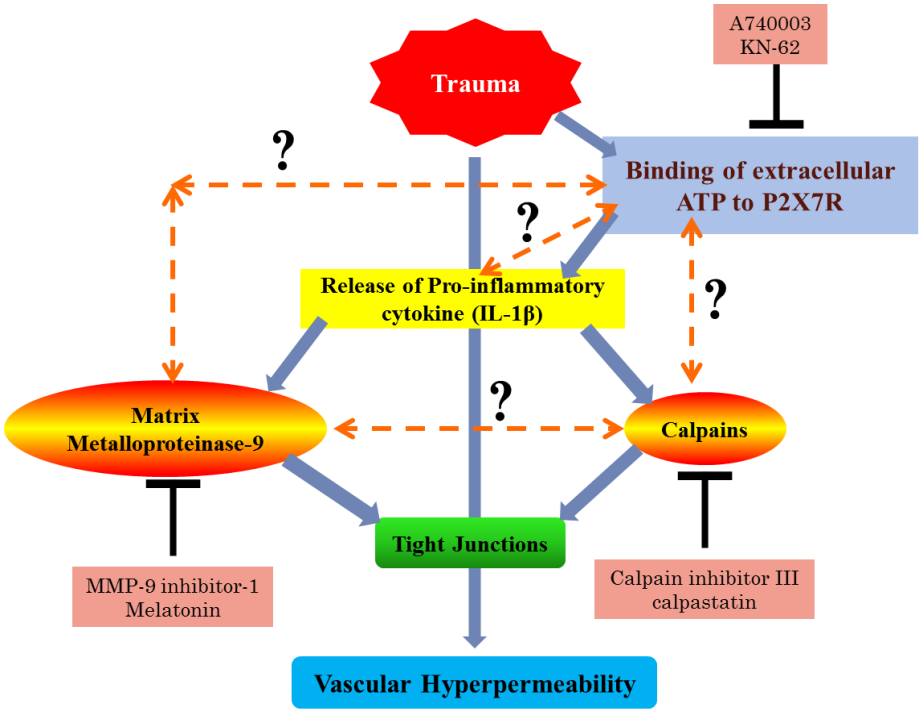

Figure 36: Mechanisms that regulate vascular hyperpermeability following brain trauma. At a structural level, the tight junctions regulate brain microvascular hyperpermeability. IL-1β is one of the main pro-inflammatory cytokine that is shown to increase following brain trauma. Our studies demonstrate that IL-1β induces matrix metalloproteinase-9 (MMP-9) and calpains activity, which in turn regulates vascular hyperpermeability by altering the tight junctional integrity. Further studies focused on employing pharmacological and endogenous inhibitors of MMP-9 (MMP-9 inhibitor 1, melatonin) and calpains (calpain inhibitor III, calpastatin) to study their effect on IL-1β-induced BBB hyperpermeability. To elucidate the pathways upstream of IL-1β; we studied the effect of extracellular ATP that is known to increase following various traumatic insults. Extracellular ATP binds to P2X7R triggering the release of IL-1β. Our studies demonstrated that pharmacological inhibition of P2X7R (A740003, KN-62) can attenuate ATP-induced BBB dysfunction and hyperpermeability. We employed melatonin, calpain inhibitor III and KN-62 as potential therapeutic agents to attenuate TBI-induced BBB hyperpermeability. Few of the potential relationships to be explored for future studies include: 1) how P2X7R-mediated mechanisms induce the release of IL-1β in brain endothelial cells, possibly via inflammasome/caspase-1-mediated pathways?, 2) how ATP binding to P2X7R affects MMP-9 or calpain activity in the endothelial cells as well as in animal models?, and 3) how are MMP-9 and calpains related; i.e., do calpains activate MMP-9 or vice-versa?.

REFERENCES

[1] Q. Shen, M. Wu, and S. Yuan, Endothelial contractile cytoskeleton and microvascular permeability. Cell health and cytoskeleton 2009 (2009) 43-50.

[2] P. Kumar, Q. Shen, C.D. Pivetti, E.S. Lee, M.H. Wu, and S.Y. Yuan, Molecular mechanisms of endothelial hyperpermeability: implications in inflammation. Expert reviews in molecular medicine 11 (2009) e19.

[3] S. Deaglio, and S.C. Robson, Ectonucleotidases as regulators of purinergic signaling in thrombosis, inflammation, and immunity. Advances in pharmacology 61 (2011) 301-32.

[4] A.D. Gean, and N.J. Fischbein, Head trauma. Neuroimaging clinics of North America 20 (2010) 527-56.

[5] Y. Xiong, A. Mahmood, and M. Chopp, Animal models of traumatic brain injury. Nature reviews. Neuroscience 14 (2013) 128-42.

[6] A.I.R. Maas, N. Stocchetti, and R. Bullock, Moderate and severe traumatic brain injury in adults. The Lancet Neurology 7 (2008) 728-741.

[7] D. Shlosberg, M. Benifla, D. Kaufer, and A. Friedman, Blood–brain barrier breakdown as a therapeutic target in traumatic brain injury. Nature Reviews Neurology 6 (2010) 393-403.

[8] S.Y. Yuan, Protein kinase signaling in the modulation of microvascular permeability. Vascular Pharmacology 39 (2002) 213-223.

[9] C.M. Miller, N.R. Boulter, S.J. Fuller, A.M. Zakrzewski, M.P. Lees, B.M. Saunders, J.S. Wiley, and N.C. Smith, The role of the P2X(7) receptor in infectious diseases. PLoS pathogens 7 (2011) e1002212.

[10] W. Dietrich, and F. Erbguth, [Increased intracranial pressure and brain edema]. Medizinische Klinik - Intensivmedizin und Notfallmedizin 108 (2013) 157-69; quiz 170.

[11] J. Guest, M. Garg, A. Bilgin, and R. Grant, Relationship between central and peripheral fatty acids in humans. Lipids Health Dis 12:79 (2013).

[12] C.J. Ek, K.M. Dziegielewska, M.D. Habgood, and N.R. Saunders, Barriers in the developing brain and Neurotoxicology. Neurotoxicology 33 (2012) 586-604.

[13] M. Bundgaard, and N.J. Abbott, All vertebrates started out with a glial blood-brain barrier 4-500 million years ago. Glia 56 (2008) 699-708.

[14] N.J. Abbott, A.A. Patabendige, D.E. Dolman, S.R. Yusof, and D.J. Begley, Structure and function of the blood-brain barrier. Neurobiology of disease 37 (2010) 13-25.

[15] N.J. Abbott, L. Ronnback, and E. Hansson, Astrocyte-endothelial interactions at the blood-brain barrier. Nature reviews. Neuroscience 7 (2006) 41-53.

[16] V. Pop, and J. Badaut, A neurovascular perspective for long-term changes after brain trauma. Translational stroke research 2 (2011) 533-45.

[17] W. Mayhan, Regulation of blood–brain barrier permeability. Microcirculation 8 (2001) 1108-1110.

[18] F. Arshad, L. Wang, C. Sy, S. Avraham, and H.K. Avraham, Blood-brain barrier integrity and breast cancer metastasis to the brain. Pathology research international 2011 (2010) 920509.

[19] S. Nag, A. Kapadia, and D.J. Stewart, Review: molecular pathogenesis of blood-brain barrier breakdown in acute brain injury. Neuropathology and applied neurobiology 37 (2011) 3-23.

[20] S.A. Liddelow, K.M. Dziegielewska, C.J. Ek, M.D. Habgood, H. Bauer, H.C. Bauer, H. Lindsay, M.J. Wakefield, N. Strazielle, I. Kratzer, K. Mollgard, J.F. Ghersi-Egea, and N.R. Saunders, Mechanisms that determine the internal environment of the developing brain: a transcriptomic, functional and ultrastructural approach. PloS one 8 (2013) e65629.

[21] B. Engelhardt, and L. Sorokin, The blood-brain and the blood-cerebrospinal fluid barriers: function and dysfunction. Seminars in immunopathology 31 (2009) 497-511.

[22] G.J. del Zoppo, Inflammation and the neurovascular unit in the setting of focal cerebral ischemia. Neuroscience 158 (2009) 972-82.

[23] S.M. Stamatovic, R.F. Keep, and A.V. Andjelkovic, Brain endothelial cell-cell junctions: how to "open" the blood brain barrier. Curr Neuropharmacology 6 (2008) 179-192.

[24] L. Paris, L. Tonutti, C. Vannini, and G. Bazzoni, Structural organization of the tight junctions. Biochimica et biophysica acta 1778 (2008) 646–659.

[25] A. Luissint, C. Artus, F. Glacial, K. Ganeshamoorthy, and C. PO, Tight junctions at the blood brain barrier: physiological architecture and disease-associated dysregulation. Fluids and barriers of the CNS 9 (2012) 23.

[26] P. Ballabh, A. Braun, and M. Nedergaard, The blood-brain barrier: an overview: structure, regulation, and clinical implications. Neurobiology of disease 16 (2004) 1-13.

[27] A.W. Vorbrodt, and D.H. Dobrogowska, Molecular anatomy of intercellular junctions in brain endothelial and epithelial barriers: electron microscopist's view. Brain Res Brain Res Rev 42 (2003) 221-242.

[28] W. Oldendorf, The blood-brain barrier. Experimental eye research 25 (1977) 177-190.

[29] R. Daneman, L. Zhou, D. Agalliu, J.D. Cahoy, A. Kaushal, and B.A. Barres, The mouse blood-brain barrier transcriptome: a new resource for understanding the development and function of brain endothelial cells. PloS one 5 (2010) e13741.

[30] P. Annunziata, C. Cioni, R. Santonini, and E. Paccagnini, Substance P antagonist blocks leakage and reduces activation of cytokinestimulated rat brain endothelium. J Neuroimmunol 131 (2002).

[31] C. Mariano, I. Palmela, P. Pereira, A. Fernandes, A.S. Falcao, F.L. Cardoso, A.R. Vaz, A.R. Campos, A. Goncalves-Ferreira, K.S. Kim, D. Brites, and M.A. Brito, Tricellulin expression in brain endothelial and neural cells. Cell and tissue research 351 (2013) 397-407.

[32] S.C. Thal, C. Luh, E.V. Schaible, R. Timaru-Kast, J. Hedrich, H.J. Luhmann, K. Engelhard, and C.M. Zehendner, Volatile anesthetics influence blood-brain barrier integrity by modulation of tight junction protein expression in traumatic brain injury. PloS one 7 (2012) e50752.

[33] A.S. Fanning, B.J. Jameson, L.A. Jesaitis, and J.M. Anderson, The tight junction protein ZO-1 establishes a link between the transmembrane protein occludin and the actin cytoskeleton. The Journal of biological chemistry 273 (1998) 29745–29753.

[34] E. Dejana, M.G. Lampugnani, O. Martinez-Estrada, and G. Bazzoni, The molecular organization of endothelial junctions and their functional role in vascular morphogenesis and permeability. Int J Dev Biol 44 (2000) 743-748.

[35] M.S. Balda, and K. Matter, Tight junctions at a glance. Journal of cell science 121 (2008) 3677-82.

[36] H. Chiba, M. Osanai, M. Murata, T. Kojima, and N. Sawada, Transmembrane proteins of tight jucntions. Biochimica et biophysica acta 1778 (2008) 588-600.

[37] G. Bazzoni, and E. Dejana, Endothelial cell-to-cell junctions: molecular organization and role in vascular homeostasis. Physiol Rev. 84 (2004) 869–901.

[38] L. Gonzalez-Mariscal, A. Betanzos, and A. Avila-Flores, MAGUK proteins: structure and role in the tight junction. Seminars in cell & developmental biology 11 (2000) 315-24.

[39] M. Furuse, Knockout animals and natural mutations as experimental and diagnostic tool for studying tight junction functions *in vivo*. Biochimica et biophysica acta 1788 (2009) 813-9.

[40] B.N. Scott, D.J. Roberts, H.L. Robertson, A.H. Kramer, K.B. Laupland, S.S. Ousman, P. Kubes, and D.A. Zygun, Incidence, prevalance and occurence rate of infection among adults hospitalized after TBI study protocol for a systemic review and meta-analysis. Syst Rev 2 (2013) 68.

[41] A.A. Hyder, C.A. Wunderlich, P. Puvanachandra, G. Gururaj, and O.C. Kobusingye, The impact of traumatic brain injuries: a global perspective. NeuroRehabilitation 22 (2005) 341–353.

[42] W.S. Pearson, D.E. Sugerman, L.C. McGuire, and V.G. Coronado, Emergency department visits for traumatic brain injury in older adults in the United States: 2006-08. The western journal of emergency medicine 13 (2012) 289-93.

[43] T.M. Sivanandam, and M.K. Thakur, Traumatic brain injury: a risk factor for Alzheimer's disease. Neuroscience and biobehavioral reviews 36 (2012) 1376-81.

[44] M.W. Greve, and B.J. Zink, Pathophysiology of traumatic brain injury. The Mount Sinai journal of medicine, New York 76 (2009) 97-104.

[45] O. Tomkins, I. Shelef, I. Kaizerman, A. Eliushin, Z. Afawi, A. Misk, M. Gidon, A. Cohen, D. Zumsteg, and A. Friedman, Blood-brain barrier disruption in post-traumatic epilepsy. Journal of neurology, neurosurgery, and psychiatry 79 (2008) 774-7.

[46] D. Strbian, P.T. Kovanen, M.-L. Karjalainen-Lindsberg, T. Tatlisumak, and P.J. Lindsberg, An emerging role of mast cells in cerebral ischemia and hemorrhage. Annals of medicine 41 (2009) 438-450.

[47] E. Neuwelt, N.J. Abbott, L. Abrey, W.A. Banks, B. Blakley, T. Davis, B. Engelhardt, P. Grammas, M. Nedergaard, J. Nutt, W. Pardridge, G.A. Rosenberg, Q. Smith, and L.R. Drewes, Strategies to advance translational research into brain barriers. The Lancet Neurology 7 (2008) 84-96.

[48] Y. Persidsky, S.H. Ramirez, J. Haorah, and G.D. Kanmogne, Blood-brain barrier: structural components and function under physiologic and pathologic conditions. Journal of neuroimmune pharmacology : the official journal of the Society on NeuroImmune Pharmacology 1 (2006) 223-36.

[49] M. Baskaya, Regional Activity of Ornithine Decarboxylase and Edema Formation after Traumatic Brain Injury. (1996).

[50] Y. Shapira, and E. Shohami, Experimental studies on brain oedema after blunt head injury: experimental approaches from animal experimentation to actual or possible clinical application. Eur J Anaesthesiol. 10 (1993) 155-73.

[51] M.D. Habgood, N. Bye, K.M. Dziegielewska, C.J. Ek, M.A. Lane, A. Potter, C. Morganti-Kossmann, and N.R. Saunders, Changes in blood-brain barrier permeability to large and small molecules following traumatic brain injury in mice. The European journal of neuroscience 25 (2007) 231-8.

[52] C. Cornelius, R. Crupi, V. Calabrese, A. Graziano, P. Milone, G. Pennisi, Z. Radak, E.J. Calabrese, and S. Cuzzocrea, Traumatic brain injury: oxidative stress and neuroprotection. Antioxidants & redox signaling 19 (2013) 836-53.

[53] B. Obermeier, R. Daneman, and R.M. Ransohoff, Development, maintenance and disruption of the blood-brain barrier. Nature medicine 19 (2013) 1584-96.

[54] P.B. Pun, J. Lu, and S. Moochhala, Involvement of ROS in BBB dysfunction. Free radical research 43 (2009) 348-64.

[55] C. Werner, and K. Engelhard, Pathophysiology of traumatic brain injury. British journal of anaesthesia 99 (2007) 4-9.

[56] S.M. Lucas, N.J. Rothwell, and R.M. Gibson, The role of inflammation in CNS injury and disease. British journal of pharmacology 147 Suppl 1 (2006) S232-40.

[57] B. Morrison, 3rd, B.S. Elkin, J.P. Dolle, and M.L. Yarmush, *In vitro* models of traumatic brain injury. Annual review of biomedical engineering 13 (2011) 91-126.

[58] T.P. Prevost, G. Jin, M.A. de Moya, H.B. Alam, S. Suresh, and S. Socrate, Dynamic mechanical response of brain tissue in indentation *in vivo*, *in situ* and *in vitro*. Acta biomaterialia 7 (2011) 4090-101.

[59] G. Morrison, D.D. Fraser, and G. Cepinskas, Mechanisms and consequences of acquired brain injury during development. Pathophysiology : the official journal of the International Society for Pathophysiology / ISP 20 (2013) 49-57.

[60] A. Al Ahmad, C.B. Taboada, M. Gassmann, and O.O. Ogunshola, Astrocytes and pericytes differentially modulate blood-brain barrier characteristics during

development and hypoxic insult. Journal of cerebral blood flow and metabolism : official journal of the International Society of Cerebral Blood Flow and Metabolism 31 (2011) 693-705.

[61] I. Cernak, Animal Models of Head Trauma. NeuroRx. 2 (2005) 410-22.

[62] W.T. O'Connor, A. Smyth, and M.D. Gilchrist, Animal models of traumatic brain injury: a critical evaluation. Pharmacology & therapeutics 130 (2011) 106-13.

[63] H. Alluri, K. Wiggins-Dohlvik, M.L. Davis, J.H. Huang, and B. Tharakan, Blood-brain barrier dysfunction following traumatic brain injury. Metabolic brain disease 30 (2015) 1093-104.

[64] M. Colicos, C.E. Dixon, and P.K. Dash, Delayed, selective neuronal death following experimental cortical impact injury in rats: possible role in memory deficits. Brain Res. 11 (1996) 111-9.

[65] A.E. Kline, A.K. Wagner, B.P. Westergom, R.R. Malena, R.D. Zafonte, A.S. Olsen, C.N. Sozda, P. Luthra, M. Panda, J.P. Cheng, and H.A. Aslam, Acute treatment with the 5-HT1A receptor agonist 8-OH-DPAT and chronic environmental enrichment confer neurobehavioral benefit after experimental brain trauma. 177 2 (2007).

[66] A.E. Kline, A.N. Hoffman, J.P. Cheng, R.D. Zafonte, and J.L. Massucci, Chronic administration of antipsychotics impede behavioral recovery after experimental traumatic brain injury. Neuroscience letters 448 (2008) 263-7.

[67] A.N. Hoffman, J.P. Cheng, R.D. Zafonte, and A.E. Kline, Administration of haloperidol and risperidone after neurobehavioral testing hinders the recovery of traumatic brain injury-induced deficits. Life sciences 83 (2008) 602-7.

[68] C.E. Dixon, G.L. Clifton, J.W. Lighthall, A.A. Yaghmai, and R.L. Hayes, A controlled cortical impact model of traumatic brain injury in the rat. Journal of neuroscience methods 39 (1991) 253-62.

[69] E.D. Hall, Y.D. Bryant, W. Cho, and P.G. Sullivan, Evolution of post-traumatic neurodegeneration after controlled cortical impact traumatic brain injury in mice and rats as assessed by the de Olmos silver and fluorojade staining methods. Journal of neurotrauma 25 (2008) 235-47.

[70] P. Lee, J. Kim, R. Williams, R. Sandhir, E. Gregory, W.M. Brooks, and N.E. Berman, Effects of aging on blood brain barrier and matrix metalloproteases following controlled cortical impact in mice. Experimental neurology 234 (2012) 50-61.

[71] P. Naik, and L. Cucullo, *In vitro* blood-brain barrier models: current and perspective technologies. Journal of pharmaceutical sciences 101 (2012) 1337-54.

[72] S.Y. Yuan, and R.R. Rigor, Integrated Systems Physiology: From Molecule to Function to Disease, Regulation of Endothelial Barrier Function, Morgan & Claypool Life Sciences. Copyright (c) 2011 by Morgan & Claypool Life Sciences., San Rafael (CA), 2010.

[73] S.J. Bolton, D.C. Anthony, and V.H. Perry, Loss of the tight junction proteins occludin and zonula occludens-1 from cerebral vascular endothelium during neutrophil-induced blood-brain barrier breakdown *in vivo*. Neuroscience 86 (1998) 1245-57.

[74] R.R. Rigor, R.S. Beard, Jr., O.P. Litovka, and S.Y. Yuan, Interleukin-1beta-induced barrier dysfunction is signaled through PKC-theta in human brain microvascular endothelium. American journal of physiology. Cell physiology 302 (2012) C1513-22.

[75] A. Simi, N. Tsakiri, P. Wang, and N.J. Rothwell, Interleukin-1 and inflammatory neurodegeneration. Biochem Soc Trans. 35 (2007) 1122-6.

[76] N. Didier, I.A. Romero, C. Créminon, A. Wijkhuisen, J. Grassi, and A. Mabondzo, Secretion of interleukin-1β by astrocytes mediates endothelin-1 and tumour necrosis factor-α effects on human brain microvascular endothelial cell permeability. Journal of neurochemistry 86 (2004) 246-254.

[77] C. Coisne, and B. Engelhardt, Tight junctions in brain barriers during central nervous system inflammation. Antioxidants & redox signaling 15 (2011) 1285-303.

[78] A. Basu, J.K. Krady, and S.W. Levison, Interleukin-1: a master regulator of neuroinflammation. Journal of neuroscience research 78 (2004) 151-6.

[79] A.M. Blamire, D.C. Anthony, B. Rajagopalan, N.R. Sibson, V.H. Perry, and P. Styles, Interleukin-1beta -induced changes in blood-brain barrier permeability,

apparent diffusion coefficient, and cerebral blood volume in the rat brain: a magnetic resonance study. J Neurosci. 20 (2000) 8153-9.

[80] H.E. de Vries, M.C. Blom Roosemalen, M. van Oosten, A.G. de Boer, T.J. van Berkel, D.D. Breimer, and J. Kuiper, The influence of cytokines on the integrity of the blood-brain barrier *in vitro*. Journal of neuroimmunology 64 (1996) 37-43.

[81] T. Sozen, R. Tsuchiyama, Y. Hasegawa, H. Suzuki, V. Jadhav, S. Nishizawa, and J.H. Zhang, Role of interleukin-1beta in early brain injury after subarachnoid hemorrhage in mice. Stroke; a journal of cerebral circulation 40 (2009) 2519-25.

[82] M. Grossetete, J. Phelps, L. Arko, H. Yonas, and G.A. Rosenberg, Elevation of matrix metalloproteinases 3 and 9 in cerebrospinal fluid and blood in patients with severe traumatic brain injury. Neurosurgery 65 (2009) 702-8.

[83] F. Chen, N. Ohashi, W. Li, C. Eckman, and J.H. Nguyen, Disruptions of occludin and claudin-5 in brain endothelial cells *in vitro* and in brains of mice with acute liver failure. Hepatology 50 (2009) 1914-23.

[84] B. Wu, Q. Ma, N. Khatibi, W. Chen, T. Sozen, O. Cheng, and J. Tang, Ac-YVAD-CMK Decreases Blood-Brain Barrier Degradation by Inhibiting Caspase-1 Activation of Interleukin-1beta in Intracerebral Hemorrhage Mouse Model. Translational stroke research 1 (2010) 57-64.

[85] K. Wiggins-Dohlvik, M. Merriman, C.A. Shaji, H. Alluri, M. Grimsley, M.L. Davis, R.W. Smith, and B. Tharakan, Tumor necrosis factor-alpha disruption of

brain endothelial cell barrier is mediated through matrix metalloproteinase-9. American journal of surgery 208 (2014) 954-60; discussion 960.

[86] D.S. Rudra, U. Pal, N.C. Maiti, R.J. Reiter, and S. Swarnakar, Melatonin inhibits matrix metalloproteinase-9 activity by binding to its active site. J. Pineal Res. 54 (2013) 398-405.

[87] K. Wiggins-Dohlvik, M.S. Han, H.W. Stagg, H. Alluri, C.A. Shaji, R.P. Oakley, M.L. Davis, and B. Tharakan, Melatonin inhibits thermal injury-induced hyperpermeability in microvascular endothelial cells. The journal of trauma and acute care surgery 77 (2014) 899-905.

[88] Y. Chen, H. Mao, K.H. Yang, T. Abel, and D.F. Meaney, A modified controlled cortical impact technique to model mild traumatic brain injury mechanics in mice. Frontiers in neurology 5 (2014) 100.

[89] M. Campolo, A. Ahmad, R. Crupi, D. Impellizzeri, R. Morabito, E. Esposito, and S. Cuzzocrea, Combination therapy with melatonin and dexamethasone in a mouse model of traumatic brain injury. The Journal of endocrinology 217 (2013) 291-301.

[90] F. Simao, A.S. Pagnussat, J.H. Seo, D. Navaratna, W. Leung, J. Lok, S. Guo, C. Waeber, C.G. Salbego, and E.H. Lo, Pro-angiogenic effects of resveratrol in brain endothelial cells: nitric oxide-mediated regulation of vascular endothelial growth factor and metalloproteinases. Journal of cerebral blood flow and metabolism : official journal of the International Society of Cerebral Blood Flow and Metabolism 32 (2012) 884-95.

[91] H.W. Stagg, J.G. Whaley, B. Tharakan, F.A. Hunter, D. Jupiter, D.C. Little, M.L. Davis, W.R. Smythe, and E.W. Childs, Doxycycline attenuates burn-induced microvascular hyperpermeability. The journal of trauma and acute care surgery 75 (2013) 1040-6; discussion 1046.

[92] P.D. Vermeer, J. Denker, M. Estin, T.O. Moninger, S. Keshavjee, P. Karp, J.N. Kline, and J. Zabner, MMP9 modulates tight junction integrity and cell viability in human airway epithelia. American journal of physiology. Lung cellular and molecular physiology 296 (2009) L751-62.

[93] A.R. Ruhul Amin, T. Senga, M.L. Oo, A.A. Thant, and M. Hamaguchi, Secretion of matrix metalloproteinase-9 by the proinflammatory cytokine, IL-1beta: a role for the dual signalling pathways, Akt and Erk. Genes Cells. 8 (2003) 515-23.

[94] L. Dong, H. Qiao, X. Zhang, X. Zhang, C. Wang, L. Wang, L. Cui, J. Zhao, Y. Xing, Y. Li, Z. Liu, and C. Zhu, Parthenolide is neuroprotective in rat experimental stroke model: downregulating NF-kappaB, phospho-p38MAPK, and caspase-1 and ameliorating BBB permeability. Mediators of inflammation 2013 (2013) 370804.

[95] M. Asahi, K. Asahi, J.C. Jung, G.J. del Zoppo, M.E. Fini, and E.H. Lo, Role for Matrix Metalloproteinase 9 After Focal Cerebral Ischemia: Effects of Gene Knockout and Enzyme Inhibition With BB-94 J Cereb Blood Flow Metab. 20 (2000) 1681-9.

[96] M.A. Seifman, A.A. Adamides, P.N. Nguyen, S.A. Vallance, D.J. Cooper, T. Kossmann, J.V. Rosenfeld, and M.C. Morganti-Kossmann, Endogenous melatonin increases in cerebrospinal fluid of patients after severe traumatic brain injury and correlates with oxidative stress and metabolic disarray. Journal of cerebral blood flow and metabolism : official journal of the International Society of Cerebral Blood Flow and Metabolism 28 (2008) 684-96.

[97] F. Dehghan, M. Khaksari Hadad, G. Asadikram, H. Najafipour, and N. Shahrokhi, Effect of melatonin on intracranial pressure and brain edema following traumatic brain injury: role of oxidative stresses. Archives of medical research 44 (2013) 251-8.

[98] S. Michinaga, and Y. Koyama, Pathogenesis of brain edema and investigation into anti-edema drugs. International journal of molecular sciences 16 (2015) 9949-75.

[99] N.J. Abbott, Inflammatory mediators and modulation of blood-brain barrier permeability. Cell Mol Neurobiol. 20 (2000) 131-47.

[100] A.M. Blamire, D.C. Anthony, B. Rajagopalan, N.R. Sibson, V.H. Perry, and P. Styles, Interleukin-1beta -induced changes in blood-brain barrier permeability, apparent diffusion coefficient, and cerebral blood volume in the rat brain: a magnetic resonance study. J Neurosci. 20 (2000) 8153-9.

[101] K.N. Murray, A.R. Parry-Jones, and S.M. Allan, Interleukin-1 and acute brain injury. Frontiers in cellular neuroscience 9 (2015) 18.

[102] S. Toulmond, and N.J. Rothwell, Interleukin-1 receptor antagonist inhibits neuronal damage caused by fluid percussion injury in the rat. Brain Res. 13 (1995) 261-6.

[103] D. Wong, K. Dorovini-Zis, and S.R. Vincent, Cytokines, nitric oxide, and cGMP modulate the permeability of an *in vitro* model of the human blood-brain barrier. Experimental neurology 190 (2004) 446-55.

[104] M. Pietsch, K.C. Chua, and A.D. Abell, calpains Attractive targets for the development of syntehtic inhibitors. Current Topics in Medicinal Chemistry 10 (2010) 270-293.

[105] A.E. Loot, I. Pierson, T. Syzonenko, A. Elgheznawy, V. Randriamboavonjy, A. Zivković, H. Stark, and I. Fleming, Ca2+-sensing receptor cleavage by calpain partially accounts for altered vascular reactivity in mice fed a high-fat diet. J Cardiovasc Pharmacol. 61 (2013) 528-35.

[106] T. Miyazaki, Y. Taketomi, M. Takimoto, X.F. Lei, S. Arita, J.R. Kim-Kaneyama, S. Arata, H. Ohata, H. Ota, M. Murakami, and A. Miyazaki, m-Calpain induction in vascular endothelial cells on human and mouse atheromas and its roles in VE-cadherin disorganization and atherosclerosis. Circulation 124 (2011) 2522-32.

[107] M. Bralić, and V. Stemberga, Calpain expression in the brain cortex after traumatic brain injury. Coll Antropol. 36 (2012) 1319-23.

[108] T. Wang, L. Wang, L. Moreno-Vinasco, G.D. Lang, J.H. Siegler, B. Mathew, P.V. Usatyuk, J.M. Samet, A.S. Geyh, P.N. Breysse, V. Natarajan, and J.G.

Garcia, Particulate matter air pollution disrupts endothelial cell barrier via calpain-mediated tight junction protein degradation. Particle and fibre toxicology 9 (2012) 35.

[109] M.A. Smith, and R.G. Schnellmann, Calpains, mitochondria, and apoptosis. Cardiovascular research 96 (2012) 32-7.

[110] S.Y. Jeong, M. Martchenko, and S.N. Cohen, Calpain-dependent cytoskeletal rearrangement exploited for anthrax toxin endocytosis. Proceedings of the National Academy of Sciences of the United States of America 110 (2013) E4007-15.

[111] M.-H. Zhou, H. Zheng, H. Si, Y. Jin, J. Peng, L. He, Y. Zhou, C. MuÃƒoz-Garay, D. Zawieja, L. Kuo, X. Peng, and S. Zhang, Stromal interaction molecule 1 (STIM1) and Orai1 mediate histamine-evoked calcium entry and nuclear factor of activated T-cells (NFAT) signaling in human umbilical vein endothelial cells. Journal of biological chemistry 289 (2014) 29446-56.

[112] A. Kampfl, R.M. Posmantur, X. Zhao, E. Schmutzhard, G.L. Clifton, and R.L. Hayes, Mechanisms of calpain proteolysis following traumatic brain injury: Implications for pathology and Therapy: A review and update. Journal of neurotrauma 14 (1997) 121-134.

[113] S. Chakraborti, M.N. Alam, D. Paik, S. Shaikh, and T. Chakraborti, Implications of calpains in health and diseases. Indian J Biochem Biophys. 49 (2012) 316-28.

[114] B. Fei, S. Yu, and R.L. Geahlen, Modulation by Syk of Bcl-2, calcium and the calpain–calpastatin proteolytic system in human breast cancer cells. Biochimica et Biophysica Acta (BBA) - Molecular Cell Research 1833 (2013) 2153-2164.

[115] O. Prangsaengtong, K. Senda, Y. Doki, J.Y. Park, M. Jo, H. Sakurai, N. Shibahara, I. Saiki, and K. Koizumi, Calpain 1 and -2 play opposite roles in cord formation of lymphatic endothelial cells via eNOS regulation. Human cell 25 (2012) 36-44.

[116] M. Ma, Role of calpains in the injury-induced dysfunction and degeneration of the mammalian axon. Neurobiology of disease 60 (2013) 61-79.

[117] R.M. Hannah, K.M. Dunn, A.D. Bonev, and M.T. Nelson, Endothelial SK(Ca) and IK(Ca) channels regulate brain parenchymal arteriolar diameter and cortical cerebral blood flow. Journal of cerebral blood flow and metabolism : official journal of the International Society of Cerebral Blood Flow and Metabolism 31 (2011) 1175-86.

[118] S.N. Thompson, K.M. Carrico, A.G. Mustafa, M. Bains, and E.D. Hall, A pharmacological analysis of the neuroprotective efficacy of the brain- and cell-permeable calpain inhibitor MDL-28170 in the mouse controlled cortical impact traumatic brain injury model. Journal of neurotrauma 27 (2010) 2233-43.

[119] T. Tsubokawa, I. Solaroglu, H. Yatsushige, J. Cahill, K. Yata, and J.H. Zhang, Cathepsin and calpain inhibitor E64d attenuates matrix metalloproteinase-9 activity after focal cerebral ischemia in rats. Stroke; a journal of cerebral circulation 37 (2006) 1888-94.

[120] M.A. Ali, A. Stepanko, X. Fan, A. Holt, and R. Schulz, Calpain inhibitors exhibit matrix metalloproteinase-2 inhibitory activity. Biochemical and biophysical research communications 423 (2012) 1-5.

[121] A. ElAli, T.R. Doeppner, A. Zechariah, and D.M. Hermann, Increased blood-brain barrier permeability and brain edema after focal cerebral ischemia induced by hyperlipidemia: role of lipid peroxidation and calpain-1/2, matrix metalloproteinase-2/9, and RhoA overactivation. Stroke; a journal of cerebral circulation 42 (2011) 3238-44.

[122] D.E. Goll, V.F. Thompson, H. Li, W. Wei, and J. Cong, The calpain system. Physiol Rev. 83 (2003) 731-801.

[123] H. Hu, X. Li, Y. Li, L. Wang, S. Mehta, Q. Feng, R. Chen, and T. Peng, Calpain-1 induces apoptosis in pulmonary microvascular endothelial cells under septic conditions. Microvascular research 78 (2009) 33-9.

[124] M. Pfaff, X. Du, and M.H. Ginsberg, Calpain cleavage of integrin beta cytoplasmic domains. FEBS Lett. 22 (1999) 17-22.

[125] Y. Zhao, N.L. Malinin, J. Meller, Y. Ma, X.Z. West, K. Bledzka, J. Qin, E.A. Podrez, and T.V. Byzova, Regulation of cell adhesion and migration by Kindlin-3 cleavage by calpain. The Journal of biological chemistry 287 (2012) 40012-20.

[126] H. Alluri, H.W. Stagg, R.L. Wilson, R.P. Clayton, D.A. Sawant, M. Koneru, M.R. Beeram, M.L. Davis, and B. Tharakan, Reactive oxygen species-caspase-3 relationship in mediating blood-brain barrier endothelial cell hyperpermeability

following oxygen-glucose deprivation and reoxygenation. Microcirculation 21 (2014) 187-95.

[127] L. Cristofori, B. Tavazzi, R. Gambin, R. Vagnozzi, S. Signoretti, A.M. Amorini, G. Fazzina, and G. Lazzarino, Biochemical analysis of the cerebrospinal fluid: evidence for catastrophic energy failure and oxidative damage preceding brain death in severe head injury: a case report. Clinical biochemistry 38 (2005) 97-100.

[128] S.M. Lee , M.D. Wong, A. Samii, and D.A. Hovda, Evidence for energy failure following irreversible traumatic brain injury. Ann N Y Acad Sci. (1999) 337-40.

[129] R.J. Rodrigues, A.R. Tome, and R.A. Cunha, ATP as a multi-target danger signal in the brain. Frontiers in neuroscience 9 (2015) 148.

[130] A.M. Choo, W.J. Miller, Y.C. Chen, P. Nibley, T.P. Patel, C. Goletiani, B. Morrison, 3rd, M.K. Kutzing, B.L. Firestein, J.Y. Sul, P.G. Haydon, and D.F. Meaney, Antagonism of purinergic signalling improves recovery from traumatic brain injury. Brain : a journal of neurology 136 (2013) 65-80.

[131] J.T. Neary, Y. Kang, K.A. Willoughby, and E.F. Ellis, Activation of extracellular signal-regulated kinase by stretch-induced injury in astrocytes involves extracellular ATP and P2 purinergic receptors. J Neurosci. 23 (2003) 2348-56.

[132] R. Le Feuvre, D. Brough, and N. Rothwell, Extracellular ATP and P2X7 receptors in neurodegeneration. Eur J Pharmacol. 447 (2002) 261-9.

[133] P. Pelegrin, and A. Surprenant, The P2X(7) receptor-pannexin connection to dye uptake and IL-1beta release. Purinergic signalling 5 (2009) 129-37.

[134] A. Brandao-Burch, M.L. Key, J.J. Patel, T.R. Arnett, and I.R. Orriss, The P2X7 Receptor is an Important Regulator of Extracellular ATP Levels. Frontiers in endocrinology 3 (2012) 41.

[135] M. Tsuda, H. Tozaki-Saitoh, and K. Inoue, Pain and purinergic signaling. Brain Res Rev 63 (2010) 222-32.

[136] N. Mehta, M. Kaur, M. Singh, S. Chand, B. Vyas, P. Silakari, M.S. Bahia, and O. Silakari, Purinergic receptor P2X(7): a novel target for anti-inflammatory therapy. Bioorganic & medicinal chemistry 22 (2014) 54-88.

[137] M. Zerr, B. Hechler, M. Freund, S. Magnenat, I. Lanois, J.P. Cazenave, C. Leon, and C. Gachet, Major Contribution of the P2Y1 Receptor in Purinergic Regulation of TNF -Induced Vascular Inflammation. Circulation 123 (2011) 2404-2413.

[138] S.D. Oliveira, R. Coutinho-Silva, and C.L. Silva, Endothelial P2X7 receptors' expression is reduced by schistosomiasis. Purinergic signalling 9 (2013) 81-9.

[139] G.I. Gorodeski, and G. J., Extracellular ATP regulates transcervical permeability by modulating two distinct paracellular pathways. Am J Physiol. 72 (1997) C1602-10.

[140] R.A. North, Molecular physiology of P2X receptors. Physiol Rev. 82 (2002) 1013-67.

[141] D.E. Kimbler, J. Shields, N. Yanasak, J.R. Vender, and K.M. Dhandapani, Activation of P2X7 promotes cerebral edema and neurological injury after traumatic brain injury in mice. PloS one 7 (2012) e41229.

[142] H. Hidaka, and K. Okazaki, KN-62: A Specific Ca2+/calmodulin-dependent Protein Kinase Inhibitor as a Putative Function-searching Probe for Intracellular Signal Transduction. Cardiovascular drug reviews 14 (1996) 84-95.

[143] S.B. Coade, and J.D. Pearson, Metabolism of adenine nucleotides in human blood. Circulation Research 65 (1989) 531-537.

[144] R. Bartlett, L. Stokes, and R. Sluyter, The P2X7 receptor channel: recent developments and the use of P2X7 antagonists in models of disease. Pharmacological reviews 66 (2014) 638-75.

[145] M.L. Cotrina, and M. Nedergaard, Physiological and pathological functions of P2X7 receptor in the spinal cord. Purinergic signalling 5 (2009) 223-32.

[146] J.G. Fitz, Regulation of Cellular Atp Release. Trans Am Clin Climatol Assoc. 118 (2007).

[147] K. Yamamoto, K. Furuya, M. Nakamura, E. Kobatake, M. Sokabe, and J. Ando, Visualization of flow-induced ATP release and triggering of Ca2+ waves at caveolae in vascular endothelial cells. Journal of cell science 124 (2011) 3477-83.

[148] E. Craigie, R.E. Birch, R.J. Unwin, and S.S. Wildman, The relationship between P2X4 and P2X7: a physiologically important interaction? Frontiers in physiology 4 (2013) 216.

[149] B.S. Khakh, and R.A. North, P2X receptors as cell-surface ATP sensors in health and disease. Nature 442 (2006) 527-32.

[150] P. Honore, D. Donnelly-Roberts, M.T. Namovic, G. Hsieh, C.Z. Zhu, J.P. Mikusa, G. Hernandez, C. Zhong, D.M. Gauvin, P. Chandran, R. Harris, A.P. Medrano, W. Carroll, K. Marsh, J.P. Sullivan, C.R. Faltynek, and M.F. Jarvis, A-740003 [N-(1-{[(cyanoimino)(5-quinolinylamino) methyl]amino}-2,2-dimethylpropyl)-2-(3,4-dimethoxyphenyl)acetamide], a novel and selective P2X7 receptor antagonist, dose-dependently reduces neuropathic pain in the rat. The Journal of pharmacology and experimental therapeutics 319 (2006) 1376-85.

[151] L.M. Zheng, A. Zychlinsky, C. Liu, D.M. Ojcius, and J.D. Young, Extracellular ATP as a Trigger for Apoptosis or Programmed Cell Death J cell Biol. 112 (1991) 279-88.

[152] D.L. Donnelly-Roberts, M.T. Namovic, P. Han, and M.F. Jarvis, Mammalian P2X7 receptor pharmacology: comparison of recombinant mouse, rat and human P2X7 receptors. British journal of pharmacology 157 (2009) 1203-14.

[153] J. Berrout, M. Jin, and R.G. O'Neil, Critical role of TRPP2 and TRPC1 channels in stretch-induced injury of blood-brain barrier endothelial cells. Brain research 1436 (2012) 1-12.

[154] M. De Bock, M. Culot, N. Wang, A. da Costa, E. Decrock, M. Bol, G. Bultynck, R. Cecchelli, and L. Leybaert, Low extracellular Ca2+ conditions induce an

increase in brain endothelial permeability that involves intercellular Ca2+ waves. Brain research 1487 (2012) 78-87.

[155] D. Pubill, G. Dayanithi, C. Siatka, M. Andres, M.N. Dufour, G. Guillon, and C. Mendre, ATP induces intracellular calcium increases and actin cytoskeleton disaggregation via P2x receptors. Cell calcium 29 (2001) 299-309.

[156] M. Bradford, and S. Soltoff, P2X7 receptors activate protein kinase D and p42/p44 mitogen-activated protein kinase (MAPK) downstream of protein kinase C. Biochem J. 15 (2002) 745-55.